Lateral Static and Dynamic Response of Single Piles in Non-Homogenous Soils using a Standalone Two-Parameter Foundation Model

Mathewos Endeshaw

School of Civil and Environmental Engineering

Addis Ababa University
Addis Ababa Institute of Technology

A thesis submitted for the degree of

Masters of Science in Civil Engineering

March 2023

Addis Ababa University
Addis Ababa Institute of Technology
School of Civil and Environmental Engineering

Lateral Static and Dynamic Response of Single Piles in Non-Homogenous Soils using a Standalone Two-Parameter Foundation Model

Mathewos Endeshaw

Advisor: Dr. Ing. Asrat Worku

Approved by board of examiners:

Advisor	Signature	Date
External Examiner	Signature	Date
Internal Examiner	Signature	Date
Chairman	Signature	Date

Statement of Originality

I hereby declare that this thesis titled Lateral Static and Dynamic Response of Single Piles in Non-Homogenous Soils using a Standalone Two-Parameter Foundation Model is my own original work and has not been submitted for any other degree in any other university or published elsewhere. I have also provided due references for all the resources and materials used for this thesis.

Student's Name _____ Signature _____ Date _____

This is to certify that the above declaration made by the student is correct to the best of my knowledge.

Advisor's Name _____ Signature _____ Date _____

Acknowledgements

First and foremost, I would like to express my sincerest gratitude to my advisor, Dr. Ing. Asrat Worku, who has provided me with invaluable guidance throughout this work. From the development of the proposal to the finalization of this thesis, Dr. Ing. Asrat has always made his time available for discussion and feedback on various topics related to this work and beyond. I have learned a lot from him, not only academically but also personally.

I would also like to thank my family and friends for their constant support and encouragement. I am especially grateful to my parents and siblings for their continuous and unyielding support in my academic endeavors.

I am also thankful to my friends who helped proofread this work and offered helpful suggestions.

Thank you!

Abstract

In the design and analysis of structures supported on piles, geotechnical engineers are required to formulate pile responses. Such a formulation involves the use of subgrade models that relate the interface forces to the displacement. The primary focus of this thesis is one such relatively new subgrade model, initially developed for shallow foundations, applied to laterally loaded piles. The model is a Kerr-equivalent two-parameter Pasternak-type continuum subgrade. Furthermore, as with most pile applications, the variable nature of the soil along the pile depth is also taken into consideration. The goal of this thesis is to investigate the applicability of the aforementioned model for predicting the static and dynamic inertial response of a single pile embedded in non-homogenous soils represented by a power function. To this end, the model in question is initially calibrated by setting equivalences between the responses predicted and results from finite element analysis. Expressions for a calibrating factor left open in the model are developed as functions of relevant parameters. The results from the calibrated model are compared with the results from the finite element method and found to be comparable. Additionally, it is demonstrated that the critical slenderness ratio and critical relative stiffness can be approximated by threshold values form expressions developed for the calibration factor. Using the calibrated subgrade model, the static response of the soil is also investigated. Expressions for the pile head flexibility influence factor and pile head stiffness terms are provided. The proposed expressions compare well with published results. In addition, utilizing the unique characteristic of the model being studied, in that the shear interaction is explicitly accounted for, its effects on static pile response are also studied. In general, neglecting the shear term results in overestimation of the pile head displacement. Similarly, the use of a calibrated lower order Winkler-type model that implicitly accounts for shear interaction is investigated which by in large provides higher displacement profiles. The calibrated model is also used in predicting the dynamic inertial response of a laterally loaded pile in non-homogeneous soil. An approximate energy method is used to arrive at the dynamic pile head stiffness and damping ratios. With the exception of fixed-head piles, it is observed that the dynamic pile head stiffness can reasonably be approximated by the static pile head stiffness for low ranges of excitation frequencies commonly encountered in seismic events. Curve fit expressions are also provided for the pile head damping ratio. The effect of shear interaction is also investigated for the dynamic inertial case. As the analysis is confined to long flexible piles, very little effect is observed with the exception of piles in rocking oscillation.

Keywords: Soil-Structure Interaction, Laterally Loaded Piles, Kerr-Equivalent Pasternak model, Inertial Interaction, Energy Method, Pile Head Stiffness, Pile Head Damping

Contents

1 Introduction **1**
1.1 Background . . . 1
1.2 Description of the problem and scope . . . 4
1.3 Objectives . . . 5
1.3.1 Specific objectives . . . 5
1.4 Methodology and thesis overview . . . 6

2 Literature Review **8**
2.1 Analysis of laterally loaded piles . . . 8
2.1.1 The Subgrade approach . . . 8
2.1.1.1 Subgrade models . . . 9
2.1.1.2 Subgrade models in dynamic analysis . . . 17
2.1.1.3 Analysis of laterally loaded piles using the subgrade approach . . . 20
2.1.2 Boundary element method . . . 23
2.1.3 Finite element method . . . 24
2.2 Representation of soil non-homogeneity . . . 33

3 Methods of Study **36**
3.1 Selection of forms of soil non-homogeneity . . . 37
3.2 Selection of a distributed dashpot model for radiation damping . . . 38
3.3 Analysis parameters . . . 39
3.4 Finite element modeling . . . 42
3.4.1 Domain geometry . . . 42
3.4.2 Element types and sizes . . . 44
3.4.2.1 Element types for the soil domain . . . 44
3.4.2.2 Element types for the pile domain . . . 45
3.4.3 Pile-soil interface . . . 47
3.4.4 Representation of soil non-homogeneity . . . 48
3.4.5 Analysis workflow . . . 48
3.4.6 Verification of finite element results . . . 49
3.5 Beam-on-Pasternak-subgrade analysis . . . 51
3.5.1 Description of soil . . . 51
3.5.2 Governing equation . . . 52
3.5.3 Boundary conditions . . . 53
3.5.4 Solution methods . . . 56
3.6 Approximate method of analysis for dynamic inertial interaction . . . 56
3.6.1 Description of soil . . . 57

3.6.2 Pile shape functions . . . 58
3.6.3 Energy formulation . . . 61
3.6.4 Evaluation of the integrals . . . 63

4 Model Calibration **64**
4.1 Effect of pile-soil relative stiffness . . . 65
4.2 Effect of pile slenderness ratio . . . 73
4.3 Effect of the soil Poisson's ratio . . . 79
4.4 Effect of pile end condition . . . 80
4.5 Comparison of calibration factor threshold values with critical slenderness ratio and critical relative stiffness . . . 81
4.6 Validation of model calibration . . . 83
4.7 Calibrated subgrade parameters . . . 86
4.7.1 Piles embedded in soils with linearly increasing elastic modulus . 86
4.7.1.1 Free-head floating piles . . . 86
4.7.1.2 Fixed-head floating piles . . . 88
4.7.1.3 Fixed-base piles . . . 89
4.7.2 Piles embedded in soils with parabolically varying elastic modulus 89
4.7.2.1 Free-head floating piles . . . 89
4.7.2.2 Fixed-head floating piles . . . 90
4.7.2.3 Fixed-base piles . . . 91

5 Static Pile Response **92**
5.1 Piles Embedded in soil with linearly increasing elastic modulus . . . 94
5.1.1 Free-head floating Piles . . . 94
5.1.2 Fixed-head floating piles . . . 98
5.1.3 Fixed-base piles . . . 100
5.2 Piles embedded in soil with parabolically increasing elastic modulus . . . 100
5.2.1 Free-head floating piles . . . 101
5.2.2 Fixed-head floating piles . . . 103
5.2.3 Fixed-base piles . . . 104
5.3 Effect of shear interaction . . . 105

6 Dynamic Analysis — Inertial Interaction **112**
6.1 Dynamic pile head stiffness . . . 114
6.2 Pile head damping . . . 119
6.2.1 Effect of Poisson's ratio . . . 120
6.2.2 Effect of relative stiffness . . . 121
6.2.3 Effect of excitation frequency . . . 125
6.3 Expressions for pile head impedance functions . . . 130
6.4 Effect of shear interaction in dynamic inertial response . . . 135

7 Conclusions and Recommendations **139**
7.1 Conclusions . . . 139
7.2 Recommendations for future research . . . 141

References **143**

A Derivation of equivalent base shear, Q_L **150**

B Derivation of energy equations for approximate analysis in inertial interaction **153**
B.1 Contribution of the pile flexural stiffness 155
B.2 Contribution of the subgrade 156
B.3 Contribution of the pile inertia 157
B.4 Contribution of the dashpot 158

List of Figures

1.1 Definition of the Problem 4

2.1 Mechanical Subgrade Models; (a) Winkler Model, (b) Pasternak Two-Parameter Model, (c) Filonenko-Borodich Two-Parameter Model, (d) Kerr Three-Parameter Model 10
2.2 Reissner's Problem Definition 12
2.3 Plan diagram of damping models 19

3.1 Profile of soil modulus 38
3.2 Normalized pile head displacement using different measures of relative pile stiffness 39
3.3 finite element domain geometry 43
3.4 Sensitivity of finite element result to distance of vertical boundary for free-head floating pile in soil with linearly increasing modulus with zero at the surface ($\nu_s = 0.3$) 44
3.5 Finite Element Model 45
3.6 Geometry of elements used in finite element analysis, (left: C3D20, right: C3D15) (ABAQUS 2022) 46
3.7 Mesh convergence for free-head floating piles embedded in soil with linearly increasing soils 47
3.8 Sign Convention 51

4.1 Model calibration workflow 65
4.2 Variation of the calibration factor with respect to the relative stiffness for free-head floating piles in soil with linearly increasing elastic modulus . . 68
4.3 Variation of the calibration factor with respect to relative stiffness for fixed-head floating piles in soil profile with linearly increasing elastic modulus . 69
4.4 Variation of the calibration factor with respect to relative stiffness for free-head fixed-base piles in soil profile with linearly increasing elastic modulus 69
4.5 Variation of the calibration factor with respect to relative stiffness for fixed-head fixed-base piles in soil profile with linearly increasing elastic modulus 70
4.6 Variation of the calibration factor with respect to the relative stiffness for free-head floating piles in soil with parabolically increasing elastic modulus 71
4.7 Variation of the calibration factor with respect to the relative stiffness for fixed-head floating piles in soil with parabolically increasing elastic modulus 72
4.8 Variation of the calibration factor with respect to the relative stiffness for free-head fixed-base piles in soil with parabolically increasing elastic modulus 72
4.9 Variation of the calibration factor with respect to the relative stiffness for fixed-head free-base piles in soil with parabolically increasing elastic modulus 73

4.10 Variation of the calibration factor with respect to slenderness ratio for free-head floating piles in soil profile with linearly increasing elastic modulus 75
4.11 Variation of the calibration factor with respect to slenderness ratio for fixed-head floating piles in soil profile with linearly increase elastic modulus 76
4.12 Variation of calibration factor with respect to the slenderness ratio for free-head floating piles in soil with parabolically increasing elastic modulus 78
4.13 Variation of the calibration factor with respect to the slenderness ratio for fixed-head floating piles in soil with parabolically increasing elastic modulus 79
4.14 Variation of the calibration factor with respect to the soil Poisson's ratio for fixed-head floating piles in soil profile with linearly increase elastic modulus 80
4.15 Comparison of calibration factor threshold with published expressions for critical relative stiffness (left) and critical pile length (right) for free-head floating piles in soil profile with linearly increasing elastic modulus 82
4.16 Comparison of calibration factor threshold with published expressions for critical relative stiffness (left) and critical pile length (right) for fixed-head floating piles in soil profile with linearly increase elastic modulus 82
4.17 Comparison of calibration factor threshold with published expressions for critical pile length for free-head floating piles in soil profile with parabolically varying elastic modulus 83
4.18 Comparison of pile displacement profile for free-head floating piles embedded in soil with linearly increasing elastic modulus 85
4.19 Comparison of pile displacement profile for fixed-head floating piles embedded in soil with linearly increasing elastic modulus 86

5.1 Comparison of influence factors for free-head floating long flexible piles embedded in soil with linearly increasing elastic modulus 96
5.2 Comparison of influence factors for free-head floating short rigid piles embedded in soil with linearly increasing elastic modulus 97
5.3 Comparison of influence factors for fixed-head floating short rigid piles embedded in soil with linearly increasing elastic modulus 99
5.4 Comparison of influence factors for fixed-head floating long flexible piles embedded in soil with linearly increasing elastic modulus 100
5.5 Comparison of influence factors for free-head floating long flexible piles embedded in soil with Parabolically increasing elastic modulus 102
5.6 Effect of shear term for free-head free-base piles in soil with linearly increasing elastic modulus 107
5.7 Effect of shear term for fixed-head free-base piles in soil with linearly increasing elastic modulus 108
5.8 Comparison of Kerr-equivalent Pasternak model and Winkler model for free-head free-base piles in soil with linearly increasing elastic modulus . 109
5.9 Comparison of Kerr-equivalent Pasternak model and Winkler model for fixed-head free-base piles in soil with linearly increasing elastic modulus . 110
5.10 Comparison of bending moment from Kerr-equivalent Pasternak model and Winkler model for piles in soil with linearly increasing elastic modulus 111

6.1 Variation of dynamic pile head stiffness with relative pile-soil stiffness for free-head piles embedded in soil with linearly increasing elastic modulus, $\nu_s = 0.4$ and $a_{0r} = 0.5$ 115

6.2 Variation of dynamic pile head stiffness with normalized frequency (a_{0r}) for free-head piles embedded in soil with linearly increasing elastic modulus, $\nu_s = 0.4$ and $E_p/mr = 10^4$ 116
6.3 Variation of dynamic pile head stiffness with relative pile-soil stiffness for free-head piles embedded in soil with parabolically increasing elastic modulus, $\nu_s = 0.4$ and $a_{0r} = 0.5$ 117
6.4 Variation of dynamic pile head stiffness with normalized frequency (a_{0r}) for free-head piles embedded in soil with parabolically increasing elastic modulus, $\nu_s = 0.4$ and $E_p/mr = 10^4$ 118
6.5 Variation of dynamic pile head stiffness with relative pile-soil stiffness for fixed-head piles, $\nu_s = 0.35$ and $a_{0r} = 0.5$ 119
6.6 Variation of dynamic pile head stiffness with normalized frequency (a_{0r}) for fixed-head piles, $\nu_s = 0.4$ and $E_p/mr = 10^4$ 119
6.7 Variation of w_{ij}^s with Poisson's ratio for $E_p/mr = 10^4$ and $a_{0r} = 0.5$ (top: free-head pile, left $n = 1$ and right $n = 0.5$, bottom: fixed-head pile) . . . 120
6.8 Variation of β_{ij}^r with Poisson's ratio for $E_p/mr = 10^4$ and $a_{0r} = 0.5$ (top: free-head pile, left $n = 1$ and right $n = 0.5$, bottom: fixed-head pile) . . . 121
6.9 Variation of w_{ij}^s with relative stiffness for free-head piles in soil with linearly increasing elastic modulus (results averaged over Poisson's ratio) 122
6.10 Variation of w_{ij}^s with relative stiffness for free-head piles in soil with parabolically increasing elastic modulus (results averaged over Poisson's ratio) . 123
6.11 Variation of w_{ij}^s with relative stiffness for fixed-head piles with $a_{0r} = 0.5$ (left: $n = 1$, right: $n = 0.5$, results averaged over Poisson's ratio) 123
6.12 Variation of β_{ij}^r with relative stiffness for free-head piles in soil with linearly increasing elastic modulus (results averaged over Poisson's ratio) 124
6.13 Variation of β_{ij}^r with relative stiffness for free-head piles in soil with parabolically increasing elastic modulus (results averaged over Poisson's ratio) . 125
6.14 Variation of β_{ij}^r with relative stiffness for fixed-head piles (left: $n = 1$, right: $n = 0.5$, results averaged over Poisson's ratio) 125
6.15 Variation of w_{ij}^s with normalized frequency for free-head piles in soil with linearly increasing elastic modulus (results averaged over Poisson's ratio) 126
6.16 Variation of w_{ij}^s with normalized frequency for free-head piles in soil with parabolically increasing elastic modulus (results averaged over Poisson's ratio) 127
6.17 Variation of w_{ij}^s with normalized frequency for fixed-head piles (left: $n = 1$, right: $n = 0.5$, results averaged over Poisson's ratio) 127
6.18 Variation of β_{ij}^r with normalized frequency for free-head piles in soil with linearly increasing elastic modulus (results averaged over Poisson's ratio) 128
6.19 Variation of β_{ij}^r with normalized frequency for free-head piles in soil with parabolically increasing elastic modulus (results averaged over Poisson's ratio) 129
6.20 Variation of β_{ij}^r with normalized frequency for fixed-head piles (left: $n = 1$, right: $n = 0.5$, results averaged over Poisson's ratio) 129
6.21 Comparison of proposed β_{ij} against published literature for free-head piles in soil with linearly increasing elastic modulus and $\beta_s = 5\%$ 133
6.22 Comparison of proposed β_{ij} against published literature for free-head piles in soil with parabolically increasing elastic modulus and $\beta_s = 5\%$ 134

6.23 Comparison of proposed β_{ij} against published literature for fixed-head piles in soil with linearly increasing elastic modulus and $\beta_s = 5\%$ 134
6.24 Variation of β_{ij} with a_{0r} for free-head piles in soil with linearly increasing elastic modulus, $^{E_p}/_{mr} = 10^4$ and $\beta^s = 5\%$ (results averaged over the Poisson's ratio) 136
6.25 Variation of β_{ij} with a_{0r} for fixed-head piles in soil with linearly increasing elastic modulus, $^{E_p}/_{mr} = 10^4$ and $\beta^s = 5\%$ (results averaged over the Poisson's ratio) 136
6.26 Variation of β_{ij} with a_{0r} for free-head piles in soil with parabolically increasing elastic modulus, $^{E_p}/_{mr} = 10^4$ and $\beta^s = 5\%$ (results averaged over the Poisson's ratio) 137
6.27 variation of β_{ij} with a_{0r} for fixed-head piles in soil with parabolically increasing elastic modulus, $^{E_p}/_{mr} = 10^4$ and $\beta^s = 5\%$ (results averaged over the Poisson's ratio) 138

List of Tables

2.1 Material damping weight factor proposed by Gazetas (1991) for free-head long flexible piles 29
2.2 Material damping weight factor proposed by Syngros (2004) for free-head and fixed-head long flexible piles 31

3.1 Summary of parameter values for finite element analysis 41
3.2 Validation of finite element results against Higgins et al. (2013) for linearly increasing soil stiffness and free-head floating piles 50
3.3 Validation of finite element results against Higgins et al. (2013) for linearly increasing soil stiffness and fixed-head floating piles 50
3.4 Validation of finite element results against Gazetas (1991) for parabolically increasing soil profile 51

4.1 Validation of model calibration for piles embedded in soil with linearly increasing elastic modulus 84
4.2 Validation of model calibration for piles embedded in soil with parabolically increasing elastic modulus 84

6.1 Proposed mean values for material damping weight factor 131

Chapter 1

Introduction

1.1 Background

Pile foundations are extensively used to support structures and safely transfer loads to the soil. Piles are used in structures such as bridges, towers and earth retaining walls. Pile foundations are also used as machine foundations, where dynamic action from the supported machines have to be safely transferred to the soil. In addition, piles as part of a structure are designed to resist actions from earthquakes. The analysis and design of such structures requires determining the responses of the supporting pile under applied load or ground motion. These responses of the pile are generally coupled to the responses of the soil in that displacement in the soil result in forces in the pile and vice-versa. Such an interaction has considerable implication in the performance of structures supported on piles under static and dynamic action (Poulos and Davis 1980; Pender 1993).

The study of static and dynamic soil-structure interaction (SSI and DSSI) is done separately mainly due to the deferring degrees of complexity between the two types of load cases and associated responses. Nevertheless, static soil-structure interaction may be viewed as a subset of DSSI. Static SSI problems for laterally loaded pile foundations involve models that relate the pile-soil interface stresses with pile deformation, termed subgrade models. In such models, the soil is idealized as either a continuum or as a system of mechanical elements (Kerr 1964; Poulos and Davis 1980; Horvath 2002; Worku 2013). The continuum idealization of the soil involves the linear elastic constitutive model. Even

with the use of such simple constitutive relation, mathematical difficulties in obtaining solutions exist. Therefore, simplifying assumptions are usually made (Reissner 1958; Vlasov and Leont'ev 1966; Sun 1994; Guo and Lee 2001; Worku 2010). Alternatively, the mechanical idealization utilizes systems of mechanical elements such as springs, tensioned membranes and shear elements distributed along the length of the pile to simulate the soil response. The most common of such models is the Winkler (1867) model which involves independent springs. Although simple and practicable, the Winkler model has been shown to be lacking, primarily for it does not account for shear transfer in the soil (Vesic and Saxena 1970; Horvath 1983a). For this reason, mechanical models of varying orders of complexity involving additional elements have been proposed (Filonenko-Borodich 1940; Pasternak 1954; Kerr 1965). While the mechanical idealizations are mathematically less demanding, the parameters of the mechanical elements are not provided. To overcome such shortcomings, synthesis of mechanical models with continuum models have been used (Horvath 2002; Worku 2013; Worku 2014). The Kerr-equivalent Pasternak model proposed by Worku (2014) is one such model. Initially developed for shallow foundations, it is a two-parameter continuum model formulated by setting equivalences with the generalized three-parameter Kerr-type continuum model of Worku (2010). Being a two-parameter Pasternak-type model, it can explicitly account for shear interaction. In addition, as it is formulated from the more rigorous generalized three-parameter Kerr-type continuum model, it is found to be of superior performance compared to models of the same order (Worku 2014).

Analysis in dynamic soil-structure interaction also progresses in the same parallel path, either continuum or mechanical. Similar to the static problem, continuum models utilize elastodynamic theories to formulate the response of the pile. Due to complexities with such an approach, proposed methods make use of simplification or numerical solutions (Novak 1974; Dobry et al. 1982; Gazetas and Dobry 1984b; Gazetas 1991; Syngros 2004; Karatzia and Mylonakis 2017). In contrast, mechanical models in DSSI predominantly utilize single parameter Winkler-type model (frequency dependent or independent) with parameters determined from continuum based methods such as the finite element method (Gazetas 1991; Syngros 2004; Karatzia and Mylonakis 2017). In addition to load-deformation characteristics, DSSI analysis must also take into consideration the energy dissipation properties of the pile-soil system. Such a mechanism is represented by

dashpot elements evenly distributed over the pile length and combining hysteric material damping associated with the pile & soil and radiation damping associated with the geometric spreading of waves. Expressions for the viscous damping coefficient of the dashpot element have been proposed by Novak (1974), Gazetas and Dobry (1984b), and Karatzia and Mylonakis (2017) all of which make use of simplified two dimensional elastodynamic formulation. Further, dynamic problems, especially seismic ones, involve two levels of interaction; kinematic, where the existence of the piles affects the ground response which in turn imposes internal forces in the pile and inertial interaction which involves the coupled response of the pile and soil under inertial forces developed within the superstructure (Pender 1993).

Both static and dynamic soil-structure problems are further complicated by the non-homogeneous nature of soils. As piles generally penetrate to deep depths in the soil strata the assumptions of homogeneity are not applicable. To this end, studies have been published by researchers for both static and dynamic problems (Randolph 1981; Gazetas 1991; Syngros 2004; Basu and Higgins 2011; Higgins et al. 2013; Karatzia and Mylonakis 2017). In such works, the continuum idealization is predominantly used and solutions are found with the use of numerical approaches such as the finite element and boundary element methods.

This thesis deals with the lateral response of a vertical pile embedded in a vertically non-homogeneous soil in static and dynamic-inertial interaction. The non-homogeneity is represented by a continuous power function of the from, $E_s(z) = mr\,(z/r)^n$. This specific profile is chosen for its practicability and as it appears to be the most investigated in the literature (Gibson 1967; Randolph 1981; Gazetas 1991; Higgins et al. 2013). The analysis approach will be the mechanical approach with the soil modeled as a two-parameter subgrade and the pile as a vertical Euler-Bernoulli beam. The stiffness parameters for the soil are obtained from Worku (2014) calibrated Kerr-equivalent Pasternak model. The model has recently been shown to be applicable to single piles embedded in homogeneous soil with appropriate calibration of the model for static, kinematic and inertial interaction Lulseged (2021), Worku and Lulseged (2023a), and Worku and Lulseged (2023b); hence, this work may viewed as an extension of that. For the dynamic-inertial interaction case, the frequency independent stiffness parameters of the model along with appropriate

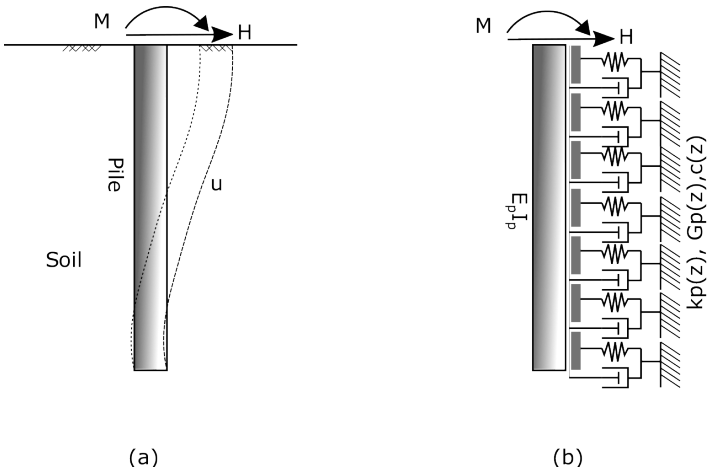

Figure 1.1: Definition of the Problem

damping coefficients are also used.

1.2 Description of the problem and scope

Referring to Figure 1.1, the problem involves a straight vertical prismatic pile of circular cross section with radius r. The pile is modeled as an Euler-Bernoulli beam with flexural stiffness, E_pI_p, embedded length, L, and material damping ratio, β_p. The soil is represented by a two-parameter Pasternak subgrade model with subgrade modulus, k_P, and shear modulus,G_P, material damping ratio, β_s, and radiation damping coefficient, c_r. Soil inhomogeneity is represented by variation in the modulus of elasticity of the soil, $E_s(z)$.

The expression for the subgrade parameters (k_P and G_P) is provided by the Kerr-equivalent Pasternak subgrade model of Worku (2014) given by (1.1) and (1.2). The model involves an open calibration factor, χ, that allows one to better fit the model to the specific problem being investigated.

$$k_P(z) = \frac{(0.4\nu_s + 0.67)\, E_s(z)}{\chi d} \tag{1.1}$$

$$G_P(z) = (1.36\nu_s + 2.28)\, G_s(z)\chi d \tag{1.2}$$

In (1.1) and (1.2), d is the diameter of the pile ($d = 2r$) , ν_s is the Poisson's ratio of the soil, $G_s(z)$ is the shear modulus of the soil and χ is the calibration factor.

The pile is subject to a lateral static force, H_0, and a moment, M_0, in static interaction and to a lateral dynamic force, $H = H_0 e^{i\omega t}$, and a moment, $M = M_0 e^{i\omega t}$, in inertial interaction. At the head, the pile may be free or fixed against rotation. Similarly, at the base, the pile may be free or fixed against both translation and rotation.

For the problem defined above, the primary requirement is to formulate and evaluate the response of the pile in static and dynamic-inertial interaction under lateral loading embedded in non-homogeneous soil.

This thesis does not address pile responses under passive actions such as lateral earth pressure on piles as in the case of earth retaining structures. It also does not investigate kinematic interaction associated with seismic excitation or other forms of ground motion.

1.3 Objectives

The general objective of this thesis is to study the application of the Kerr-equivalent Pasternak model developed by Worku (2014) for laterally loaded piles in non-homogeneous soils. The model's applicability is studied for both static and dynamic-inertial interaction cases.

1.3.1 Specific objectives

The specific objectives of this study are:

1. to evaluate the calibration factor used in the Kerr-equivalent Pasternak subgrade model for non-homogeneous soils.
2. to study the response of a single vertical pile embedded in non-homogeneous soil under static loads.
3. to study the response of a single vertical pile embedded in non-homogeneous soil

under dynamic-inertial interaction.

4. to formulate critical pile slenderness ratio for piles embedded in non-homogeneous soils.

5. to study the direct influence of soil shear resistance on the response of a pile.

1.4 Methodology and thesis overview

To arrive at any form of solution to the problem described in Section 1.2, one has to first calibrate the model by determining the value of the calibration factor left open in the Worku (2014) Kerr-equivalent Pasternak subgrade. In order to do this, comparisons are made between solutions from other methods and results using the current model. For the work at hand, the finite element method is used. Pile head displacements from finite element analysis are compared with pile head displacement from a beam-on-Pasternak subgrade analysis using the model in question and an assumed calibration factor. If the pile head displacements are within 1% of one another the calibration factor is saved otherwise the factor is successively varied until the required difference is reached. This is done for quite a wide range of relevant parameters.

Once the model is calibrated, the beam-on-Pasternak subgrade analysis is used again to investigate the static pile responses. These responses are primary formulated in the form of pile head flexibility coefficients. Furthermore, for investigating dynamic inertial interaction, an approximate energy method is used to formulate the dynamic pile head stiffness and pile head damping ratio.

This thesis is structured following the methodology outlined above. Chapter 2 presents a review of literature relevant to the current work. Chapter 3 provides a detailed discussion of the methods used in subsequent chapters, including finite element modeling, beam-on-Pasternak subgrade and an approximate energy approach. Parameter values that are used throughout the thesis are also set in this chapter. Chapter 4 sets out the model calibration process, and the effect of relevant parameters on the calibration factor is investigated. In addtion, curve fit expressions for the calibration factor are provided. In Chapter 5 static pile responses are investigated and curve fit expressions are provided

for the pile head flexibility factors and stiffness coefficients. Furthermore, the effect of shear interaction explicitly represented in the subgrade model is investigated. Chapter 6 presents an approximate energy based solution for the pile head impedance functions. The effect of shear interaction for the dynamic inertial interaction case are investigated in this chapter as well. Finally, Chapter 7 provides the conclusions drawn from the results of the work done and recommendations for future research.

Chapter 2

Literature Review

This chapter presents a review of relevant literature on the analysis of laterally loaded piles in both static and inertial pile-soil interaction. In addition, a review of the various forms of representation of soil non-homogeneity, especially as used in the analysis of piles, is presented.

2.1 Analysis of laterally loaded piles

The methods for analysis of laterally loaded piles are grouped into two, the subgrade approach and continuum approach (Poulos and Davis 1980; Pender 1993).

2.1.1 The Subgrade approach

The subgrade approach utilizes subgrade models to characterize the soil response. A subgrade model is a mathematical model for the presentation of the soil response involved in soil-structure interaction problems. Specifically, subgrade models provide a relation between contact stresses and interface deformation. The models are designed to provide reasonably accurate estimates of structural responses such as deformation, bending moment, shear force and contact stress (Horvath 2002).

2.1.1.1 Subgrade models

The subgrade models themselves can be further categorized into two classes, mechanical and continuum subgrade models. Mechanical subgrade models utilize mechanical elements such as springs, shear elements, tensioned membranes and flexural elements or combinations of this elements to represent the soil-structure interaction (Kerr 1964; Horvath 2002).

The earliest and most ubiquitous of mechanical subgrade models is the Winkler model (Winkler 1867). The model, also called the Winkler hypothesis, uses a single layer of independent springs to represent the soil. Such a configuration implies a load applied at a point only causes deformation at that point; hence, the model, results in a discontinuous deformation profile (Kerr 1964; Horvath 2002). Mathematically, the Winkler model is a linear equation of the form given by (2.1).

$$p = k_w u \tag{2.1}$$

where k_w is Winkler's coefficient of subgrade reaction, representing the stiffness of the soil to applied force per unit area and having dimension of force per unit length cubed. For applications involving linear structural elements like piles or beams, instead of the coefficient of subgrade reaction, the subgrade modulus, which is the product of coefficient of subgrade reaction and width (or diameter) of the beam or pile is used. To differentiate the geometry of the problem, authors have used the term horizontal coefficient of subgrade reaction to represent the coefficient for the case of laterally loaded piles (Terzaghi 1955). Winkler's coefficient of subgrade reaction is not an inherent soil property and is dependent on the flexibility characteristics of the structural element involved. Furthermore, the coefficient of subgrade reaction is spatially variable and dependent on stress levels (non-linearity) (Horvath 2002; Vesic and Saxena 1970).

The Winkler model by itself does not provide mechanisms for the evaluation of the coefficient of subgrade reaction. This is true of all mechanical subgrade models. Hence, various researchers have attempted to provided estimates for k_w. Terzaghi (1955) proposed a formulation for horizontal coefficient of subgrade reaction in sand based on the theory of

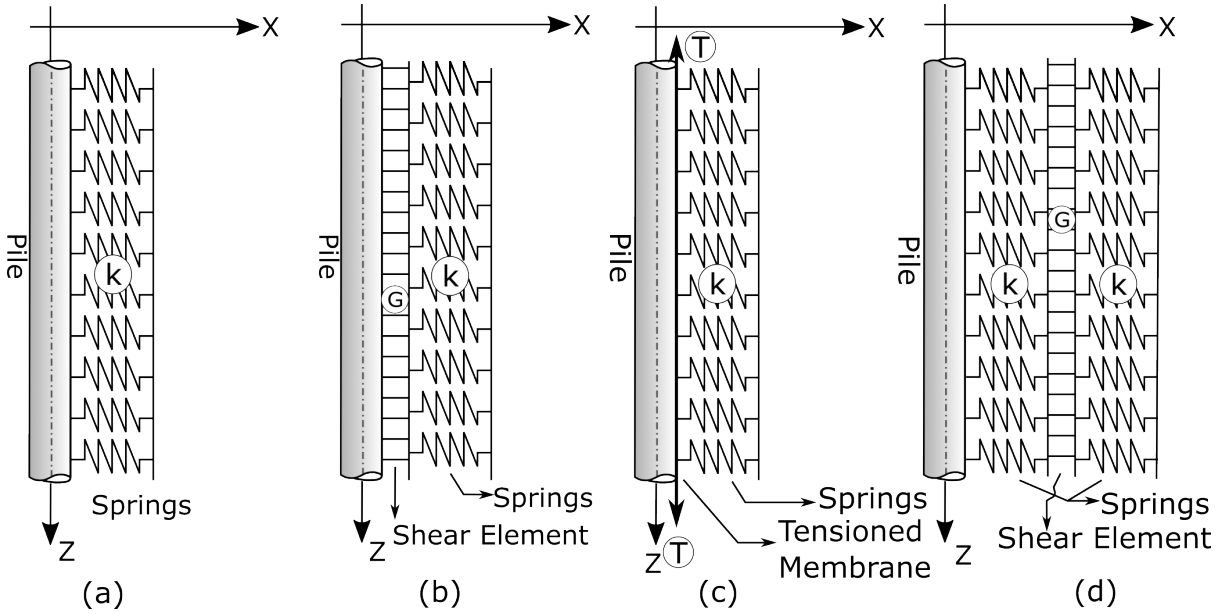

Figure 2.1: Mechanical Subgrade Models; (a) Winkler Model, (b) Pasternak Two-Parameter Model, (c) Filonenko-Borodich Two-Parameter Model, (d) Kerr Three-Parameter Model

elasticity with a linearly varying young's modulus and assuming the deformation is confined to three times the width of the pile. For clays, values based on the undrained shear strength are proposed and in both cases the width of the pile is also included as a parameter. Vesic (1961) developed an expression for the coefficient of subgrade reaction by using the theory of elasticity and equating the maximum moment in a beam obtained from a beam on Winkler foundation analysis with solutions from an elastic analysis (Horvath 1983b). Vesic's expression for k_w is given by (2.2). Equating values of a design parameter from an analysis based on a Winkler model to another method to determine the coefficient of subgrade reaction may result in inaccurate estimate of other design parameters (other than those used to determine the coefficient). For example, Vesic and Saxena (1970) found that for infinite slabs, the coefficient obtained by equating the maximum bending moment from an analysis using the Winkler subgrade to an elastic analysis is 2.4 times larger than the coefficient obtained by equating the maximum displacements using the same analysis.

$$k_w d = 0.65 \left(\frac{E_s d^4}{E_p I_p} \right)^{\frac{1}{12}} \frac{E_s}{1 - \nu_s^2} \tag{2.2}$$

In an attempt to overcome the weaknesses of the Winkler hypothesis, models involving

additional mechanical elements to introduce coupling between the springs were developed. The Pasternak model (Pasternak 1954) involves a shear element introducing interaction among the springs, see Figure 2.1. Mathematically, the Pasternak model has the form given by (2.3) and requires two parameters, Pasternak's coefficient of subgrade reaction, k_p, associated with the springs and a modulus of rigidity, G_p, associated with the shear element.

$$p = k_P u - G_P \nabla^2 u \tag{2.3}$$

Similarly, Filonenko-Borodich (1940) proposed a subgrade model with two mechanical elements; a spring layer characterized by the coefficient of subgrade reaction, k_{fb} and a tensioned membrane characterized by a tension force, T. Mathematically, the model has the form shown by (2.4).

$$p = k_{fb} u - T \nabla^2 u \tag{2.4}$$

An extension of the Pasternak model is proposed by Kerr (1965) that involves two layers of springs, characterized by coefficients of subgrade reaction $k_{kl}$and $k_{ku}$and a shear element with modulus of rigidity, G_k, embedded in between the springs (Figure 2.1). Mathematically, the model has the from given by (2.5)

$$\left(1 + \frac{k_{kl}}{k_{ku}}\right) p - \frac{G_k}{k_{ku}} \nabla^2 p = k_{kl} u - G_k \nabla^2 u \tag{2.5}$$

Models involving additional springs (or shear) elements or involving other structural elements such as beams have also been proposed. For example, Hetényi (1950) proposed a model involving a beam embedded between two beds of springs.

As noted above, mechanical subgrade models by themselves do not provide values for parameters of the elements used nor is there any rational basis for the replacement of soil media with structural elements. Nevertheless, soil inhomogeneity can be accounted for with ease by spatially varying the parameters used for the mechanical elements (Poulos and Davis 1980). In addition, nonlinear behavior can also be taken into consideration with

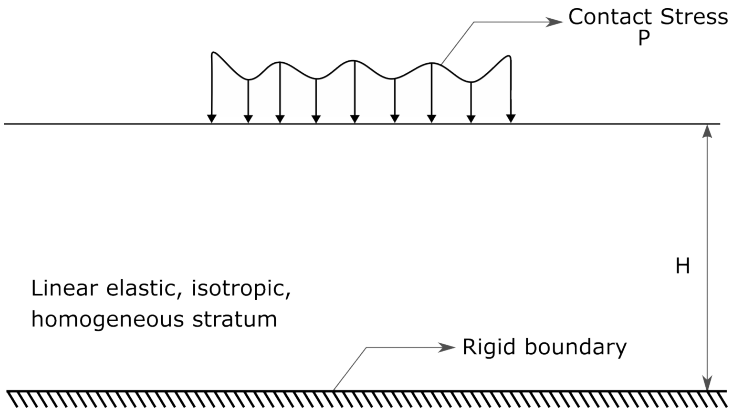

Figure 2.2: Reissner's Problem Definition

ease through an iterative scheme (Reese and Van Impe 2010). Owing to this simplicity and ease of implementation, mechanical models are extensively used in practice; especially, the Winkler model (Horvath 2002).

Continuum subgrade models use continuum mechanics, mostly employing isotropic linear elastic constitutive laws to represent the soil and develop mathematical relations between contact stresses and interface deformation. To arrive at such relations most researchers utilize simplifying assumptions regarding the stresses and displacement within the elastic continuum (Reissner 1958; Vlasov and Leont'ev 1966; Kerr and Rhines 1967; Horvath 1983a; Horvath 1983b; Worku 2010).

Reissner (1958) first proposed a continuum model where the soil was idealized as an elastic layer of thickness H underlain by a rigid base. To develop the model, Reissner made the simplifying assumption $\sigma_x = \sigma_y = \tau_{xy} = 0$. From consideration of equilibrium, this assumption results in the shear stresses, τ_{yz} and τ_{zx}, being independent of depth, significantly simplifying the problem. Reissner's subgrade model is given in Equation (2.6).

$$p - \frac{1}{12}\frac{GH^2}{E_s}\nabla^2 p = \frac{E_s}{H}w_0 - \frac{1}{3}G_s H\nabla^2 w_0 \tag{2.6}$$

Horvath (1983b) formulated a Winkler equivalent subgrade model by neglecting all but the vertical normal stress and strain. Hence, providing a continuum based interpretation for the Winkler hypothesis whereby all shear interaction and lateral stresses are neglected (Horvath 1983a).

Vlasov and Leont'ev (1966) developed a continuum subgrade model by representing the displacement components as a finite series of separable functions, see Equations (2.7) - (2.9), where φ_i, γ_g and ϕ_k are assumed to be known beforehand. The governing equation that relates the external forces (surface traction and body forces) to displacements are then obtained by the use of the principle of virtual work.

$$u(x,y,z) = \sum_{i=1}^{m} u_i(x,y)\varphi_i(z) \text{ for } i = 1,2,3... \tag{2.7}$$

$$v(x,y,z) = \sum_{g=1}^{l} v_g(x,y)\gamma_g(z) \text{ for } g = 1,2,3... \tag{2.8}$$

$$w(x,y,z) = \sum_{k=1}^{n} w_k(x,y)\phi_k(z) \text{ for } k = 1,2,3... \tag{2.9}$$

For the general three dimensional case, such an approach reduces the degree of freedom of the problem from infinite in all three directions to infinite in the lateral directions and finite DOF $(m+l+n)$ in the vertical direction. This results in a set of partial differential equations in $u_i(x,y), v_g(x,\text{y})$ and $w_k(x,\text{y})$ involving integrals of the displacement profile functions (φ_i, γ_g and ϕ_k). Such a formulation offers an advantage, where variations in soil properly and geometry of the problem in the vertical direction can be handled with relative ease.

By making an assumption on the geometry of the problem and neglecting displacements components results in various forms of subgrade models. For example, for a homogeneous soil, by neglecting the lateral displacement and applying a predetermined function to the displacement profile, Vlasov and Leont'ev reduced the set of partial differential equations to that shown in Equation (2.10).

$$p = k_{VL}w_0 - G_{VL}\nabla^2 w_0 \tag{2.10}$$

where k_{VL} and G_{VL} involve elastic parameters and integrals of the assumed displacement profile. It is to be noted that this equation is of the same form as the Pasternak mechanical subgrade model.

Sun (1994) extended Vlasov and Leont'ev's 1966 work for laterally loaded piles in homogeneous and multilayered elastic media. Unlike Vlasov and Leont'ev's formulation, the displacement profile function, $\varphi(r)$, is not assumed in advance. Instead, it is evaluated using the principle of variational calculus from consideration of the soil around the pile and is found to be a function of a parameter designated as γ, which represents the rate of decay of the lateral displacement as one moves away from the pile-soil interface. The parameter in turn is dependent on the pile-soil interface displacement, the primary unknown; therefore, the evaluation of γ involves an iterative process (Sun 1994).

Further extension of this work was done by Guo and Lee (2001), who in addition to using separable displacement functions, employed a simplified stress field instead of those obtained from the separable displacement functions through elastic theory. The formulation also made use of a modified shear modulus, initially proposed by Randolph (1981), to account for the effects of the Poisson's ratio. The use of the simplified stress field is justified by better performance of the subgrade model and the resulting pile response when compared to solutions from numerical continuum methods (Guo and Lee 2001).

The aforementioned approaches based on Vlasov and Leont'ev's 1966 work all result in a subgrade model that has the same mathematical form as the Pasternak's mechanical model. In addition, such an approach results in non zero stress at boundaries where there is no traction. Such discrepancies can be explained by the use of the variational approach, where equilibrium is satisfied in a global manner instead of at every point within the problem domain (Vlasov and Leont'ev 1966; Sun 1994).

Similarly, a Pasternak-type two-parameter continuum model (2.11) was developed by Kerr and Rhines (1967), assuming $\sigma_x = \sigma_y = \tau_{xy} = 0$ and $u = v = 0$. These assumptions are only valid for $\nu = 0$ and when boundary conditions are taken into consideration, lead to a contradiction.

$$p = \frac{E_s}{H} w_0 - \frac{1}{2} G H \nabla^2 w_0 \tag{2.11}$$

In the same work, Kerr and Rhines (1967) presented a formulation using series expansion of a solution function for two dimensional elasticity problems. By retaining different

terms in the expansion, various subgrade model of varying complexity are obtained. For example, retaining the first order term results in an equation similar to the Winkler model and second order approximation results in a Pasternak-like equation, but more interestingly, higher order approximation results in models, whose mechanical equivalents involve multiple elements of springs, shear and flexural elements.

Worku (2010)presented a generalized continuum model (2.16) where relatively minimal simplifying assumptions were made regarding the stress and displacements. To formulate such a model, the lateral normal stress were assumed to be related to the vertical normal stress through a function of the vertical coordinate. Furthermore, the two shear stresses components are assumed to be separable into a function of the vertical coordinate and another function of the lateral coordinates.

$$\sigma_x(x,y,z) = g_x(z)\sigma_z(x,y,z) \tag{2.12}$$

$$\sigma_y(x,y,z) = g_y(z)\sigma_z(x,y,z) \tag{2.13}$$

$$\tau_{yz}(x,y,z) = I_z(z)\bar{\tau}_{yz}(x,y) \tag{2.14}$$

$$\tau_{zx}(x,y,z) = I_z(z)\bar{\tau}_{zx}(x,y) \tag{2.15}$$

$$p - \frac{G}{E}\frac{1}{K_I}\left(L_{gI} - \frac{K_{gI}L_g}{K_g}\right)\nabla^2 p = \frac{E}{K_g}w_0 - \frac{GL_{gI}}{K_gK_I}\nabla^2 w_0 \tag{2.16}$$

where: K_I,L_{gI}, K_{gI}, $L_g$and $K_g$involve integrals of g_x, $g_y$and I_z

This model is a three-parameter model similar to that by Kerr and Rhines (1967) and involving second order derivatives of both the displacement and traction. By making reasonable assumption on the nature of $g_x(z)$, $g_y(z)$ and $I_z(z)$, Worku (2010) was able to develop various forms of the model including a variant that is equivalent to Reissner's model. Furthermore, by neglecting the lateral displacement and the shear stress components (τ_{yz} and τ_{zx}), Pasternak-type two parameter and Winkler-Type one-parameter models, respectively, were developed Worku (2010).

In the aforementioned formulations, the presence of the layer thickness, H, in the de-

nominator of the interface displacement term results in unrealistic estimates of the displacement for deep deposits where H is large. To limit this, Worku (2010) replaced the term in question with χd; where, χ is used as a dimensionless calibration factor and d is the width of structural element. Values for the calibration factor can be determined through comparison with results from numerical or direct measurements (Worku 2010; Worku and Degu 2010; Worku 2013; Worku 2014; Lulseged 2021). This in effect implies a reduction of the stress/strain influence depth to less than H for a thick soil deposit.

While continuum models may present a rational approach to the Soil-Structure Interaction problem, they involve considerable mathematical rigor. Mechanical models on the other hand, while simpler, do not provide means of determining parameters of the mechanical elements used. To best utilize the advantages of both models, the parameters of the mechanical model are determined from the continuum models of similar mathematical order. Such a synthesis of the two approaches is a best-of-both worlds solution where the practicability of the mechanical subgrade models is supplemented by the rigor of the continuum models (Kerr and Rhines 1967; Horvath 2002; Worku 2013; Worku 2014).

Synthesized parameters of the Pasternak foundation from the generalized continuum model of Worku (2010) are presented in Worku (2013) and Worku (2014). In the former, the parameters of the Pasternak foundation are determined from a lower order simplified variant of the generalized continuum model having a mathematical form similar to the two parameter model. In the latter, Pasternak parameters are determined by setting equivalence with the rigorous Worku (2010) model. This is done by incorporating the stiffness contributions of the two spring layers and shear layer of the three-parameter model to the stiffness of the spring of the two-parameter model and equating the shear contributions (Worku 2014). The resulting parameters are given by:

$$K_P = \frac{(0.4\nu_s + 0.67)E_s}{\chi d} \tag{2.17}$$

$$G_P = \frac{(0.68\nu_s + 1.14)}{1+\nu_s} E_s \chi d \tag{2.18}$$

This model, since synthesized with the higher order generalized continuum model of

Worku (2010), was shown to be of superior performance compared to similar models of the same order, when compared with against solutions from the finite element method (Worku 2014).

2.1.1.2 Subgrade models in dynamic analysis

Subgrade models are also used in dynamics analysis. In fact, static analysis may be viewed as a specialized case of dynamic analysis where the excitation frequency is zero. In general, due to complications associated with dynamic soil-structure interaction, dynamic subgrade models are limited to one-parameter Winkler-type models and their formulation involves significant simplifying assumptions (Novak 1974; Dobry et al. 1982; Gazetas and Dobry 1984b; Mylonakis 1995; Karatzia and Mylonakis 2017).

Dynamic subgrade models, in addition to describing load-deformation characteristic of the pile-soil system, must also specify energy dissipation mechanisms. For a pile-soil system, energy is dissipated by hysteretic damping in the pile and soil, termed material damping, and by stress waves propagating away from the pile-soil interface known as radiation (geometric) damping. In a mechanical model, this mechanism is represented by dashpots.

Therefore, a dynamic Winkler subgrade model involves springs and dashpots connected in parallel and uniformly distributed over the pile length. The subgrade coefficient is represented as a complex valued function given by:

$$k_x + i\omega c_x \tag{2.19}$$

where k_x is the dynamic stiffness coefficient, c_x is the dashpot coefficient, ω is the excitation frequency and $i = \sqrt{-1}$. The stiffness coefficient, k_x is commonly expressed as:

$$k_x = \delta E_s \tag{2.20}$$

where δ is a non-dimensional parameter dependent on geometric, load-deformation and

inertial characteristics of the pile-soil system. The damping coefficient is also dependent on geometric, load-deformation and energy dessipation characteristic of the pile-soil system. Both parameters are also dependent on the excitation frequency (Mylonakis 1995; Syngros 2004; Karatzia and Mylonakis 2017). Alike the static case, the dynamic Winkler models do not provide values for the coefficients. Hence, values are obtained from other methods through synthesis (Gazetas 1991; Syngros 2004; Karatzia and Mylonakis 2017).

Novak (1974) proposed a dynamic subgrade model based on a solution for the plane strain problem. The soil is modeled as an equivalent linear viscoelastic material and is divided into discrete infinitesimal layers. Each layer is assumed to be independent of the others and inter-layer shear and normal stresses are neglected. Such an assumption is equivalent to the Winkler hypothesis discussed in the previous section and results in a model of the form given by:

$$p(z,t) = (S_{u1} + iS_{u2}) \times G_s \times u(z,t) \tag{2.21}$$

where S_{ui} for $i = 1$ and 2 is a real valued coefficient dependent on the normalized excitation frequency, a_0, Poisson's ratio and G_s is the shear modulus of the soil. This is a Winkler-type model with a frequency dependent, complex valued coefficient of subgrade reaction.

At low frequencies, the stiffness coefficient from Novak (1974) rapidly vanishes becoming zero at $a_0 = 0$; hence, the model cannot be used for static analysis. In addition, the resulting components of the pile head impedance function are independent of the pile-soil stiffness and slenderness ratio, contrary to what is observed through the use of more rigorous methods developed more recently for both static and dynamic analysis (Mylonakis 2001).

Mylonakis (2001) extended Novak's 1974 model by introducing shear and normal stress interaction between the distinct infinitesimal layers. In the strictest sense, the model is not three-dimensional as the lateral (u and v) and vertical (w) displacements are uncoupled. The solution to the resulting differential equation is solved by the Vlasov and Leont'ev (1966) method discussed in the previous section. It is remembered that this method

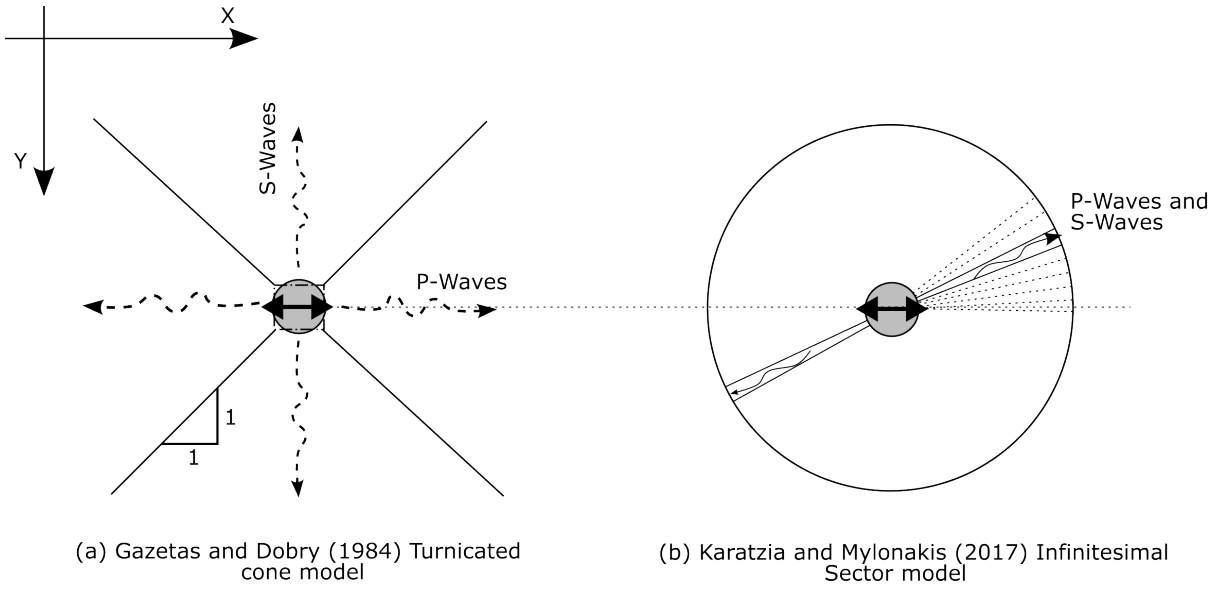

(a) Gazetas and Dobry (1984) Turnicated cone model

(b) Karatzia and Mylonakis (2017) Infinitesimal Sector model

Figure 2.3: Plan diagram of damping models

made use of assumed shape functions that reduced the DOF of the system and involved an energy method where the resulting equations were integrated in a direction perpendicular to the structure-soil interface. This method resulted in two-parameter models (Vlasov and Leont'ev 1966; Sun 1994; Guo and Lee 2001). On the other hand, Mylonakis (2001) integrated the resulting equations in the direction parallel to the interface resulting in a 1-parameter Winkler-type dynamic subgrade model. This approach overcomes the shortcomings of the Novak's 1974 model.

Gazetas and Dobry (1984b) proposed an expression for the radiation damping coefficient based on a two-dimensional formulation similar to that of Novak (1974). Gazetas and Dobry (1984b) assumed that only some fraction of the soil in the horizontal xy-plane would be responsible in energy dissipation through transmission of stress waves. To this end, they replaced a circular pile by a square pile of the same perimeter and divided the surrounding soil into four independent truncated quarter planes with boundaries extending at 45^0 from the edges of the pile. In the two quarters parallel to the direction of displacement extension-compression waves are transmitted while shear waves are transmitted in the quarters perpendicular to the direction of motion, see Figure 2.3. The energy dissipated in the four quarters is summed up and given by the expression (Gazetas and Dobry 1984b):

$$\frac{c_r}{4r\rho_s V_s} = \left\{1 + \left[\frac{3.4}{\pi\left(1-\nu_s\right)}\right]^{\frac{5}{4}}\right\}\left(\frac{\pi}{4}\right)^{\frac{3}{4}} a_0^{-\frac{1}{4}} \tag{2.22}$$

where $V_s = \sqrt{\frac{G_s}{\rho_s}}$ is the shear wave velocity, G_s is the shear modulus of the soil, ρ_s is the mass density of the soil and $a_0 = \frac{\omega r}{V_s}$ is the non-dimensional frequency.

Karatzia and Mylonakis (2017) extended Gazetas's and Dobry's 1984 work by considering a circular pile and subdividing the surrounding soil into infinitesimal sectors. In each sector, the soil is assumed to transmit both shear and extension-compression waves, see Figure 2.3. In addtion, the vertical normal stress, σ_z is assumed to be zero instead of the plane-strain assumption, $\epsilon_z = 0$, used by Gazetas and Dobry (1984b) and Novak (1974). The resulting expression for the radiation damping is given by (2.23) and is applicable over the range of $0 \leq a_0 \leq 1$.

$$\frac{c_r}{d\pi\rho_s V_s} = \left[0.25 + 0.8\left(\frac{2}{1-\nu_s}\right)^{1/2}\right] a_0^{-0.4} \tag{2.23}$$

Gazetas's and Dobry's expression in (2.22) is very similar in form to Karatzia's and Mylonakis's expression with some difference being the result of how the pile was modeled. It should be noted that both expressions, as presented above, are curve fit from complex equations that involve special functions. Equation (2.23) differs from (2.22) by a mean value of 16.9% for $\nu_s = 0.2$ and 24.3% for $\nu_s = 0.4$ with the largest difference occurring as the excitation frequency increases. Part of this difference may be attributed to curve fitting as the curves reported by Karatzia and Mylonakis (2017) using the original expressions show less deviation, at least graphically.

2.1.1.3 Analysis of laterally loaded piles using the subgrade approach

The method of analysis of laterally loaded piles under static loading using the subgrade approach makes use of the classical Euler-Bernoulli beam theory, Equation (2.24). For the case of piles, no external distributed load term exists and the expression only involves the pile-soil interface pressure term, p, which is related to the subgrade model used. The resulting differential equation is then solved for the pile displacement profile, $u(z)$.

Once the displacement profile is found, the remaining pile responses, such as the bending moment and shear force are found as derivatives of the displacement profile using classical mechanics of material formulation for the Euler-Bernoulli beam. Such analysis is termed as beam-on-elastic foundation analysis. Further, to highlight the subgrade model used, terms such as beam-on-winker subgrade (when the Winkler model is employed) may be used (Hetényi 1946; Scott 1981).

$$E_p I_p \frac{d^4 u(z)}{dz^4} + p(z) = 0 \tag{2.24}$$

Gupta and Basu (2018) investigated the applicability of the Euler-Bernoulli beam, Timoshenko beam and rigid beam models for analysis of laterally loaded piles. They found that for solid section piles, the classical Euler-Bernoulli beam theory and Timosheko beam theory gave similar bending moments and soil reaction force for pile length and stiffness used in practice. Further, comparing with finite element analysis, the Timoshenko beam theory gave the closest results in terms of pile head displacement and rotation. For hollow sections, at low relative stiffness values, irrespective of the pile slenderness ratio, pile head displacement obtained using the Euler-Bernoulli beam theory deviate from those obtained using the Timoshenko beam theory (Gupta and Basu 2018).

For dynamic loading, the equation of motion of the vibration of the classical Euler-Bernoulli beam is used (2.25). In this case, the interface pressure term is related to both the load-deformation relationships from subgrade models and equivalent dashpot reaction from the damping models. Primarily, the steady state solution is sought and in most applications the displacement amplitude is computed by reducing the partial differential equation in (2.25) to an ODE by assuming the form of the steady-state displacement time history (Scott 1981; Mylonakis 1995; Karatzia and Mylonakis 2017). Once the the displacement amplitude is obtained the amplitudes of the rest of the pile response are found in a similar fashion to the static case.

$$m \frac{\partial^2 u(z,t)}{\partial t^2} + E_p I_p \frac{\partial^4 u(z,t)}{\partial z^4} + p(z,t) = 0 \tag{2.25}$$

Alternatively, Dobry et al. (1982) proposed a solution method analogous to the finite

element method involving assumed shape functions for the deformed shape of a pile due to a unit head displacement and unit head rotation. The method utilizes the virtual work principle to formulate the pile head stiffness and damping. This approach is especially suited for non-homogenous media where closed-form solutions for the pile response are difficult to obtain. In such cases, the shape function can be approximated from the homogenous solutions (Mylonakis 1995; Karatzia and Mylonakis 2017). The approach has been successfully employed for beam-on-dynamic-Winkler-subgrade analysis involving non-homogenous media by Mylonakis (1995) and Karatzia and Mylonakis (2017).

Recently, Worku and Lulseged (2023b) used Worku's 2014 Kerr-equivalent Pasternak subgrade model with a beam-on-Pasternak subgrade analysis to formulate closed form analytical expressions for the pile response for both finite and infinite length piles embedded in homogenous soils. Even though the model was developed for shallow foundations, by utilizing the calibration factor left open in the model, and properly calibrating it against finite element analysis, reasonably accurate solutions were obtained. Furthermore, Worku and Lulseged (2023a), using the same Kerr-equivalent Pasternak subgrade model and calibration factors from Worku and Lulseged (2023b), investigated the kinematic interaction of a single pile embedded in homogenous medium. The effect of shear interaction, which is explicitly represented in the Worku (2014) model, is also presented.

An extension to the beam-on-elastic foundation analysis is the $p-y$ method, which introduces non-linearity both in the response of the pile and soil (Matlock 1970; O'Neill, Reese, and Cox 1990; Reese and Van Impe 2010). Unlike the subgrade models discussed so far, $p-y$ models involve non-linear relationships between the pile-soil interface contact stress and displacement (Matlock 1970; O'Neill, Reese, and Cox 1990). These relationships are developed empirically and are dependent on local conditions (Basu, Salgado, and Prezzi 2008). Non-dimensional $p-y$ models for varying soil conditions have been proposed by various researchers (Matlock 1970; O'Neill, Reese, and Cox 1990; Reese and Van Impe 2010). These involve a family of curves, where each curve represents a specific depth to account for non-homogeneity. Due to the non-linearity of the subgrade models, analysis involving the $p-y$ method is done in an iterative manner (Reese and Van Impe 2010).

2.1.2 Boundary element method

The boundary element method (BEM) is a form of numerical method based on discretization of the boundary only instead of the entire domain. BEM formulations may follow a direct or indirect approach. The indirect formulation of the boundary element method involves utilizing a singular solution such as that of Mindlin (1936) for point load inside an elastic half-space, which is then distributed using a fictitious distribution function over the surface of the problem domain. In order to be a solution, the sum (integral) of this distribution function over the boundary must satisfy boundary conditions along with compatibility consideration resulting in integral equations. The integral equations can then be solved numerically for the fictitious distribution function which is then used to approximate the actual traction and displacement (Poulos 1971; Butterfield and Banerjee 1971; Banergee and Driscoll 1976; Banerjee 1976).

The boundary element method offers the advantage of reducing the size of the computation as the discretization is limited to the boundary of the domain, making it especially useful for problems with a low surface to volume ratio commonly found in foundation engineering. On the other hand, the resulting matrices are fully populated as compared to the banded matrices common in the finite element method adding to the computational cost (Banergee and Driscoll 1976). Furthermore, the approach requires that there be a formulation for a singular solution (Banerjee and Davies 1978).

Initial use of the boundary element method for laterally loaded piles involved a rectangular strip embedded in homogeneous isotropic elastic media. The strip was divided into segments over which a fictitious lateral traction acted. The flexural displacement of the beam (due to the fictitious lateral traction) in the from of finite difference equation is equated to an algebraic equation for the displacement of the soil obtained by integrating Mindlin's 1936 singular solution along with additional equations from lateral force and moment equilibrium. The solution for the fictitious lateral force then leads to the response of the beam (Poulos 1971; Poulos and Davis 1980). Solutions for the various permutations of end conditions, for example free head floating pile are given in Poulos and Davis (1980) in graphical form, utilizing 21 elements for the pile. The authors admit that the solution provided may be limited by the number of elements used and may result

in non-conservative estimates of the pile head response (Poulos and Davis 1980).

Banerjee and Davies (1978) presented a boundary element approximate solution for axially and laterally loaded piles in a non-homogeneous ideally elastic medium, where the Young's modulus varied linearly with depth. A solution for a point load at the interface of a two layer elastic half-space developed by Davies and Banerjee (1978) was used as the particular solution for the BEM formulation. This work was a continuation of Banergee and Driscoll (1976), where a BEM program for a raked pile group in an ideal elastic homogeneous medium was developed. Comparison of the results of the program for laterally loaded vertical piles with experimental results showed favorable results. Their work showed that soil inhomogeneity and relative stiffness of the pile has significant influence on all measures of the response of the pile and soil reaction. In addition, the slenderness ratio is shown to have negligible effect, for laterally loaded piles (Banerjee and Davies 1978). However, it may be argued that the range of slenderness ratio investigated, $20 \leq \frac{L}{d} \leq 60$, is confined to intermediate and long piles where the influence of slenderness ratio is reduced.

2.1.3 Finite element method

The finite element method (FEM) is a numerical method that involves discretization of the domain of a problem. The method is capable of handling problems with complex geometries, non-linearities and inhomogeneities. Unlike the boundary element method, FEM does not require a singular solution to the problem and results in banded matrices.

Kuhlemeyer (1979) and Randolph (1981) investigated response of laterally loaded piles using the Fourier method, proposed by Wilson (1965), for non-axisymmetric loadings on symmetric bodies. The method involves using the Fourier expansion of the non-axissymetric load and employing the orthogonality property to reduce the three-dimensional problem into n two-dimensional uncoupled problems, where n is the number of terms in the series. The finite element method is then used to solve for the displacement amplitudes associated with each term in Fourier expansion of the non-axissymetric load. Finally, each displacement amplitude is superimposed to obtain the solution.

Randolph (1981), using the aforementioned method with triangular elements and a linear

interpolation scheme, developed expressions for the pile head responses of free head, floating, long flexible piles embedded in homogenous and linearly increasing elastic modulus soil by fitting the expressions to the finite element solution. Furthermore, the critical slenderness ratio (or equivalently the active pile length) were also proposed from observations of the pile head displacement with respect to the pile length . The effect of Poisson's ratio was taken into account by using a modified shear modulus $G_s^* = G_s\left(1 + \frac{3}{4}\nu_s\right)$. The equation developed for the critical slenderness ratio of the pile is given by:

$$\left(\frac{L}{r}\right)_{cr} = 2\psi^{-\frac{2}{9}}\left(\frac{E_P}{mr}\right)^{\frac{2}{9}} \tag{2.26}$$

where $\psi = \frac{1+0.75\nu_s}{2(1+\nu_s)}$

The critical slenderness ratio, or equivalently, the active pile length, delineates long flexible piles from the rest. As the pile length increases, the pile response becomes less dependent on the pile length and pile base conditions (Basu and Higgins 2011; Higgins et al. 2013). For a given piles soil system, if the slenderness ratio is larger than the critical value, the pile behaves as a long flexible pile. The critical slenderness ratio is correlated to the relative stiffness as shown in (2.27).

Similarly, Basu and Higgins (2011) and Higgins et al. (2013) employed the Fourier method to study the response of free and fixed head piles in homogenous, double layered and linearly increasing elastic modulus soil. The study involved an extensive range of slenderness ratio and pile-soil relative stiffness to include short rigid, transitional and long flexible piles. For soils with linearly increasing modulus, at relative stiffness values of $\frac{E_p}{mr} > 10^5$, pile head response becomes independent of the relative stiffness irrespective of slenderness ratio. On the other hand, for the case of $\frac{L}{r}$ >80 the pile head response becomes independent of the slenderness ratio irrespective of relative stiffness. From these observations Basu and Higgins (2011) and Higgins et al. (2013) developed expressions for the boundaries of short rigid piles (critical stiffness ratio), long flexible piles (critical slenderness ratio), pile head responses and maximum pile head moment (fixed head piles) for both short and long piles. The expressions for the critical stiffness ratio is given by:

$$\left(\frac{E_P}{mr}\right)_{cr} = 119\psi\left(\frac{L}{r}\right)^{3.45} \tag{2.27}$$

The critical relative stiffness, demarcates short rigid piles from the rest. For a given pile-soil system, if the relative stiffness is larger than the critical value, the pile behaves as a short rigid pile. As the relative stiffness increases the pile response becomes less dependent on it (Basu and Higgins 2011; Higgins et al. 2013). The critical relative stiffness is correlated to the slenderness ratio of the pile as shown in (2.27).

Note that Basu and Higgins (2011) and Higgins et al. (2013) utilized Randolph's 1981 active pile length expression given in (2.26). In addtion, the critical slenderness ratio and critical relative stiffness expressions (2.26) and (2.27) were found to be both applicable to free and fixed head piles.

Expressions for the pile head responses for short rigid $\left(\frac{E_p}{mr} > \left(\frac{E_P}{mr}\right)_{cr}\right)$ free head piles embedded in soil with linearly increasing modulus are given by (Basu and Higgins 2011; Higgins et al. 2013):

$$u_0 = 0.37\frac{H_0}{mr^2}\psi^{-1}\left(\frac{L}{r}\right)^{-1.14} + 0.29\frac{M_0}{mr^3}\psi^{-1}\left(\frac{L}{r}\right)^{-1.99} \tag{2.28}$$

$$\theta_0 = 0.29\frac{H_0}{mr^3}\psi^{-1}\left(\frac{L}{r}\right)^{-1.99} + 0.33\frac{M_0}{mr^4}\psi^{-1}\left(\frac{L}{r}\right)^{-2.93} \tag{2.29}$$

and for long flexible piles $\left(\frac{L}{r} > \left(\frac{L}{r}\right)_{cr}\right)$:

$$u_0 = 0.55\frac{H_0}{mr^2}\psi^{-0.67}\left(\frac{E_p}{mr}\right)^{-0.33} + 0.53\frac{M_0}{mr^3}\psi^{-0.46}\left(\frac{E_p}{mr}\right)^{-0.54} \tag{2.30}$$

$$\theta_0 = 0.50\frac{H_0}{mr^3}\psi^{-0.46}\left(\frac{E_p}{mr}\right)^{-0.54} + 1.23\frac{M_0}{mr^4}\psi^{-0.22}\left(\frac{E_p}{mr}\right)^{-0.78} \tag{2.31}$$

Similarly, for short rigid $\left(\frac{E_p}{mr} > \left(\frac{E_P}{mr}\right)_{cr}\right)$ fixed head piles, the pile head responses are given by:

$$u_0 = 0.14\frac{H_0}{mr^2}\psi^{-1}\left(\frac{L}{r}\right)^{-1.50} \tag{2.32}$$

and

$$u_0 = 0.31\frac{H_0}{mr^2}\psi^{-0.65}\left(\frac{E_p}{mr}\right)^{-0.35} \tag{2.33}$$

for long flexible $\left(\frac{L}{r} > \left(\frac{L}{r}\right)_{cr}\right)$ fixed-head piles.

where H_0 and M_0 are the pile head resultant forces and moment, respectively; while u_0 and θ_0 represent the pile head transition and rotation.

For two-layered soils, Higgins et al. (2013), proposed an approach based on a limited study of the effects of relative layer thickness and relative stiffness of the two soil layers. They observed that for a given pile-soil stiffness ratio (with respect to stiffness of the top layer) and relative thickness of the layers, as the stiffness of the bottom layer increased the pile head displacement reduced. Further, for a weaker bottom layer, as the relative thickness of the top layer is reduced then the pile head displacement increases and vice versa. Based on this observations, expressions for pile head displacement due to a pile head traction are developed. The approach is at best approximate and only applicable to free head piles under lateral loading only Higgins et al. (2013).

Gazetas (1991) using the finite element method for laterally loaded piles under dynamic loading also presented expressions for static and dynamic pile head stiffness and active length for free head piles in homogenous, linearly increasing modulus and parbolically varying profile soils. The static pile head stiffness of free head piles embedded in soils with a linearly increasing modulus are given by:

$$\frac{K_{HH}}{md^2} = 0.6\left(\frac{E_p}{md}\right)^{0.35} \tag{2.34}$$

$$\frac{K_{HM}}{md^2} = 0.17\left(\frac{E_p}{md}\right)^{0.6} = \frac{K_{MH}}{md^3} \tag{2.35}$$

$$\frac{K_{MM}}{md^4} = 0.15\left(\frac{E_p}{md}\right)^{0.8} \tag{2.36}$$

and for a free-head pile embedded in soil with a parabolically varying profile:

$$\frac{K_{HH}}{md^2} = 0.8\left(\frac{E_p}{md}\right)^{0.28} \tag{2.37}$$

$$\frac{K_{HM}}{md^2} = 0.24\left(\frac{E_p}{md}\right)^{0.53} = \frac{K_{MH}}{md^3} \tag{2.38}$$

$$\frac{K_{MM}}{md^4} = 0.15\left(\frac{E_p}{md}\right)^{0.77} \tag{2.39}$$

Gazetas (1991) also provided expressions for the active length of the pile for the soil profiles investigated. The active length was defined as the pile length below which the pile displacement was less than $\frac{1}{1000}$th of the pile head displacement and for $\nu_s = 0.4$ (Syngros 2004). The expression for the active length of a free head pile embedded in soils with linearly increasing modulus are given by:

$$\left(\frac{L}{d}\right)_{cr} = 2\left(\frac{E_P}{md}\right)^{0.20} \tag{2.40}$$

and for soils with parabolic increase in modulus:

$$\left(\frac{L}{d}\right)_{cr} = 2\left(\frac{E_P}{md}\right)^{0.22} \tag{2.41}$$

In addtion, Gazetas (1991) also provided expressions for pile head damping and dynamic pile head stiffness. The dynamic pile head stiffness were found to be similar to the static ones. Expressions for the pile head damping involved a constant coefficient to the material

Table 2.1: Material damping weight factor proposed by Gazetas (1991) for free-head long flexible piles

Soil profile	w^s_{HH}	w^s_{HM}	w^s_{MM}
Homogenous	0.80	0.80	0.35
Linearly increasing	0.60	0.30	0.20
Parabolically increasing	0.70	0.60	0.22

damping parameter and a term dependent on normalized frequency and relative pile soil stiffness associated with the radiation damping. The expressions have the general form given by:

$$\beta_{ij} = w^s_{ij}\beta_s + \beta^r_{ij}(a_{0d}, {}^{E_p}/_{E_{sd}}) \tag{2.42}$$

where w^s_{ij} is a constant weighing factor and $\beta^r_{ij}(a_{0d}, {}^{E_p}/_{E_{sd}})$ is the radiation damping ratio. The values for w^s_{ij} are given in Table 2.1.

The expressions for the radiation damping ratio, β^r_{ij}, proposed by Gazetas (1991) are given by:

$$\beta^r_{HH} = \frac{1.10}{2\pi} a_0 \left(\frac{E_p}{E_s}\right)^{0.17} \tag{2.43}$$

$$\beta^r_{HM} = \frac{0.85}{2\pi} a_0 \left(\frac{E_p}{E_s}\right)^{0.18} \tag{2.44}$$

$$\beta^r_{MM} = \frac{0.35}{2\pi} a_0 \left(\frac{E_p}{E_s}\right)^{0.20} \tag{2.45}$$

for piles embedded in homogenous soil,

$$\beta^r_{HH} = \frac{1.80}{2\pi} a_{0d} \tag{2.46}$$

$$\beta^r_{HM} = \frac{1}{2\pi} a_{0d} \tag{2.47}$$

$$\beta^r_{MM} = \frac{0.40}{2\pi} a_{0d} \tag{2.48}$$

for piles embedded in soil with linearly increasing elastic modulus and,

$$\beta^r_{HH} = \frac{1.20}{2\pi} a_{0d} \left(\frac{E_p}{E_{sd}} \right)^{0.08} \tag{2.49}$$

$$\beta^r_{HM} = \frac{0.70}{2\pi} a_{0d} \left(\frac{E_p}{E_s} \right)^{0.05} \tag{2.50}$$

$$\beta^r_{MM} = \frac{0.35}{2\pi} a_{0d} \left(\frac{E_p}{E_s} \right)^{0.10} \tag{2.51}$$

for piles embedded in soil with parabolically increasing elastic modulus.

Syngros (2004) developed a program called K-PAX employing the Fourier method for non-axissymetric loads in axissymetric solids. Using the program, Syngros studied the static and dynamic response of laterally loaded floating piles (mostly long piles) embedded in homogenous and linearly increasing modulus soil. In terms of the static analysis, pile head responses in the form of pile head stiffness coefficients were provided through curve fitting with the results from K-PAX. For free head piles in soils with linearly increasing modulus:

$$\frac{K_{HH}}{md^2} = 0.28 \left(\frac{E_p}{md} \right)^{0.35} \tag{2.52}$$

$$\frac{K_{HM}}{md^2} = 0.17 \left(\frac{E_p}{md} \right)^{0.6} = \frac{K_{MH}}{md^3} \tag{2.53}$$

$$\frac{K_{MM}}{md^4} = 0.13 \left(\frac{E_p}{md} \right)^{0.8} \tag{2.54}$$

and for fixed head piles:

$$\frac{K_{HH}}{md^2} = 0.64 \left(\frac{E_p}{md} \right)^{0.35} \tag{2.55}$$

In addtion, Syngros (2004) also provided expressions for the active length (critical slenderness ratio) of piles embedded in soil of homogenous and linearly increasing modulus

Table 2.2: Material damping weight factor proposed by Syngros (2004) for free-head and fixed-head long flexible piles

Soil profile	Pile head condition	w^s_{HH}	w^s_{HM}	w^s_{MM}
Homogenous	Free-head	0.80	0.60	0.40
	Fixed-head	0.80	–	–
Linearly increasing	Free-head	0.70	0.55	0.80
	Fixed-head	0.70	–	–

using a definition similar to that used by Gazetas (1991). Expressions for the critical slenderness of free head piles embedded in soil with linearly increasing modulus are given as:

$$\left(\frac{L}{d}\right)_{cr} = 2.0\left(\frac{E_p}{md}\right)^{2.0} \tag{2.56}$$

and for fixed head piles:

$$\left(\frac{L}{d}\right)_{cr} = 2.5\left(\frac{E_p}{md}\right)^{2.0} \tag{2.57}$$

Similar to Gazetas (1991), Syngros reported dynamic pile head stiffness that are identical to the static ones. Syngros (2004) also provided expressions for the pile head damping ratio in a form similar to Equation (2.42). Values for the material damping weight factor proposed by Syngros are given in Table

The expressions for the radiation damping ratio, β^r_{ij}, proposed by Syngros (2004) are given by:

$$\beta^r_{HH} = 0.19a_0\left(\frac{E_p}{E_s}\right)^{0.18} \tag{2.58}$$

$$\beta^r_{HM} = 0.3\left[a_0 + 0.03\left(\frac{E_p}{E_s}\right)^{0.27}\right] \tag{2.59}$$

$$\beta^r_{MM} = 0.1a_{0d}\left[a_0 + 0.013\left(\frac{E_p}{E_s}\right)^{0.4}\right] \tag{2.60}$$

for free-head piles embedded in homogenous soil,

$$\beta_{HH}^{r} = 0.17 \left[a_0 \left(\frac{E_p}{E_s} \right)^{0.15} - 0.7 \left(\frac{E_p}{E_s} \right)^{-0.7} \right] \tag{2.61}$$

for fixed-head piles embedded in homogenous soil,

$$\beta_{HH}^{r} = 0.3 a_{0d} \tag{2.62}$$

$$\beta_{HM}^{r} = 0.12 \left[a_{0d} + 0.52 \left(\frac{E_p}{E_{sd}} \right)^{-0.04} \right] \tag{2.63}$$

$$\beta_{MM}^{r} = 0.055 a_{0d} \left(\frac{E_p}{E_{sd}} \right)^{-0.02} \tag{2.64}$$

for free-head piles embedded in soil with linearly increasing elastic modulus,

$$\beta_{HH}^{r} = 0.7 \left(\frac{E_p}{E_{sd}} \right)^{-0.07} a_{0d}^{2.7(E_p/E_{sd})^{-0.15}} \tag{2.65}$$

Evidently, the critical slenderness ratio of fixed head piles is 25% more than that of free head piles which contradicts the findings of Higgins et al. (2013) and Basu and Higgins (2011). Furthermore, comparing Equations (2.56) and (2.40), it is observed that both are identical. In regards to the pile head stiffness components, it is noted that all the exponents are identical for corresponding stiffness components. The coefficients are also similar with the exception of the swaying stiffness components where Syngros's solution is 53% smaller than Gazetas's. In terms of energy dissipation, it is noted that the damping ratio provided by Syngros is generally larger than Gazetas. Both sets of expressions for radiation damping (2.43 - 2.51 and 2.58 - 2.65) are applicable to excitation frequencies above the cut-off frequency. A cut-off frequency is the excitation frequency below which the there exists no radiation damping (Syngros 2004). For an elastic half-space the cut-off frequency is zero (i.e. radiation damping is initiated at very small frequencies), on the

other hand in a bounded medium, such as that involved in FEM modeling, the cut-off frequency is larger than zero (Syngros 2004).

2.2 Representation of soil non-homogeneity

Soils are inherently heterogeneous materials as a result of processes associated with their formation, transportation, deposition and insitu mechanical phenomena such as increase in vertical stresses with depth, aging, cementation and more. The depth-wise variation in soil property has received much attention, and various investigators have put forward means of representation of such variations (Randolph 1981; Gazetas 1991; Syngros 2004; Basu, Salgado, and Prezzi 2008; Higgins et al. 2013; Karatzia and Mylonakis 2017). In applications involving laterally loaded piles, soil non-homogeneity is represented by a spatially variable elastic modulus or an equivalent shear modulus. Although there exists some evidence regarding the variation of Poisson's ratio with depth (Fulan 1981), the Poisson's ratio is assumed to be constant in most works with the exception of multi-layered soils (Basu, Salgado, and Prezzi 2008).

The most common form of representation of soil non-homogeneity is the linear depth-wise variation commonly associated with Gibson (1967), who initially studied the response of shallow foundations resting on soil modeled as an elastic half space with this form of non-homogeneity. see Equation (2.66). A special kind of the linear depth-wise variation, where the surface stiffness is zero and the Poisson's ratio is set to 0.5 is called Gibson soil (Selvadurai 2007). Interestingly, for foundations resting on Gibson soil, rigorous continuum based formulation for the surface displacement results in a Winkler-like discontinuous displacement profile (Gibson 1967). The Gibson form is best suited for representation of granular soils where the soil stiffness increases with depth (Poulos and Davis 1980).

$$G_s(z) = G_{s0} + mz \tag{2.66}$$

where G_{s0} is the surface shear modulus and m is the rate of increase of the shear modulus

Another depth-wise variation that is commonly studied is the power function, given in Equation (2.67).

$$E_s(z) = E_{sd}\left[\eta + (1-\eta)^{z}/_{d}\right]^n \tag{2.67}$$

where E_{sd} is the elastic modulus at $z = d$, $\eta = {}^{E_{s0}}/_{E_{sd}}$, E_{s0} is the elastic modulus at the ground surface ($z = 0$) and n is a parameter that controls the form of the variation. By varying the parameters η and n various forms of soil non-homogeneity may be represented. For example, Davisson and Prakash (1963) studying pole foundations recommended $\eta = 0$ and $n = 0.15$ with the aim of representing the reduction in stiffness at the soil surface associated with non-linear response. Gazetas (1991) used $\eta = 0$ with $n = 1$, linear profile, and $n = 0.5$, parabolic profile, to study dynamic response of piles in non-homogenous soil. Poulos and Davis (1980) also note that the most common assumption for clays is $\eta = 0$ and $n = 0$ which is equivalent to a homogenous profile.

The aforementioned depth-wise variation forms are unbounded, in that the elastic modulus increases indefinitely with depth. Selvadurai, Singh, and Vrbik (1986) used a bounded exponential form to investigate the Reissner-Sagoci problem which involves the torsional rotation of a rigid circular disc perfectly bonded to to surface of an elastic half-space. The specific form they used decreases with depth asymptotically approaching a constant value. Similarly, Vrettos (1998) investigated the Boussinesq problem involving an elastic medium where the shear modulus increases exponentially to a bounding value. The expression used by Vrettos is given by:

$$G_s(z) = G_{s0} + (G_{s\infty} - G_{s0})(1 - e^{-\alpha z}) \tag{2.68}$$

Vrettos's 1998 bounded exponential form has also been used by Karatzia and Mylonakis (2017) for the analysis of laterally loaded piles in inertial interaction.

Multi-layering, another common form of soil non-homogeneity is also extensively studied in regards to laterally loaded piles (Basu, Salgado, and Prezzi 2008; Gazetas and Dobry 1984a; Karatzia and Mylonakis 2017; Higgins et al. 2013). Multi-laying simply involves distinct layers with differing properties. It should be noted that layering inherently results

in transverse isotropy in addtion to non-homogeneity and depending on the scale of the problem may be interpreted as either (Selvadurai 2007).

Non-homogeneity is not confined to depth-wise variations only, there exist lateral variation; especially, for pile foundations where radial stresses may introduce artificial variability. To this end, radial variations of the form given by Equation (2.69) have been implemented by Syngros (2004) to study static and dynamic pile responses in such cases.

$$E_s(r) = E_{sr\infty}\left[1 - \left(\frac{Ad}{2r}\right)^{3/4}\right] \tag{2.69}$$

where A is a parameter defining the rate of decay of soil stiffness as one moves closer to the pile-soil interface and $E_{sr\infty}$ is the soil elastic modulus at very large radial distance from the pile-soil interface.

Chapter 3

Methods of Study

To achieve the stated goals, namely, to investigate the static and dynamic inertial response of a pile in a Kerr-equivalent Pasternak subgrade, one first has to calibrate the subgrade model. Calibration entails evaluation of the calibration factor by setting equivalences of a selected response type of the pile obtained by using the subgrade model in question and another relevant method. The other method could be the finite element method, the boundary element method, other analytical approaches or measured data.

For this work, the finite element method is used to calibrate the subgrade model. To this end, finite element analysis is first used to determine pile response in two types of inhomogeneities and four different pile end conditions. The responses are then compared against corresponding solutions from static beam-on-elastic-foundation analysis using Kerr-equivalent Pasternak subgrade to determine the calibration factor. Once the calibration factor is determined, the beam-on-elastic-foundation analysis is again used to evaluate the static pile responses. On the other hand, the dynamic pile head responses are approximated by using assumed shape functions obtained from the solution for homogeneous soil profile. An energy method is then used to compute the pile head impedance functions while still employing the calibration factors obtained from the static analysis. This chapter presents a discussion on the method used.

3.1 Selection of forms of soil non-homogeneity

The specific formulation for the variation of modulus of elasticity is given by (3.1). This expression is the power function form discussed in Section 2.2, with the surface stiffness, E_{s0}, dropped.

This specific power function form is chosen because of the following reasons:

- The power function form can incorporate various forms of non-homogeneity by varying the parameter n.
- For most pile lengths in application, a significant portion of the displacement is confined to shallow depths Poulos and Davis (1980) and Gazetas (1991). Such large displacements result in non-linear response both associated with non-linear material constitutive behavior and contact non-linearity associated with the separation of the soil from the pile . These non-linearites would undoubtedly result in reduction in stiffness at shallow depths. Hence, surface stiffness, E_{s0}, is dropped from the expression.
- Mathematically, it is one of the simplest forms, easing the amount of computation. Further, it has been used extensively (Randolph 1981; Gazetas 1991; Syngros 2004; Higgins et al. 2013), possibly due to its simplicity. In addtion, from a practical standpoint, validation of results can be readily done against published results that used this form.

$$E_s(z) = mr\left(\frac{z}{r}\right)^n \tag{3.1}$$

In Equation (3.1), mr is a reference modulus of elasticity at $z = r$ (i.e. E_{sr}) and n is a parameter that defines the specific pattern of variation of the modulus of elasticity with depth. Two specific values for n are studied, namely, linearly increasing elastic modulus ($n = 1$) and parabolically increasing elastic modulus ($n = 0.5$), see Figure 3.1. Note that mr is generally treated as a single parameter, E_{sr}, but for the case of $n = 1$, the parameter m represents the rate of increase (slope) of the soil modulus.

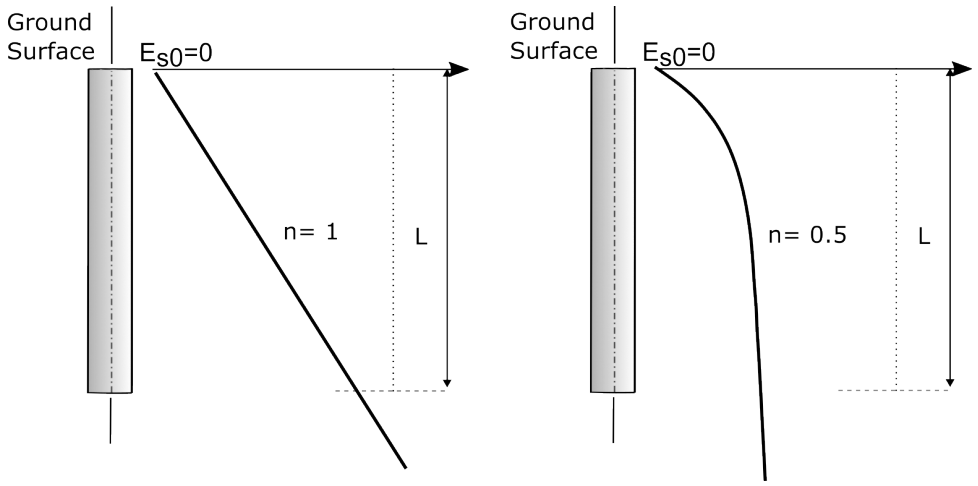

Figure 3.1: Profile of soil modulus

3.2 Selection of a distributed dashpot model for radiation damping

As noted in section 2.1.1.2 and 2.1.3, in dynamic analysis of piles, energy dissipation is represented by evenly distributed dashpot elements. Two relevant models for the damping characteristics of the dashpots have been discussed in section 2.1.3, Gazetas's truncated cone model (Gazetas 1984) and Syngros's infinite sector model (Syngros 2004). From these two models, Syngros's infinite sector model is chosen for this work. This is done because the infinite sector model is a relatively recent extension of the former where each infinite sector is capable of transmitting p and s-waves instead of only in predefined zones as employed by the former (Gazetas and Dobry 1984b; Karatzia and Mylonakis 2017). See section 2.1.3. The Karatzia and Mylonakis (2017) infinite sector model is given by:

$$\frac{c_r}{d\pi\rho_s V_s} = \left[0.25 + 0.8\left(\frac{2}{1-\nu_s}\right)^{1/2}\right] a_0^{-0.4} \tag{3.2}$$

where ρ_s is the density of the soil, V_s is the shear wave velocity $\left(V_s = \sqrt{\frac{G_s}{\rho_s}}\right)$, a_0 is the normalized frequency $\left(a_0 = \frac{\omega d}{V_s}\right)$ and ω is the excitation frequency. Equation (3.2) is applicable over the range $0 \leq a_0 \leq 1$.

The distributed dashpots incorporate both the radiation damping (whose model is selected above) and material damping components. The material damping components are

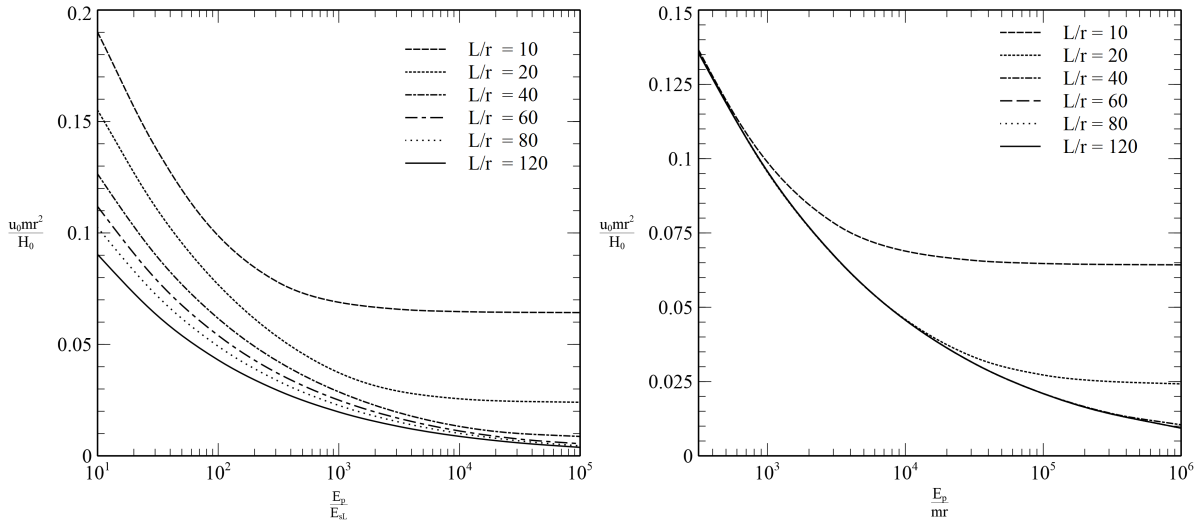

Figure 3.2: Normalized pile head displacement using different measures of relative pile stiffness

constant values. see section 3.3 for parameter values of the material damping ratio for the soil and pile.

3.3 Analysis parameters

Numerical values of parameters for the finite element method and subsequent analysis are selected based on real world values. For the soil domain, the parameters under consideration are the modulus of elasticity, $E_s(z)$, and Poisson's ratio, ν_s. While for the pile, the pile radius, r, slenderness ratio, $\frac{L}{r}$ or $\frac{L}{d}$, modulus of elasticity, E_p, and Poisson's ratio, ν_p, are considered.

Furthermore, a measure of the relative stiffness of pile to soil is also included. Multiple researchers have employed different measures of relative stiffness. Banerjee and Davies (1978) used $K_R = \frac{E_p I_p}{E_{sL} L^4}$, where E_{sL} is the modulus of elasticity of the soil at the pile base. More recently Higgins et al. (2013) used $\frac{E_p}{m^* r}$, where $m^* = \frac{dG_s^*}{dz} = \frac{d}{dz}\left[G_s\left(1 + 0.75\nu_s\right)\right]$ and for homogenous soils $\frac{E_p}{E_s}$ has been implemented by Lulseged (2021). In the current work, K_R, $\frac{E_p}{E_{sL}}$ and $\frac{E_p}{mr}$ where $m = \frac{dE_s(z)}{dz}$ have been investigated as alternative options. Plots of the normalized pile head displacement versus $\frac{E_p}{E_{sL}}$ and $\frac{E_p}{mr}$ are shown in Figure 3.2.

Evidently, the normalized pile-head response is independent of the slenderness ratio when

employing $\frac{E_p}{mr}$ for values of $\frac{L}{r} > 60$ $\left(\frac{L}{d} > 30\right)$ and within the range of $\frac{E_p}{mr}$ investigated. This is inline with published responses of long piles(Randolph 1981; Higgins et al. 2013). On the contrary, when $\frac{E_p}{E_{sL}}$ is used pile-head response is dependent on slenderness ratio across the full range of parameters investigated. This may be attributed to the fact that $\frac{E_p}{E_{sL}}$ implicitly incorporates the effect of the pile length in the denominator. This argument can also be extended to the use of K_R where the pile length is explicitly involved in the formulation $\left(K_R = \frac{E_p I_p}{E_{sL} L^4}\right)$ (Randolph 1981).

The use of a modified shear modulus was also investigated as alternative to directly incorporating the effect of the Poisson's ratio. The approach, proposed by Randolph (1981), involves a modified shear modulus $G_s^* = (1 + 0.75\nu_s)G_s$. This approach cannot be implemented for the formulation of the calibration factor; primarily, since expressions for the subgrade parameters $k_p$and $G_p$directly incorporate the Poisson's ratio. Hence, an unmodified relative stiffness factor $\frac{E_p}{mr}$ is used, where the slope m represents the rate of increase of the elastic modulus for linearly increasing modulus profile. Although, for parabolicaly increasing modulus, the parameter m is less meaningful. A more apt interpretation is to consider mr as a single parameter representing the elastic modulus at the reference depth of $z = r$; therefore, $mr = E_s(r)$. It is this interpretation that is used through out this work. Following a similar work by Higgins et al. (2013) the values for the relative stiffness, $\frac{E_p}{mr}$, are set to$10^{2.5} - 10^6$, these values are equivalent to approximately $2MPa - 3GPa$ of soil elastic modulus at the pile base depending up on the pile length and material. This range encompasses typical values of modulus of elasticity of soil recommended in literature (Kulhawy and Mayne 1990; Bowles 1997).

Since $\frac{E_p}{mr}$ is used as a relative stiffness parameter, it is convenient to define the slenderness ratio as $\frac{L}{r}$ $\left(= 2\frac{L}{d}\right)$. The range of pile slenderness ratio investigated is $\frac{L}{r} = 5 - 120$. The specific values used are $5, 10, 20, 40, 60, 80, 120$ with the additional values of $12.5, 15, 17.5$ employed when more data is found necessary. This values are based on those used in the works of Higgins et al. (2013) and Lulseged (2021)

Values for the modulus of elasticity of the pile material are taken by considering Timber, Concrete and Steel. For concrete piles, $E_p = 30GPa$ is considered representative. This value is obtained by averaging the typical values proposed by ACI (2019), AASHTO (2007) and ES EN 1992-1-1:2015 (2015) for normal weight standard strength concrete

(i.e C20/25 to C50/60). The Poisson's ratio is taken to be 0.2 (AASHTO 2007; ES EN 1992-1-1:2015 2015). For timber piles $E_p = 10GPa$ and $\nu_s = 0.4$ are considered. Admittedly, timber is an orthotropic material; hence, it requires 9 independent elastic parameters, but for convenience an average modulus of elasticity obtained from bending tests is used (Forest Products Laboratory 1999; BSI 2016). For the Poisson's ratio, primarily considering flexural response, an average value associated with stress in the longitudinal direction and deformation in the radial direction is used (Collin 2002). For steel $E_p = 210GPa$ and $\nu_s = 0.2$, this values are based on ES EN 1993-1-1:2015 (2015) and AASHTO (2007).

The Poisson's ratio for the soil is assumed to be constant with depth. Numerical values for the Poisson's ratio are taken from Kulhawy and Mayne (1990) and Bowles (1997). Based on the values recommended, the range of Poisson's ratio used is $\nu_s = 0.20 - 0.50$.

The material damping ratio for the soil is taken to be $\beta^s = 0.5$ and an identical value is considered for the pile ($\beta^p = 0.5$) (Gazetas 1991; AASHTO 2007). A summary of all parameter values proposed is given in Table 3.1.

Table 3.1: Summary of parameter values for finite element analysis

	Domain	Parameter	Symbol	Unit	Value
1	Pile	Modulus of Elasticity (Concrete)	E_p	GPa	30
2		Modulus of Elasticity (Steel)			210
3		Modulus of Elasticity (Timber)			10
4		Poisson's Ratio (concrete)	ν_p	–	0.2
5		Poisson's Ratio (Steel)			0.3
6		Poisson's Ratio (Timber)			0.4
7		Slenderness Ratio	$\frac{L}{r}$	–	$5 - 120$
8		Material Damping Ratio	β^p	–	0.5
9	Soil	Relative Stiffness	$\frac{E_p}{mr}$	–	$10^{2.5} - 10^6$
10		Poisson's Ratio	ν_s	–	$0.20 - 0.50$
11		Non-homogeneity Parameter	n	–	$n = 1$ and $n = 0.5$
12		Material Damping Ratio	β^s	–	0.5

3.4 Finite element modeling

The Finite element analysis is conducted using ABAQUS (2022) software suite. ABAQUS is a general finite element analysis program with an extensive material and element library and support for both implicit and explicit integration schemes for time dependent problems through the Abaqus/Standard and Abaqus/Explicit solver modules, respectively. Preprocessing and postprocessing is accomplished through the Abaqus/CAE module. Additional material models, elements and fields can be added through user subroutines using the FORTRAN programming language. Further extension and automation of ABAQUS's capabilities can be done by scripts written in the Python programming language (ABAQUS 2022).

Compering with other finite element software, especially those purpose built for analysis in geotechnical engineering, notably PLAXIS 3D (2020), ABAQUS (2022) provides better support for modeling non-homogeneity. PLAXIS 3D only provides support for modeling homogeneous, layered and linearly varying soil profiles. Modeling other forms of soil non-homogeneity is accomplished by dividing the soil into layers, which in effect is a step interpolation method. On the other hand, in ABAQUS (2022) one can set the material properties to vary with predefined fields and set this fields to vary in any direction. This is further simplified for temperature independent stress/displacement analysis as the inbuilt temperature field can be used.

The specific ABAQUS version used in this work is ABAQUS 2022. The program is run on a system with a six core Intel Core i7-9750H processor and 8 GB of RAM.

3.4.1 Domain geometry

Since the problem involves an axisymetric domain geometry with a non-axisymetric load, three-dimensional analysis is conducted. The domain is cylindrical in shape with a cylindrical pile at its center. The problem is symmetric about the X-Z plane; thus, only one-half of the domain is considered. The lateral extent of the domain (i.e. distance from the pile center axis to the vertical boundaries) is set at a minimum of $2L$, see Figure 3.3. This is done following a similar implementation by Higgins et al. (2013).

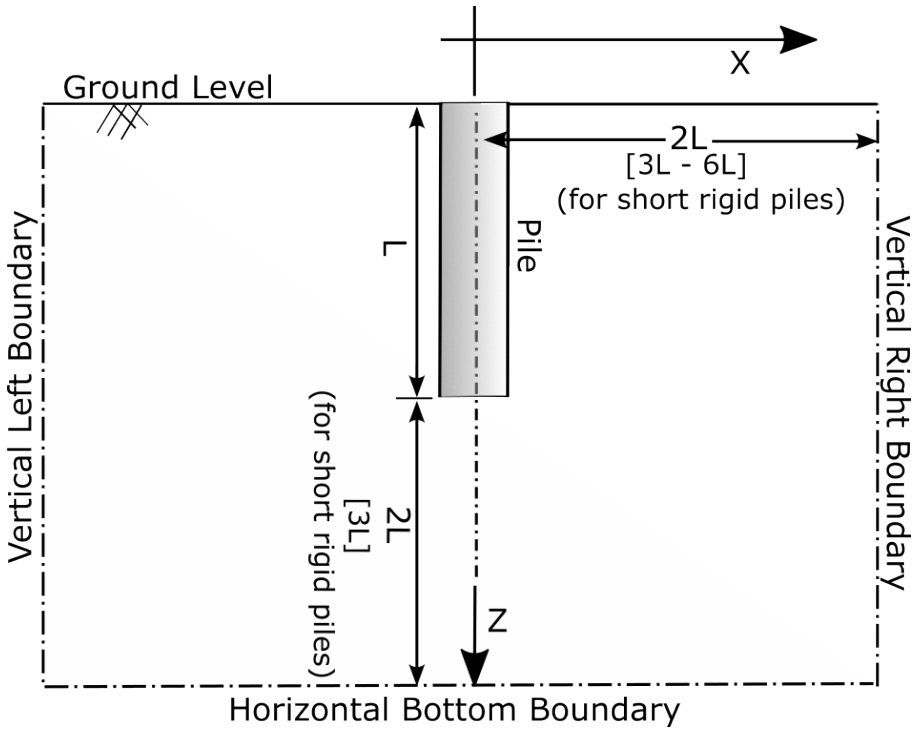

Figure 3.3: finite element domain geometry

Furthermore, boundary sensitivity analysis was conducted. It was observed that for relatively short and rigid piles (Figure 3.4, green curve with green axis), the solution became more dependent on the location of boundary. On the other hand, for relatively longer flexible piles (see Figure 3.4 red curve with red axis) the solution is less dependent on the distance of the boundary from the pile axis (note the difference in the scale of the red and green axis). This may be explained by the fact that a relatively rigid pile implies a smaller soil stiffness; hence, resulting in larger magnitude of displacement at radial distance further from the pile (closer to the boundary).

Comparing short rigid fixed-head and free-head piles, fixed-head piles show more dependence on the distance of the boundary. Normalized pile head displacements for fixed-head short rigid piles increased by 12.3% while the the value was 3.0% for there free-head counter parts. Over all, for most pile sizes the radial boundary distance of $2L$ was found to be adequate, with the exception of short rigid piles. In those cases, a distance of $30m$ was chosen. This value increases the boundary distance to $3L - 6L$ for the short pile lengths investigated. The distance from the base of the pile to the horizontal boundary is set at $2L$. Again, for short pile, this value was increased to $15m$ (about $3L$ for the short piles studied).

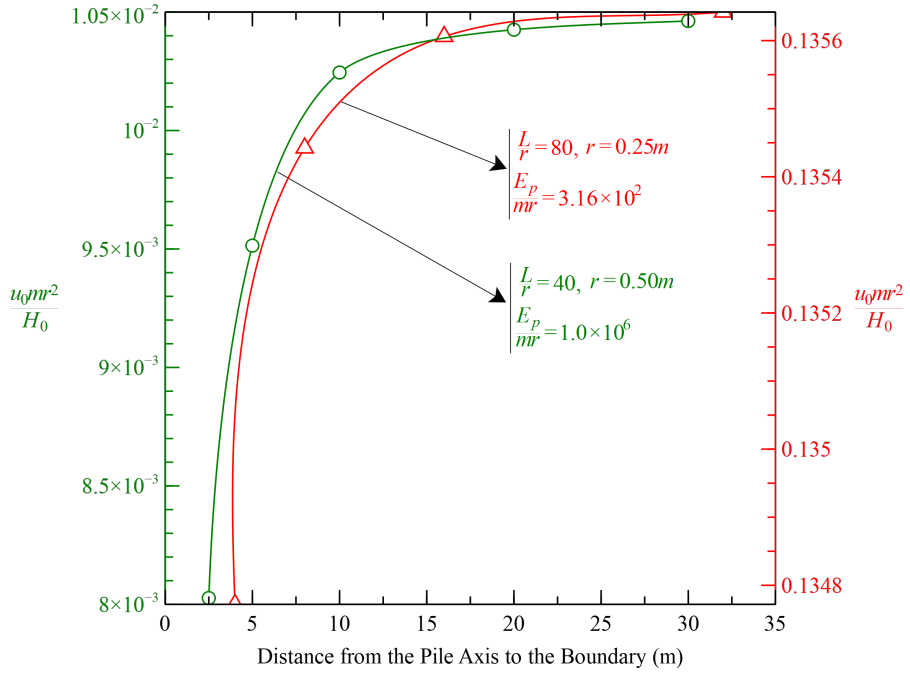

Figure 3.4: Sensitivity of finite element result to distance of vertical boundary for free-head floating pile in soil with linearly increasing modulus with zero at the surface ($\nu_s = 0.3$)

The appropriate boundary conditions are applied to the domain boundaries. The Y-symmetry boundary condition ($u_y = \theta_x = \theta_z = 0$) is applied to the X-Z plane of symmetry, while rollers ($u_z = 0$) are applied to the pile base and pins ($u_x = u_y = 0$) to the curved boundary.

3.4.2 Element types and sizes

A structured meshing scheme with three dimensional solid quadrilateral elements was employed for the soil. The number of elements generated ranged from the order of 20,000 to 40,000 depending up on the extent of the domain.

3.4.2.1 Element types for the soil domain

The 20-node quadratic brick (three-dimensional) element with reduced integration scheme is used for the most parts of soil domain with the exception of the cylindrical region under the pile. The choice of an element with quadratic interpolation over a less computationally expensive linear one was so as take advantage of the better performance afforded by

second order elements. The specific element used is designated as C3D20R. The reduced integration scheme is chosen for the advantages it affords in reducing analysis time and the provision of generally more accurate results for second order elements (ABAQUS 2022).

For the special case, where the soil response approaches volumetric incompressiblity ($\nu_s > 0.45$), a hybrid variant, C3D20RH is employed in view of overcoming any possible volumetric locking . The hybrid element formulation allows for separate interpolation of hydrostatic stress overcoming the hypersensitivity of nodal displacements to hydrostatic pressure associated with volumetric locking (ABAQUS 2022).

The cylindrical soil region under the pile is modeled using quadratic wedge (three-dimensional) elements, designated as C3D15. For this region a hybrid variant C3D15H was also used as required ($\nu_s > 0.45$). Element geometries are shown in Figure 3.6 and the locations where they are employed is presented in Figure 3.5.

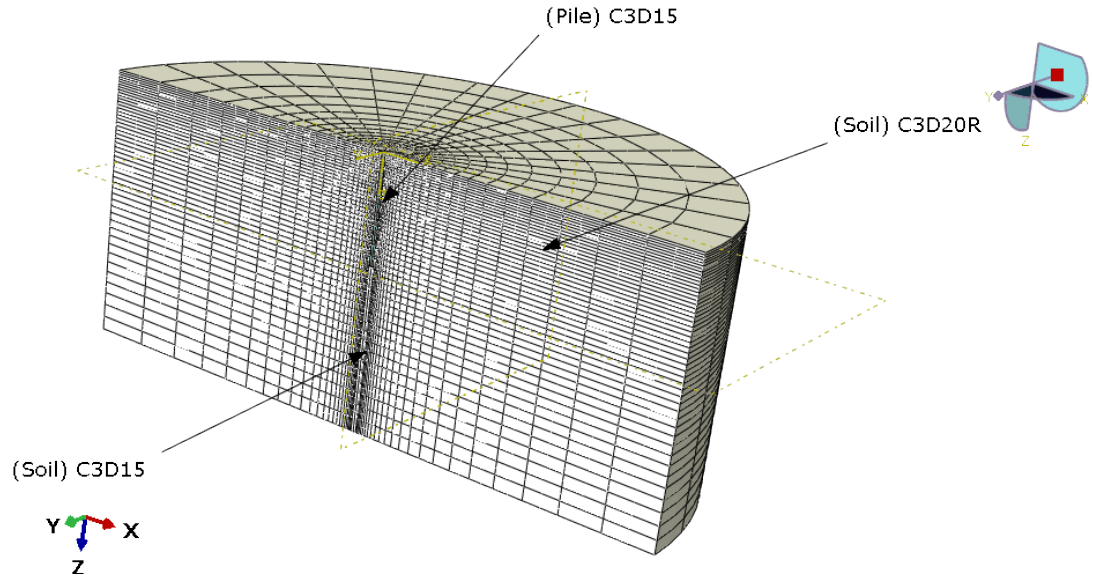

Figure 3.5: Finite Element Model

3.4.2.2 Element types for the pile domain

The pile is modeled using wedge (three-dimensional) elements, similar to the cylindrical soil region under it. The specific element used is designated as C3D15. The element is formulated using a quadratic interpolation scheme. The use of three-dimensional element

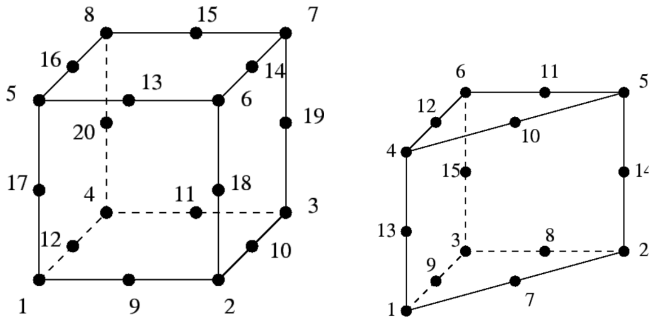

Figure 3.6: Geometry of elements used in finite element analysis, (left: C3D20, right: C3D15) (ABAQUS 2022)

for the pile has the limitation that sections forces, such as, bending moment are not readily available. While there exist beam elements, as will be discussed in the following section, use of three-dimensional elements affords better flexibility when it comes to modeling the pile-soil interface, in that, tie-constraints can be used instead of using embedded beam-in-solid elements. The hybrid element variant is not used for the pile as Poisson's ratios are under 0.45.

Regarding element sizes, the mesh is structured so that smaller elements sizes are used close to the pile-soil interface where there is a large displacement gradient. Along the pile soil interface, element size in the vertical direction are constant and vary from $0.25m - 0.75m$ depending on the length of the pile. Below the pile tip, the element size gradually increase away from the pile to a maximum of 2.5 times the sizes along the pile length at the domain bottom boundary. In the radial direction, element sizes also increase away from the pile with a minimum size at the pile-soil interface of $0.1m$. This values are selected based on a mesh convergence study conducted in parallel with the boundary sensitivity study. Different element sizes, especially at the pile soil interface where used to select the most efficient one. For example, referring to Figure 3.7, for free-head short-rigid piles in soil with linearly increasing elastic modulus, FEM solutions for mesh configurations beyond $30,000$ elements converge. On the other hand, for intermediate and long flexible piles convergence is attained for mesh configurations resulting in a total of $20,000 - 25,000$ or more elements.

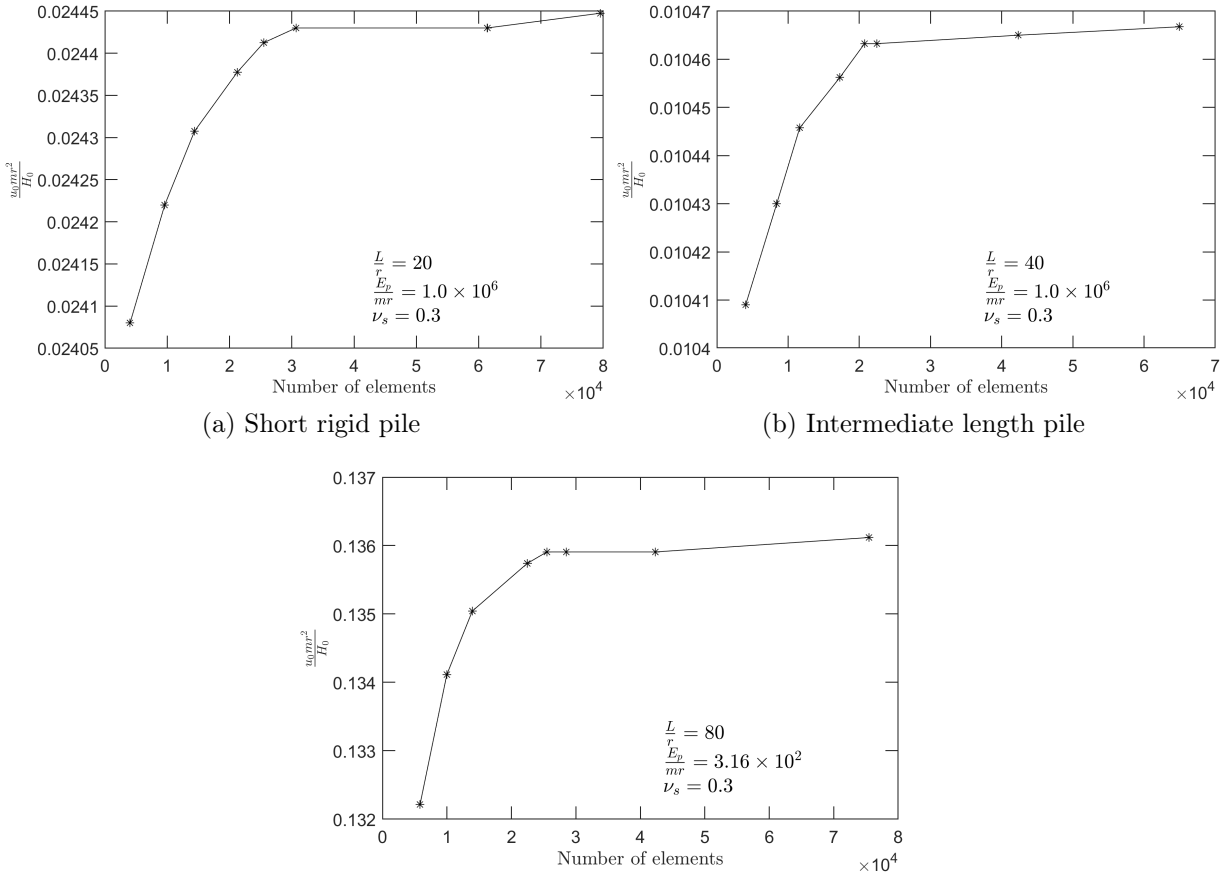

(a) Short rigid pile

(b) Intermediate length pile

(c) Long flexible pile

Figure 3.7: Mesh convergence for free-head floating piles embedded in soil with linearly increasing soils

In regards to element shape, element aspect ratios larger than the ideal unity do occur; especially, for the wedge elements. In general, less than 20% of elements exhibit aspect ratio larger than 10 and even in that case most are away from the pile-soil interface. Additionally, other mesh analysis checks provided by ABAQUS did not result in any errors or warnings.

3.4.3 Pile-soil interface

The pile-soil interface is assumed to be perfectly bonded. While there exist advanced interface elements involving either zero or finite thicknesses (Desai et al. 1984; Day and Potts 1994), for such a simple interface where there exists no separation and the primary concern is compatibility, a simple constraint is adequate. To achieve this, the interface was modeled using tie constraints. The tie elements, constrain the degrees of freedom

of one node to the other (ABAQUS 2022). In the current case, this implies that the displacement degrees of freedom of the soil elements at the interface are bound to the displacement degrees of freedom on of the pile elements at the interface. The default surface-to-surface approach is used when specifying the tie constraints and no explicit position tolerances are provided.

3.4.4 Representation of soil non-homogeneity

For representing the soil non-homogeneity, a dummy field approach was used. As the problem is not temperature dependent the dummy field used was a temperature field which has built-in support in ABAQUS. The modulus of elasticity is set to be temperature dependent. The temperature variation is then used as a depth coordinate. The modulus of elasticity is input into ABAQUS at discrete points along the depth, which is provided as the temperature. ABAQUS interpolates modulus of elasticity values between the discrete points.

For the linearly varying profile, values at the pile head and the domain bottom are adequate. For the parabolically varying profile, due to its non-linearity, as many as 94 discrete inputs are used depending on the size of the domain. The depth (temperature) interval between the points is set at $0.25m$ along the pile length and $1.0m$ below the pile.

3.4.5 Analysis workflow

Based on the range of parameters selected from the previous section, a total of 272 model permutations exist for each pile end condition and soil non-homogeneity profile investigated. This results in a total of 2176 model runs. Considering the significant number of models, the embedded python interpreter in ABAQUS is used to automate the model generation, analysis and output collection process. The primary output, pile displacement, for each model is then saved in a comma separated values (CSV) file for model calibration purposes.

Python scripts used for modeling and output processing are provided at the author's GitHub page at https://github.com/MathewosEnd/Response-of-Laterally-Loaded-piles-

in-Kerr-Equivalent-Pasternak-subgrade

3.4.6 Verification of finite element results

The finite element method implemented in this work forms the basis for the determination of the calibration factor; hence, it is of the utmost importance that the analysis results are accurate. Accordingly, results from ABAQUS, in the form of normalized pile head displacements $\left(\frac{u_0 mr^2}{H_0}\right)$ are compared with similar published works when available. For floating piles embedded in soil with linearly increasing modulus, results were compared against Higgins et al. (2013) whose expression are provided in Section 2.1.3. They formulated finite element solution for laterally loaded piles in elastic media with constant and linearly varying Young's modulus. A summary of this validation is given in Tables 3.2 and 3.3. Finite element results for long flexible piles for both free-head and fixed-head piles match those in published literature, while result for short rigid piles deviate. For free-head short rigid piles, this is explained by the fact that their formulation uses a modified shear modulus, initially proposed by Randolph (1981), to account for the effect of Poisson's ratio for long flexible piles. For the range of parameters investigated for short rigid piles, the difference in solution diminishes from a maximum value at $\nu_s = 0.2$ to a minimum value at $\nu_s = 0.5$ irrespective of all other parameters. Moreover the expressions from Higgins et al. (2013) are obtained through curve fitting which ultimately are statistical approximations.

For fixed-head short rigid piles, comparisons deviate by a more significant margin. One possible explanation for the aforementioned differences of fixed-head short rigid piles may be that the size of the boundary used by Higgins et al. (2013) is smaller than required as explained above. This argument is made based on the observation that the differences are all positive (i.e. the FEM results are larger than the published results) for all short rigid pile cases, irrespective of pile head condition. while, the differences in the results of long flexible piles include both positive and negative values. As discussed above for short rigid piles, larger lateral boundary distances are required. Higgins et al. (2013) state that they employed "*at least 2L*" distance from the pile axis but this statement is ambiguous. There is no explicit statement about the distances used for short rigid

Table 3.2: Validation of finite element results against Higgins et al. (2013) for linearly increasing soil stiffness and free-head floating piles

Pile type	Min. Abs. difference (%)	Max. Abs. difference (%)	Mean Abs. diff. (%)
Short rigid	7.9	13.2	11.3
Long flexible	0.04	6.4	2.5

Table 3.3: Validation of finite element results against Higgins et al. (2013) for linearly increasing soil stiffness and fixed-head floating piles

Pile type	Min. Abs. difference (%)	Max. Abs. difference (%)	Mean Abs. diff. (%)
Short rigid	20.4	33.9	28.3
Long flexible	0.6	9.5	4.6

piles. To further this argument, a limited FEM study for short rigid fixed head piles in soil with linearly increasing elastic modulus and using a boundary distance of $2L$ instead of $3L - 6L$ was done. The pile head displacements were compared with Basu and Higgins (2011) and the mean difference was found to be 11.3%. The corresponding result using $3L - 6L$ boundary distance was 27.6%. Hence, the difference reduce as distance to the boundary is reduced. Interestingly, for free-head piles, using the same approach, the difference in results between the FEM and Higgins et al. (2013) was found to be 9.1% using the $2L$ boundary distance while it increased to 12.4% when using $3L - 6L$ boundary distance. This indicates a greater dependence on boundary distance for short rigid fixed-head piles compared to short rigid free-head piles, which was noted above. But this dependence is apparently amplified when comparing such results. As will be noted in later sections, these differences will also be observed when comparing critical relative stiffness and comparing static pile head flexibility influence factors.

For parabolically varying soil profile and free-head floating piles, FEM results were compared with those provided by Gazetas (1991) for long flexible piles (Table 3.4). The ABAQUS results match those provided in the literature to a reasonable degree.

Over all, for the current work the finite element results are found to be adequate with the exception of fixed-head short rigid piles, for which the finite element analysis domain is enlarged to improve accuracy as discussed above.

Table 3.4: Validation of finite element results against Gazetas (1991) for parabolically increasing soil profile

Pile type	Min. Abs. difference (%)	Max. Abs. difference (%)	Mean Abs. diff. (%)
Long flexible	1.9	11.6	5.7

3.5 Beam-on-Pasternak-subgrade analysis

For the calibration of the subgrade model and the subsequent evaluation of the static response of a single pile in non-homogeneous media, the beam-on-Pasternak subgrade analysis is used. In this analysis, the pile is modeled as a transversely loaded straight prismatic Euler-Bernoulli beam. The use of this beam theory is justified for solid sections by the work Gupta and Basu (2018) as noted in Section 2.1.1.3. The assumed positive direction of the relevant quantities involved is shown in Figure 3.8

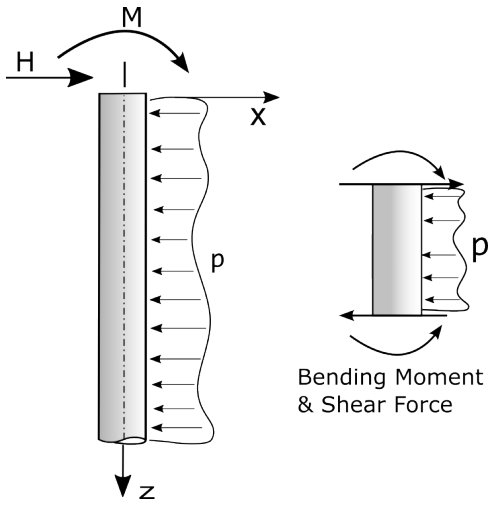

Figure 3.8: Sign Convention

3.5.1 Description of soil

From the Kerr-equivalent Pasternak model of Worku (2014) and considering the variation of soil modulus of elasticity with depth, the subgrade parameters are given by:

$$k_P(z) = \frac{(0.4\nu_s + 0.67)E_s(z)}{\chi} \tag{3.3}$$

$$G_p(z) = (1.36\nu_s + 2.28)G_s(z)\chi d^2 \tag{3.4}$$

Note that in (3.3) and (3.4) the terms are multiplied by the pile diameter d as linear structural elements are involved to represent the pile. In addtion, it is also found convenient to re-express (3.4) in terms of the elastic modulus (3.5); i.e.

$$G_p(z) = \frac{(2.72\nu_s + 4.56)}{1 + \nu_s} E_s(z)\chi r^2 \tag{3.5}$$

Inserting (3.1) into (3.3) and (3.5), the Kerr-equivalent Pasternak subgrade parameters become:

$$k_p(z) = \frac{(0.4\nu_s + 0.67)}{\chi} mr \left(\frac{z}{r}\right)^n \tag{3.6}$$

$$G_p(z) = \frac{(2.72\nu_s + 4.56)}{1 + \nu_s} \chi m r^3 \left(\frac{z}{r}\right)^n \tag{3.7}$$

3.5.2 Governing equation

From the equation of the elastic line of a beam (Hetényi 1946);

$$E_p I_p \frac{d^4 u(z)}{dz^4} + p = 0 \tag{3.8}$$

where p is the lateral pile-soil contact force per unit length, and $E_p I_p$ is the flextural stiffness of the pile.

Form the Pasternak subgrade model:

$$p = K_p u(z) - G_p \frac{d^2 u(z)}{dz^2} \tag{3.9}$$

Combining (3.8) and (3.9), and allowing the subgrade parameters to vary with depth, one obtains:

$$E_p I_p \frac{d^4u(z)}{dz^4} - G_P(z)\frac{d^2u(z)}{dz^2} + k_p(z)u(z) = 0 \tag{3.10}$$

The governing deferential equation is then obtained by inserting (3.6) and (3.7) into (3.10).

$$E_p I_p \frac{d^4u(z)}{dz^4} - \left[\frac{(2.72\nu_s + 4.56)}{1+\nu_s}\chi m r^3\right]\left(\frac{z}{r}\right)^n \frac{d^2u(z)}{dz^2} + \left[\frac{(0.4\nu_s + 0.67)}{\chi} m r\right]\left(\frac{z}{r}\right)^n u(z) = 0 \tag{3.11}$$

This governing linear ordinary differential equation with variable coefficients must be solved to obtain the pile resistance.

3.5.3 Boundary conditions

At each end of the pile, two boundary conditions are considered, namely, free and fixed end.

For the free-head boundary, from consideration of moment and force equilibrium of the pile head and accounting for the continuity provided by the shear element, the boundary conditions can be expressed by (Sun 1994; Guo 2012; Lulseged 2021):

$$E_p I_p \frac{d^2u(z)}{dz^2} - M_0 = 0, \qquad z = 0 \tag{3.12}$$

$$E_p I_p \frac{d^3u(z)}{dz^3} - G_p(z)\frac{du(z)}{dz} - H_0 = 0, \qquad z = 0 \tag{3.13}$$

inserting (3.7) into (3.13) the boundary conditions become:

$$E_p I_p \frac{d^2u(z)}{dz^2} - M_0 = 0, \qquad z = 0 \tag{3.14}$$

$$E_p I_p \frac{d^3u(z)}{dz^3} - \left[\frac{(2.72\nu_s + 4.56)}{1+\nu_s}\chi m r^3\right]\left(\frac{z}{r}\right)^n \frac{du(z)}{dz} - H_0 = 0, \qquad z = 0 \tag{3.15}$$

for the fixed-head boundary;

$$\frac{du(z)}{dz} = 0, \qquad z = 0 \tag{3.16}$$

$$E_p I_p \frac{d^3u(z)}{dz^3} - G_p(z)\frac{du(z)}{dz} - H_0 = 0, \qquad z = 0 \tag{3.17}$$

similarly, inserting (3.7) into (3.17):

$$\frac{du(z)}{dz} = 0, \qquad z = 0 \tag{3.18}$$

$$E_p I_p \frac{d^3u(z)}{dz^3} - \left[\frac{(2.72\nu_s + 4.56)}{1+\nu_s}\chi m r^3\right]\left(\frac{z}{r}\right)^n \frac{du(z)}{dz} - H_0 = 0, \qquad z = 0 \tag{3.19}$$

In the case of the floating-base boundary, since the Pasternak subgrade accounts for shear interaction, resulting in continuity, effects of the soil below the pile is taken into consideration. This effect can be represented by an equivalent shear force, Q_L at the base of the pile (Sun 1994; Guo 2012). Considering the soil segment below the pile, this yields:

$$k_P(z)u(z) - G_p(z)\frac{d^2u(z)}{dz^2} = 0, \quad z > L \tag{3.20}$$

With the conditions that for $z = L$, $u(z) = u_L$ and as $z \to \infty$, $u(z) \to 0$, Equation (3.20) can be solved for $u(z)$. This solution can then be used to formulate an expression for the shear force, Q_L at the pile base and is given by Equation (3.21). Details of the

formulation are given in Appendix A.

$$Q_L = -u_L\sqrt{k_{pL}G_{pL}} \tag{3.21}$$

Then from consideration of equilibrium at the pile base the boundary conditions are:

$$E_pI_p\frac{d^2u(z)}{dz^2} = 0, \qquad z = L \tag{3.22}$$

$$E_pI_p\frac{d^3u(z)}{dz^3} - G_p(z)\frac{du(z)}{dz} - Q_L = 0, \qquad z = L \tag{3.23}$$

inserting (3.7) and (3.21) into (3.23):

$$E_pI_p\frac{d^2u(z)}{dz^2} = 0, \quad z = L \tag{3.24}$$

$$E_pI_p\frac{d^3u(z)}{dz^3} - \left[\frac{(2.72\nu_s + 4.56)}{1+\nu_s}\chi m r^3\right]\left(\frac{z}{r}\right)^n\frac{du(z)}{dz} + u_L\sqrt{k_{pL}G_{pL}} = 0, \quad z = L \tag{3.25}$$

Finally, for the fixed-base boundary;

$$\frac{du(z)}{dz} = 0 \qquad z = L \tag{3.26}$$

$$u(z) = 0 \qquad z = L \tag{3.27}$$

The boundary conditions considered above result in a total of four permutations to be investigated. They are designated as:

- FHFB (free-head, free-base),
- FxHFB (fixed-head, free-base),
- FHFxB (free-head, fixed-base) and,

- FxHFxB (fixed-head, fixed-base)

3.5.4 Solution methods

As pointed out above, the governing equation (3.11) is a fourth order homogeneous linear ordinary differential equation with non-constant coefficients. Even though the equation is linear, the existence of non-constant coefficients introduces difficulties in obtaining a closed form solution, especially for higher order equations as in this case. Attempts to obtain a closed form solution using analytical methods were unsuccessful. Furthermore, to the best of the author's knowledge, there are no published closed form solutions for ODE of this kind. Therefore, numerical solution methods are used.

The specific solution algorithm implemented is provided by the MATLAB function *bvp5c* (MATLAB 2022). The function uses a four-point Lobatto IIIA formula accurate to the fifth order with adaptive meshing where the scaled residual is controlled (Kierzenka and L. Shampine 2008). This algorithm is used for its convenience in that even at more relaxed error tolerances, its use results in better performance compared to other available functions (MATLAB 2022). The function utilizes combined absolute and relative error tolerances, with default values of $10^{-6}$and 10^{-3}, respectively (MATLAB 2022). The absolute tolerance represents the value beyond which the solution is insignificant while relative tolerance represents the normalized residual (L. F. Shampine, Gladwell, and Thompson 2003). The absolute error tolerance is found to be adequate as it represents a displacement of $0.001mm$. On the other hand, the relative error tolerance was reduced to 10^{-4} but comparison of solutions using the changed relative tolerance to the default one showed no difference; hence, the default relative tolerance is used.

3.6 Approximate method of analysis for dynamic inertial interaction

For dynamic loading an approximate approach is used. The approach utilizes the virtual work method with assumed shapes for the pile deformation derived from the solutions

for piles in homogenous soil. The pile head response (components of the impedance function) are then computed as the sum of the contribution of the distributed stiffness and damping elements. Due to mathematical complexity associated with the problem, only long flexible piles are treated (Dobry et al. 1982; Mylonakis 1995; Karatzia and Mylonakis 2017).

3.6.1 Description of soil

As the calibration factors are to be obtained from static analysis, these frequency independent values will be used in the dynamic analysis as well. Hence, the Kerr-equivalent Pasternak subgrade parameters presented in section 3.5.1 remain the same in both the static and dynamic analyses.

For dynamic analysis, dashpot coefficients are required to represent energy dissipation. As discussed in section 3.2, the energy dissipation mechanism in soils involves material hysteresis damping and radiation damping. The material damping is represented by a constant equivalent damping ratio, β_s, while the radiation damping is represented by a radiation dashpot coefficient $c_r(z)$ which is variable with depth. Additionally, material damping for the pile is considered by a constant equivalent damping ratio β_p. The radiation dashpot coefficient is given by:

$$\frac{c_r(z)}{d\pi\rho_s V_s(z)} = \left[0.25 + 0.8\left(\frac{2}{1-\nu_s}\right)^{1/2}\right] a_0(z)^{-0.4} \tag{3.28}$$

For use in the current work, it is found convenient to expand (3.28) using (3.1) to the form:

$$c_r(z) = c_{rr}\left(\frac{z}{r}\right)^{0.7n} \tag{3.29}$$

where,

$$c_{rr} = \frac{\pi d^{0.6}\rho_s^{0.3}\omega^{-0.4}}{\left[2/(1+\nu_s)\right]^{0.7}}\left[0.25 + 0.8\left(\frac{2}{1-\nu_s}\right)^{1/2}\right](mr)^{0.7}$$

Interestingly, Karatzia and Mylonakis (2017) approximate $c_r(z) \approx c_{rr}\left(\frac{z}{r}\right)^{0.5n}$ for use with non-homogenous soil profiles, which is similar to that obtained above.

3.6.2 Pile shape functions

Shape functions defining the normalized deformed shape of a pile due to a unit head displacement $\varphi_H(z)$ and due to a unit head rotation $\varphi_M(z)$ are first assumed as a basis for this approach. For non-homogenous media, the shape functions are approximated by using normalized terms from the solution of the same pile embedded in a homogenous medium (Karatzia and Mylonakis 2017).

For the vibration of an Euler-Bernoulli beam under harmonic excitation with frequency, ω, having flexural stiffness, E_pI_p, and mass per unit length, $\bar{m}$, embedded in a homogenous soil modeled as a Pasternak subgrade, k_p and G_p, with viscous damping, c, the equation of motion is given by:

$$\bar{m}\frac{\partial^2 u(z,t)}{\partial t^2} + c\frac{\partial u(z,t)}{\partial t} + E_pI_p\frac{\partial^4 u(z,t)}{\partial z^4} - G_P\frac{\partial^2 u(z,t)}{\partial z^2} + K_p u(z,t) = 0 \tag{3.30}$$

Assuming a harmonic response,

$$u(z,t) = u(z)e^{i\omega t} \tag{3.31}$$

where $u(z)$ is the displacement amplitude, e is the natural exponent and $i = \sqrt{-1}$. Inserting (3.31) into (3.30) one obtains:

$$E_pI_p\frac{d^4u(z)}{dz^4} - G_P\frac{d^2u(z)}{dz^2} + \left[K_p - \bar{m}\omega^2 + i\omega c\right]u(z) = 0 \tag{3.32}$$

Using the characteristic equation method, the general solution to (3.30) is given by (Lulseged 2021):

$$u(z) = e^{-\alpha z}\left[A\cos(\beta z) + B\sin(\beta z)\right] + e^{\alpha z}\left[C\cos(\beta z) + D\sin(\beta z)\right] \tag{3.33}$$

Where A, B,C and D are constants of integration and

$$\alpha = \sqrt{\lambda^2 + \frac{G_p}{4E_pI_p}} \tag{3.34}$$

$$\beta = \sqrt{\lambda^2 - \frac{G_p}{4E_pI_p}} \tag{3.35}$$

$$\lambda = \sqrt{\frac{K_p + i\omega c - \bar{m}\omega^2}{4E_pI_p}} \tag{3.36}$$

For long flexible piles, $u(z) \to 0$ for $L \to \infty$; hence, (3.33) reduces to:

$$u(z) = e^{-\alpha z}\left[A\cos(\beta z) + B\sin(\beta z)\right] \tag{3.37}$$

Following Mylonakis (1995) and using (3.37) the shape functions for a pile in non-homogenous medium are approximated as shown in Equation (3.38) - (3.40). For the shape functions associated with a free-head pile, Equations (3.38) and (3.39) are obtained by considering the shape described by (3.37). In order to do that the coefficients A and B associated with the magnitude of displacement are first set to unity. Then for the shape function associated with a unit head rotation at the pile head, φ_M, the cosine term is dropped since a rotation at the pile head implies zero head displacement. This ensures that the shape function is consistent with the prescribed displacement boundary. Further, it was observed that a scaling factor was required as the resulting displacement using this shape deviated from published curves in the literature by an approximately constant value. In addtion, in Mylonakis's 1995 work a similar scaling factor is used for the parameter φ_M. Hence following Mylonakis's work, a scaling factor equal to the mean of the two wave numbers η and μ is proposed. Mylonakis's scale factor only involved a single wave number, λ, as it was based on a single parameter model. In this work, the scaling value is not chosen arbitrary, instead, various expressions including the sum and difference of the the two parameters were initially investigated in terms of there ability to predict the dynamic pile head stiffness. The use of the mean value gave the better results when compared to published data. No other consideration are required for the

shape function φ_H.

Similarly, for the shape function associated with fixed head piles (Equation 3.40), the coefficients A and B are set to unity. Further from observations of Mylonakis's 1995 formulation, the sine term was also removed. No additional scaling factor was necessary in this case.

$$\varphi_H = e^{-\mu z}\left[\cos(\eta z) + \sin(\eta z)\right] \tag{3.38}$$

$$\varphi_M = \frac{e^{-\mu z}}{\gamma}\sin(\eta z) \tag{3.39}$$

where $\gamma = \frac{\mu+\eta}{2}$, for free head piles and,

$$\varphi_H = e^{-\mu z}\cos(\eta z) \tag{3.40}$$

For fixed head piles.Where μ and η represent the non-homogeneous equivalents of α and β; respectively, and are computed as the mean values of their homogenous counterparts over the pile length. Accordingly,

$$\mu = \frac{1}{L_a}\int_0^{L_a}\alpha(z)dz \tag{3.41}$$

$$\eta = \frac{1}{L_a}\int_0^{L_a}\beta(z)dz \tag{3.42}$$

Inserting (3.3), (3.5) and (3.29) into (3.34) - (3.36), the integrands in (3.41) and (3.42) can be expressed as:

$$\alpha(z),\ \beta(z) = \sqrt{\pm\frac{G_{pr}}{4E_pI_p}\left(\frac{z}{r}\right)^n + \sqrt{\frac{k_{pr}\left(\frac{z}{r}\right)^n + ic_{rr}\omega\left(\frac{z}{r}\right)^{0.7n} - \bar{m}\omega^2}{4E_pI_p}}} \tag{3.43}$$

3.6.3 Energy formulation

The primary design parameter in inertial pile-soil interaction is the complex valued impedance function given by Novak (1974) and Gazetas (1991):

$$\mathcal{K}_{\mathrm{x}} = K_x + iC_x \tag{3.44}$$

The real part represents the dynamic pile head stiffness while the imaginary part represents the equivalent pile head damping. In effect, the impedance represents the cumulative contribution of stiffness and damping elements distributed over the pile length to the pile head response.

In order to develop expressions for components of the pile head impedance function (pile head stiffness K and pile head damping C) the virtual work method is used. The pile head stiffness and damping terms are expressed as the sum of the contributions of the distributed stiffness and dashpot elements. Hence, the total work done by (against) the distributed stiffness (spring and shear) elements and dashpots along the pile length is equated to the work done at the pile head by the spring and dashpot element, respectively. Accordingly, the expressions for pile head stiffness and damping are given by (3.45) and (3.46). The expressions are taken from Mylonakis (1995) but an additional virtual work term for the shear interaction is added. The derivation of Equations (3.45) and (3.46) is given in Appendix B.

$$K_{ij} = E_p I_p \int_0^L \varphi_i'' \varphi_j'' dz - \int_0^L G_p(z) \varphi_i' \varphi_j' dz + \int_0^L k_p(z) \varphi_i \varphi_j dz - m\omega^2 \int_0^L \varphi_i \varphi_j dz \tag{3.45}$$

$$C_{ij} = \frac{2\beta_p}{\omega} E_p I_p \int_0^L \varphi_i'' \varphi_j'' dz + \frac{2\beta_s}{\omega} \left[- \int_0^L G_p(z) \varphi_i' \varphi_j' dz + \int_0^L k_p(z) \varphi_i \varphi_j dz \right] + \int_0^L c_r(z) \varphi_i \varphi_j dz \tag{3.46}$$

Where i and j represent the different modes of oscillation. For $i = j = H$, K_{HH} and C_{HH} represent the pile head impedance components for the swaying mode. Similarly,

for $i = j = M$, K_{MM} and C_{MM} represent the pile head impedance components for the rocking mode, and for $i = H$ and $j = M$ or vice-versa, K_{HM} and C_{HM} represent the cross swaying-rocking mode of vibration.

The first terms in (3.45) and (3.46) represents the contribution of the pile to the stiffness and damping at the pile head, while the middle terms represent the contributions of the soil. The last term in (3.46) represents the contribution the radiation damping.

The final term in (3.45) represents the contribution of the pile inertia, which in most applications involving seismic excitation is small; hence, it is neglected (Karatzia and Mylonakis 2017). Therefore, the stiffness component of the impedance function may be estimated from the static pile head stiffness for laterally loaded piles. For long flexible piles the upper limit of the integration is taken to be $L \to \infty$ (Karatzia and Mylonakis 2017). This significantly reduces the computations effort and removes the pile length from being an additional parameter to be considered. Note that this is why the analysis is confined to long flexible piles. For most applications this is justified since most piles in the real world are long (Randolph 1981). This is exemplified by the fact that of the 2176 analyses run for the various combination of parameter, only about 10% are classed as short rigid.

Following Karatzia and Mylonakis (2017), Equation (3.46) can be expressed as follows:

$$C_{ij} = \frac{2K_{ij}\beta_{ij}}{\omega} = \frac{2\beta_p}{\omega} E_p I_p \int_0^L \varphi_i'' \varphi_j'' dz + \frac{2\beta_s}{\omega} \left[- \int_0^L G_p(z) \varphi_i' \varphi_j' dz + \int_0^L k_p(z) \varphi_i \varphi_j dz \right] + \int_0^L c_r(z) \varphi_i \varphi_j dz$$

$$\beta_{ij} = \beta_p \frac{E_p I_p \int_0^L \varphi_i'' \varphi_j'' dz}{K_{ij}} + \beta_s \frac{\left[- \int_0^L G_p(z) \varphi_i' \varphi_j' dz + \int_0^L k_p(z) \varphi_i \varphi_j dz \right]}{K_{ij}} + \frac{\omega \int_0^L c_r(z) \varphi_i \varphi_j dz}{2K_{ij}}$$

$$\beta_{ij} = \beta_p w_{ij}^p + \beta_s w_{ij}^s + \beta_{ij}^r \tag{3.47}$$

where,

$$w_{ij}^{p} = \frac{E_p I_p \int_0^L \varphi_i'' \varphi_j'' dz}{K_{ij}} \tag{3.48}$$

$$w_{ij}^{s} = \frac{\left[-\int_0^L G_p(z) \varphi_i' \varphi_j' dz + \int_0^L k_p(z) \varphi_i \varphi_j dz \right]}{K_{ij}} \tag{3.49}$$

$$\beta_{ij}^{r} = \frac{\omega \int_0^L c_r(z) \varphi_i \varphi_j dz}{2K_{ij}} \tag{3.50}$$

w_{ij}^{p} and w_{ij}^{s} are weights specifying the relative contribution of the material damping from the pile and soil to the pile head damping ratio β_{ij}, respectively. β_{ij}^{r} represents the contribution of radiation damping to the pile head damping ratio. Note that if the inertial contribution of the pile (last term in (3.45)) is neglected, $w_{ij}^{p} + w_{ij}^{s} = 1$.

3.6.4 Evaluation of the integrals

Unfortunately, closed-form analytical expressions for the integrals in (3.41) - (3.46) could not be obtained. This is for the most part due to the complicated form of the complex function in Equation (3.43). Simplified approaches of separately treating $n = 1$ and $n = 1/2$ and even neglecting the dynamic components, as their contribution is significantly small (an approach used by Karatzia and Mylonakis (2017)) did not result in any success. Furthermore, the computer algebra system Mathematica (2022) was used but without positive results.

Therefore, numerical integration is used to evaluate the integrals. The MATLAB function "integral" which employs a vectorized adaptive quadrature was used in MATLAB (2022).

Chapter 4

Model Calibration

The calibration factor in Worku's 2014 Kerr-equivalent Pasternak model is evaluated by comparing pile head displacements from static beam-on-Pasternak subgrade analysis using the model at hand with three dimensional static finite element analysis. In order to do this, the calibration factor is initially assumed. The assumed calibration factor along with the a combinations of relevant parameters is then used in the beam-on-Pasternak subgrade analysis from which the pile head displacement is obtained. In parallel, a static finite element analysis is conducted for the given combination of parameters, and the pile head displacement is determined. If the percentage difference between the pile head displacements from the two methods is less than 1% the assumed calibration factor is saved as an acceptable value. Otherwise, the calibration factor is increased by 0.001 and the static beam-on-Pasternak subgrade analysis is redone with the new calibration factor. A flowchart of the process is presented in Figure 4.1.

The aforementioned analysis is done for a wide range of relevant parameters including pile slenderness ratio, pile-soil relative stiffness, soil Poisson's ratio, pile end conditions and the two forms of non-homogenous soil profiles (see section 3.3). Details regarding the values of each parameter and specifics of the finite element analysis are discussed in the previous chapter, while details of the static beam-on-Pasternak subgrade analysis are presented in the next chapter.

In essence, the calibration process constitutes a parametric study, whereby the relationship between the aforementioned parameters and the calibration factor is studied. In what

follows, this relationship between the parameters and the calibration factor is discussed and expressions obtained for the calibration factor are presented.

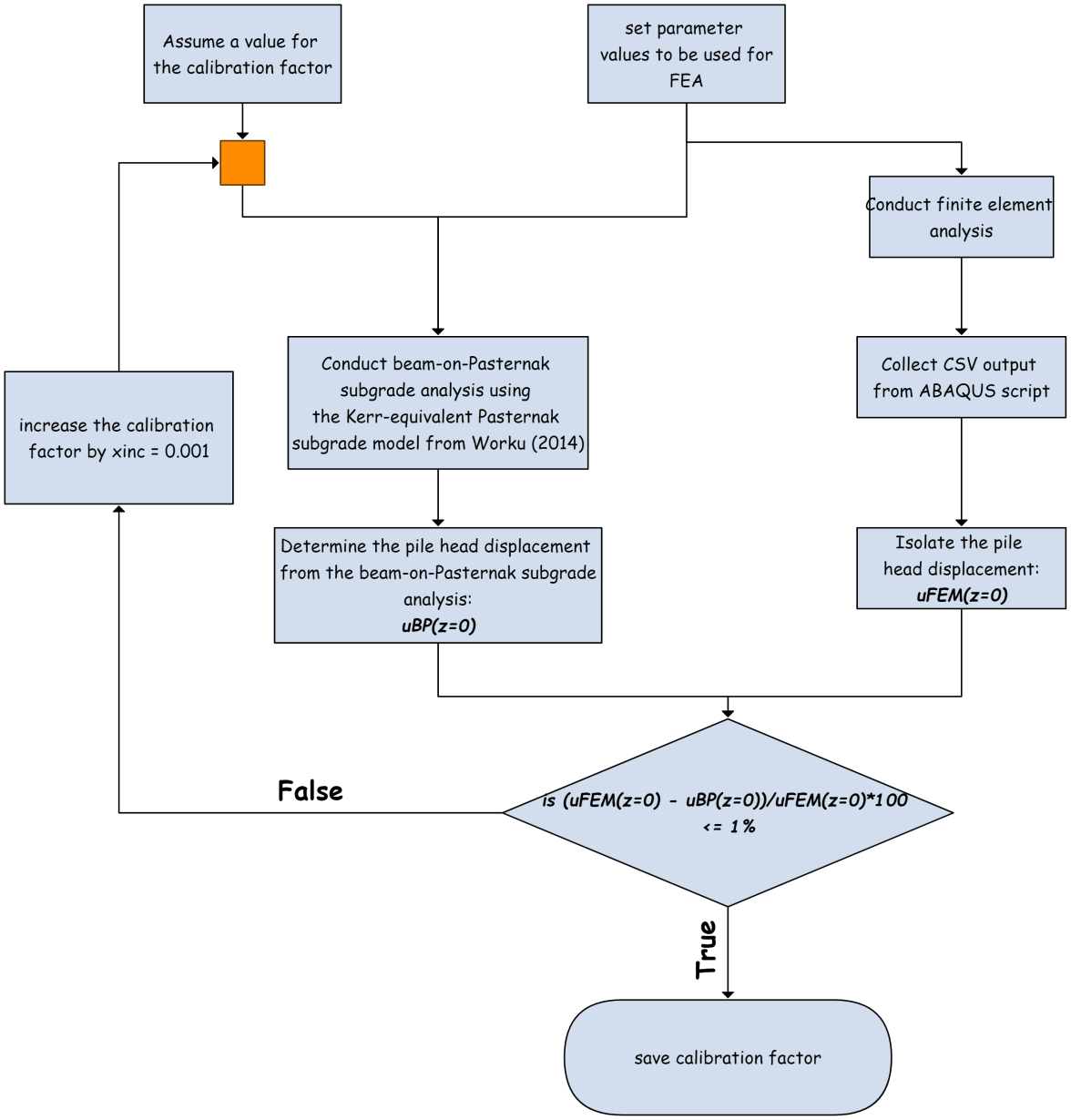

Figure 4.1: Model calibration workflow

4.1 Effect of pile-soil relative stiffness

As noted in Section 2.1.3, the response of a pile is dependent on the relative stiffness. An increase in relative stiffness implies a more rigid pile. As the relative stiffness increases the response of the pile becomes less dependent on the relative stiffness. The boundary,

beyond which the pile response ceases to be dependent on the relative stiffness is termed critical relative stiffness and designated by $\left(\frac{E_p}{mr}\right)_{cr}$ (Guo 2012; Higgins et al. 2013).

The calibration factor exhibits such trends. Figures 4.2 - 4.5 present the calibration factor versus the relative stiffness for various Poisson's ratios and different pile end conditions for piles embedded in soil with linearly increasing modulus. For floating piles and slenderness ratio less than 60, an increase in the relative stiffness results in an increase in the calibration factor up to a certain $\frac{E_p}{mr}$ value, beyond which the factor is independent of the relative stiffness, similar to that of the response of rigid piles.

For fixed-base piles and slenderness ratios less than 60, the calibration factor increases in an unbounded manner as the relative stiffness increases. This is explained by the fact that ideal short rigid piles fixed at the base against displacement and rotation will not exhibit any deflection. Consequently, in the model calibration process, the calibration factor, associated with the stiffness of the soil, must increase significantly to meet the conditions of no displacement.

For the case of floating piles, expressions are proposed for the threshold relative stiffness value, $\left(\frac{E_p}{mr}\right)_{tr}$, beyond which the calibration factor is independent of $\frac{E_p}{mr}$. These expressions are developed through the use of curve fitting and are given by:

$$\left(\frac{E_p}{mr}\right)_{tr} = 11.24\left(\frac{L}{r}\right)^{3.25} \tag{4.1}$$

for free-head floating piles and,

$$\left(\frac{E_p}{mr}\right)_{tr} = 47.8\left(\frac{L}{r}\right)^{3.34} \tag{4.2}$$

for fixed-head floating piles.

For slenderness ratios greater than or equal to 60, irrespective of the pile end condition, the calibration factor monotonically increases with the relative stiffness. Furthermore, the plots of the calibration factor in this range become independent of the slenderness ratio and converge into a single curve. For the fixed-head cases, the convergence of these curves is not as well defined. This is most likely attributed to numerical inaccuracies associated

with the method used to solve the boundary value problem. Fixed-head piles, in general, exhibit relatively lower displacements than their free-head counterparts requiring higher order accuracy for solution convergence and estimation of the calibration factor.

The values of the calibration factor over this range (i.e. $\frac{L}{r} \geq 60$) for free-head floating piles and free-head fixed-base piles are identical. Similarly, the difference between the value of the calibration factor for fixed-head floating piles and fixed-head fixed-base piles is within 1.8%. The stated minor deviation in the latter case may be attributed to the aforementioned challenges in numerical accuracy. Hence, for all practical purposes the calibration factor for $\frac{L}{r} \geq 60$ is independent of the pile base condition.

Through the use of curve fitting, expressions for the convergent curves are given as follows:

$$\chi = (0.12 + 0.06\nu_s)\left(\frac{E_p}{mr}\right)^{0.11} \tag{4.3}$$

for free-head (floating and fixed-base) piles and,

$$\chi = (0.20 + 0.11\nu_s)\left(\frac{E_p}{mr}\right)^{0.08} \tag{4.4}$$

for fixed-head (floating and fixed-base) piles.

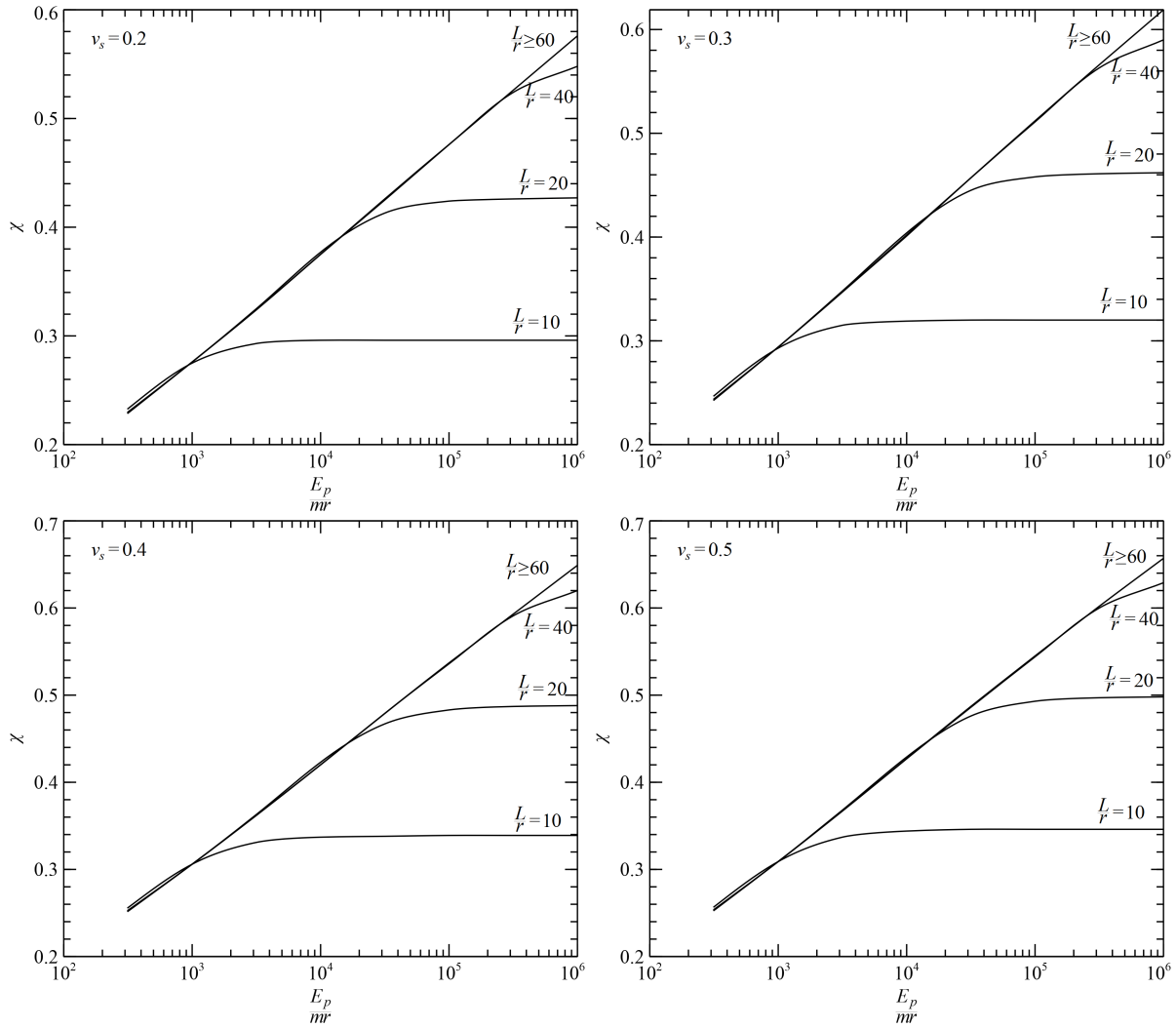

Figure 4.2: Variation of the calibration factor with respect to the relative stiffness for free-head floating piles in soil with linearly increasing elastic modulus

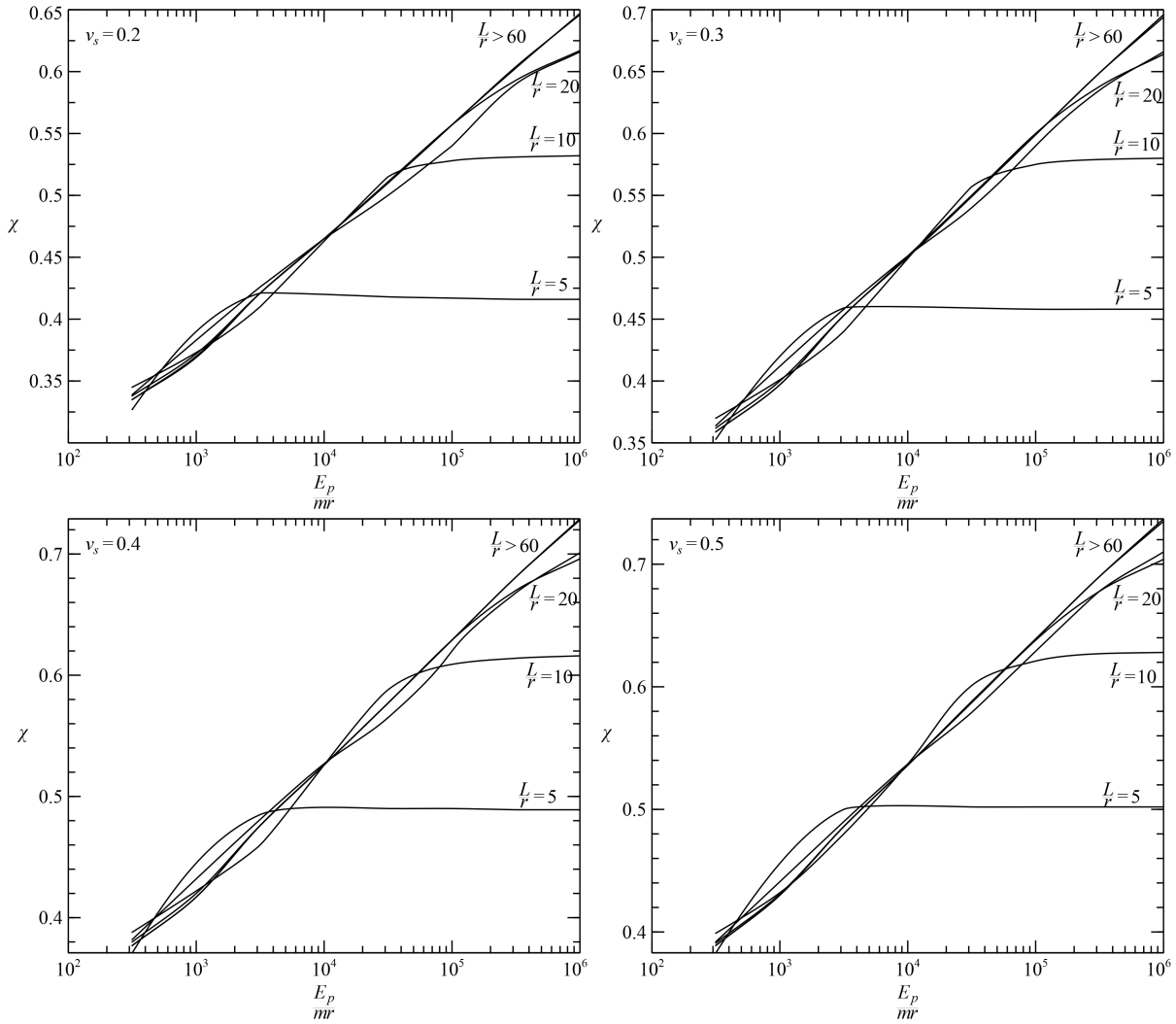

Figure 4.3: Variation of the calibration factor with respect to relative stiffness for fixed-head floating piles in soil profile with linearly increasing elastic modulus

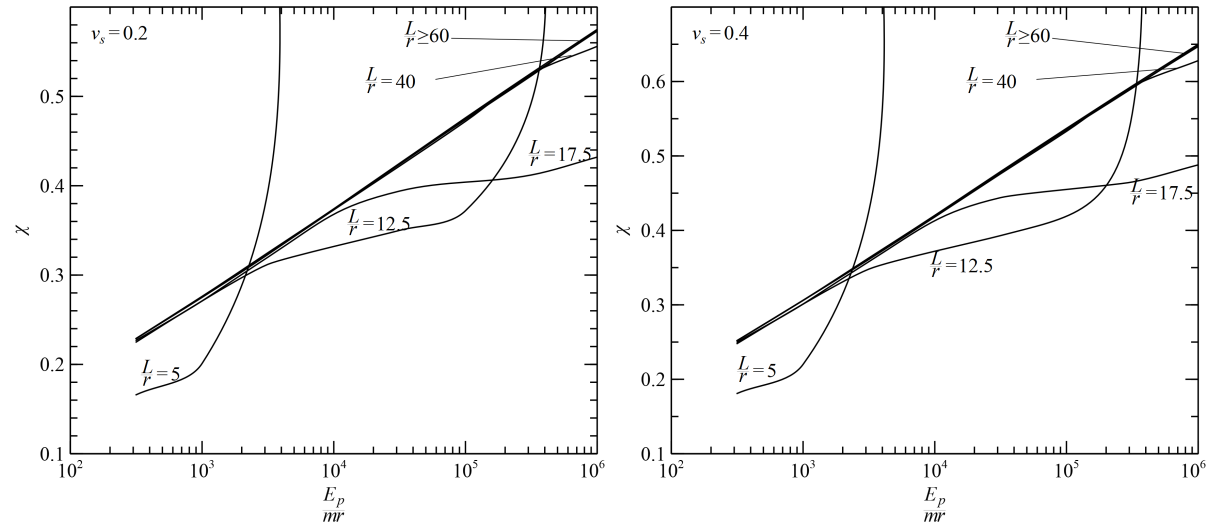

Figure 4.4: Variation of the calibration factor with respect to relative stiffness for free-head fixed-base piles in soil profile with linearly increasing elastic modulus

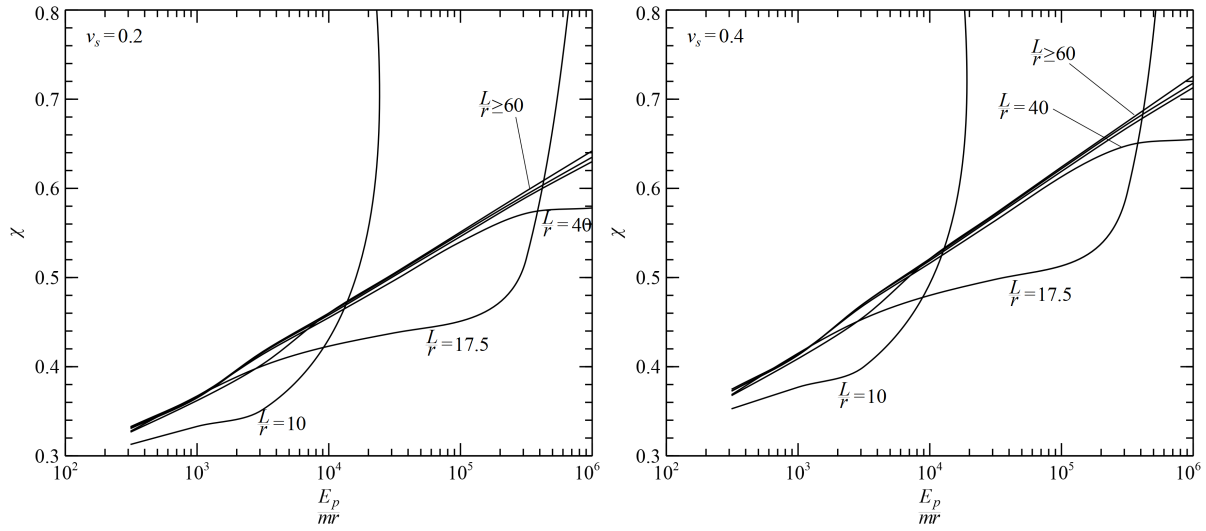

Figure 4.5: Variation of the calibration factor with respect to relative stiffness for fixed-head fixed-base piles in soil profile with linearly increasing elastic modulus

For piles embedded in soil with parabolically varying elastic modulus, referring to Figures 4.6 - 4.9 and in a similar fashion to the linearly increasing modulus case, for floating piles with $\frac{L}{r} < 80$, the calibration factor increases with the relative stiffness until a threshold value. In the case of fixed-base piles the calibration factor increases indefinitely as the relative stiffness increases, for the lower range of slenderness ratios investigated.

The threshold values are given by:

$$\left(\frac{E_p}{mr}\right)_{tr} = 3.56\left(\frac{L}{r}\right)^{3.25} \tag{4.5}$$

for free-head floating piles and,

$$\left(\frac{E_p}{mr}\right)_{tr} = 21.46\left(\frac{L}{r}\right)^{3.07} \tag{4.6}$$

for fixed-head floating piles.

For $\frac{L}{r} \geq 80$ and irrespective of the pile base condition, plots of the calibration factor at different slenderness ratios with respect to $\frac{E_p}{mr}$ converge to a single curve that monotonically increases with the relative stiffness. Expressions for these curves are given by:

$$\chi = (0.17 + 0.09\nu_s)\left(\frac{E_p}{mr}\right)^{0.10} \tag{4.7}$$

for free-head floating and fixed-base piles and,

$$\chi = (0.27 + 0.15\nu_s)\left(\frac{E_p}{mr}\right)^{0.07} \tag{4.8}$$

for fixed-head floating and fixed-base piles.

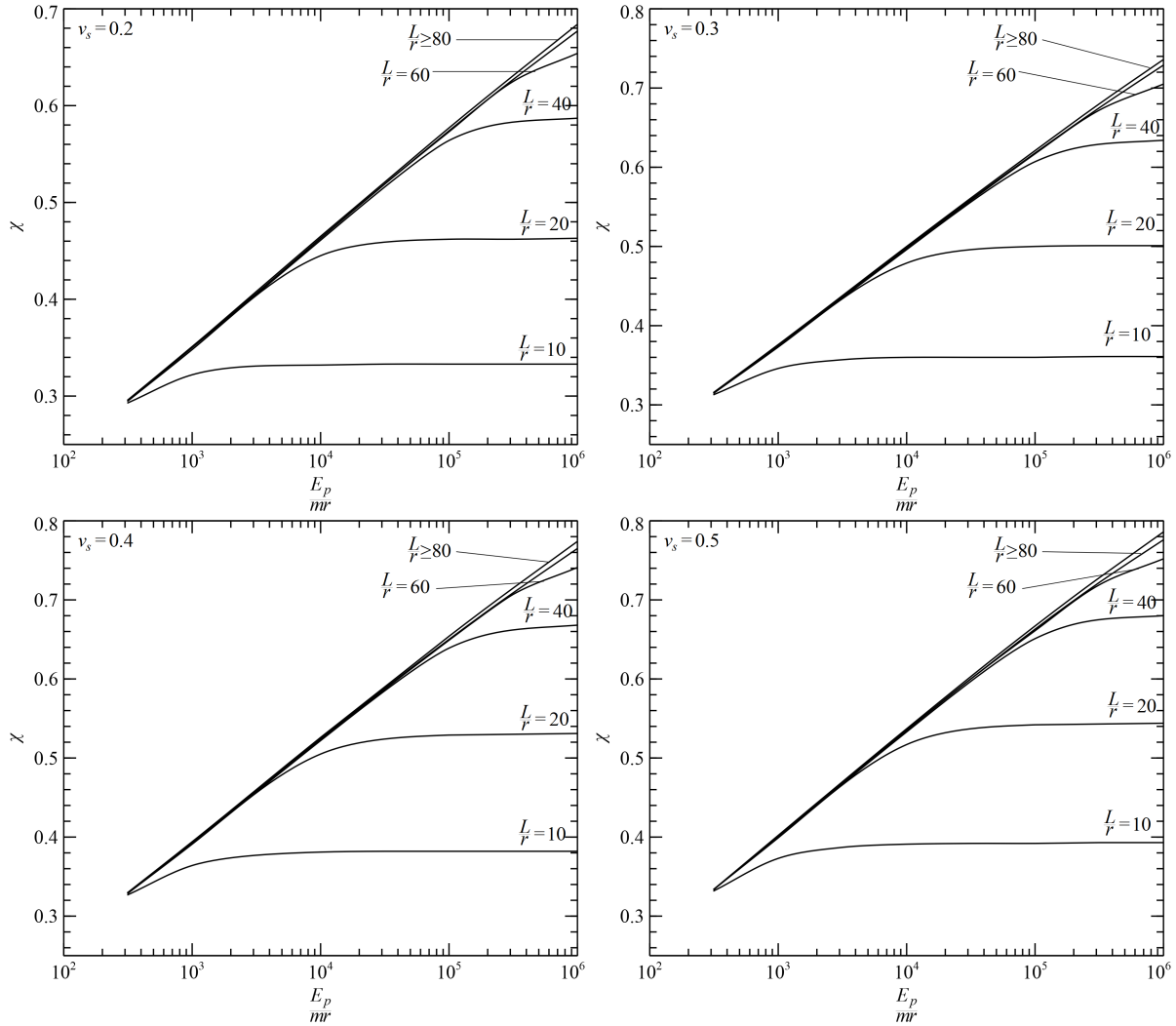

Figure 4.6: Variation of the calibration factor with respect to the relative stiffness for free-head floating piles in soil with parabolically increasing elastic modulus

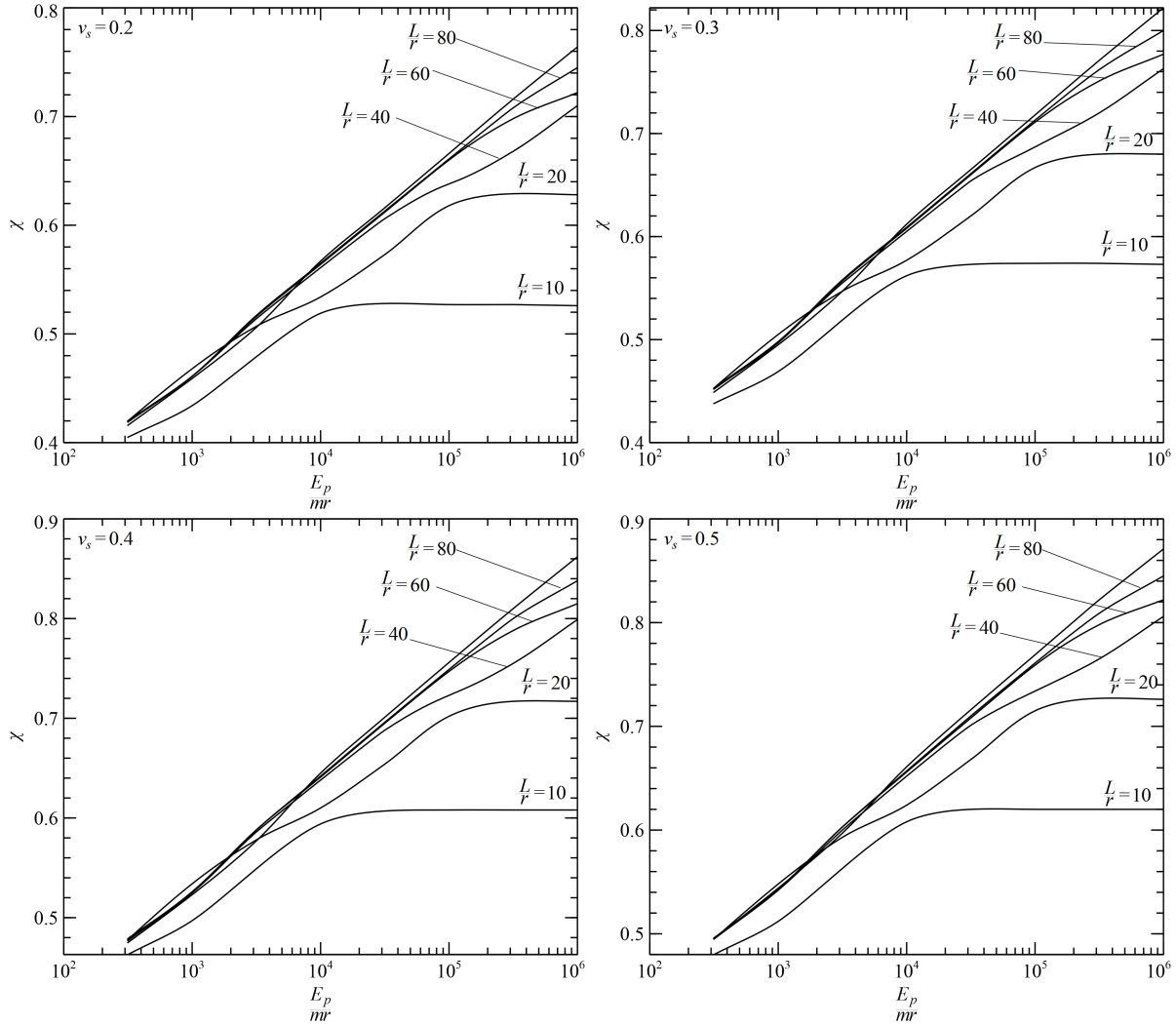

Figure 4.7: Variation of the calibration factor with respect to the relative stiffness for fixed-head floating piles in soil with parabolically increasing elastic modulus

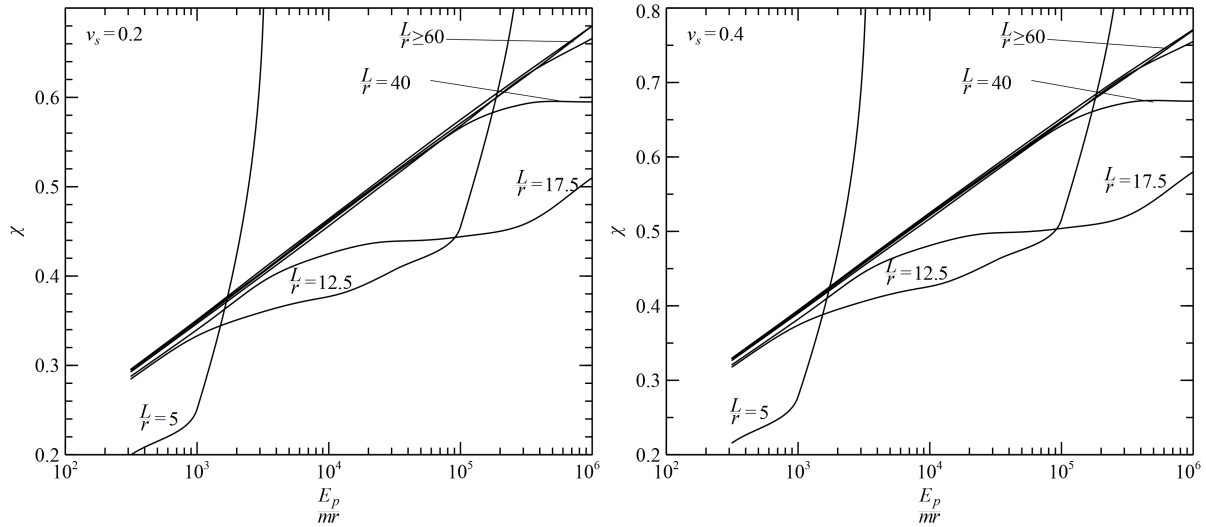

Figure 4.8: Variation of the calibration factor with respect to the relative stiffness for free-head fixed-base piles in soil with parabolically increasing elastic modulus

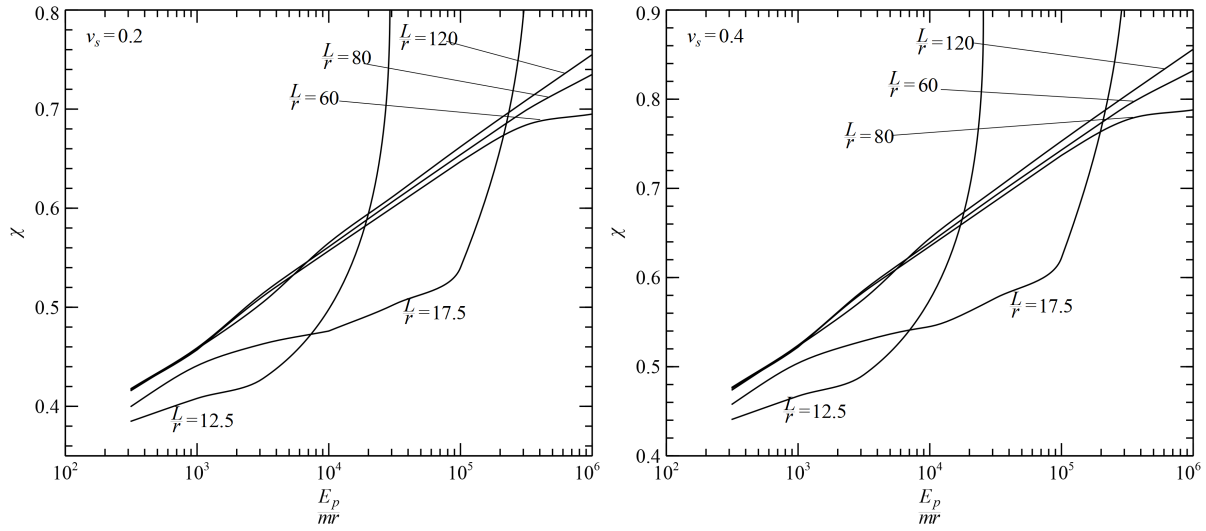

Figure 4.9: Variation of the calibration factor with respect to the relative stiffness for fixed-head free-base piles in soil with parabolically increasing elastic modulus

4.2 Effect of pile slenderness ratio

As noted in Section 2.1.3, an increase in the slenderness ratio is accompanied by the piles response being less affected by the pile base condition. Furthermore, the pile response becomes practically independent of the slenderness ratio beyond a critical value, $\left(\frac{L}{r}\right)_{cr}$, the critical slenderness ratio (Gazetas 1991; Guo and Lee 2001; Syngros 2004; Higgins et al. 2013).

Figures 4.10 and 4.11 present the variation of the calibration factor with respect to the pile slenderness ratio for linearly increasing elastic modulus. The plots are for the range of $5 \leq \frac{L}{r} \leq 20$. The calibration factor increases with the slenderness ratio up to a threshold value. Beyond this range (not shown in the figures) the calibration factor become independent of the slenderness ratio as observed by the converging curves of Figures 4.2 - 4.5 from the previous subsection.

It is also to be noted that within this range, the calibration factor increases indefinitely for fixed-base piles, though as the slenderness ratio increases, finite values independent of the $\frac{L}{r}$ and equivalent to the values for floating piles are obtained, as presented in Figures 4.4, 4.5, 4.8 and 4.9.

Expressions for the threshold slenderness ratio are proposed through the use of curve

fitting and are given by:

$$\left(\frac{L}{r}\right)_{tr} = 3.13\left(\frac{E_p}{mr}\right)^{0.21} \tag{4.9}$$

for free-head floating piles and

$$\left(\frac{L}{r}\right)_{tr} = 3.86\left(\frac{E_p}{mr}\right)^{0.205} \tag{4.10}$$

for fixed-head floating piles.

For fixed-head piles values for $\left(\frac{L}{r}\right)_{tr}$were found to be similar to their free-head counterparts with differences between the two being under 3%.

The plots of the calibration factor at different relative stiffness converge to a single curve as the relative stiffness increases. This is concurrent with the independence of the calibration factor with respect to $\frac{E_p}{mr}$ for short rigid piles as observed in the previous section.

Expressions for the convergent curves is given by:

$$\chi = (0.09 + 0.05\nu_s)\left(\frac{L}{r}\right)^{0.48} \tag{4.11}$$

for free-head piles and,

$$\chi = (0.28 + 0.26\nu_s)\left(\frac{L}{r}\right)^{0.20} \tag{4.12}$$

for fixed-head piles.

Equation (4.11) when used with the corresponding expressions for the pile response, provide pile head displacement values within 7.6% of those obtained using finite element analysis with the exception that for $\frac{L}{r} < 10$ the deviation grows to 19.3%. In such cases, a more precises expression is proposed (4.13), where the deviation diminishes to 3.8%.

$$\chi = -0.003509 + 0.03738\frac{L}{r} + 0.001237\nu_s - 0.001255\left(\frac{L}{r}\right)^2 + 0.02105\nu_s\frac{L}{r} + 1.59\times10^{-5}\left(\frac{L}{r}\right)^3 - 0.0003582\nu_s\left(\frac{L}{r}\right)^2 \quad (4.13)$$

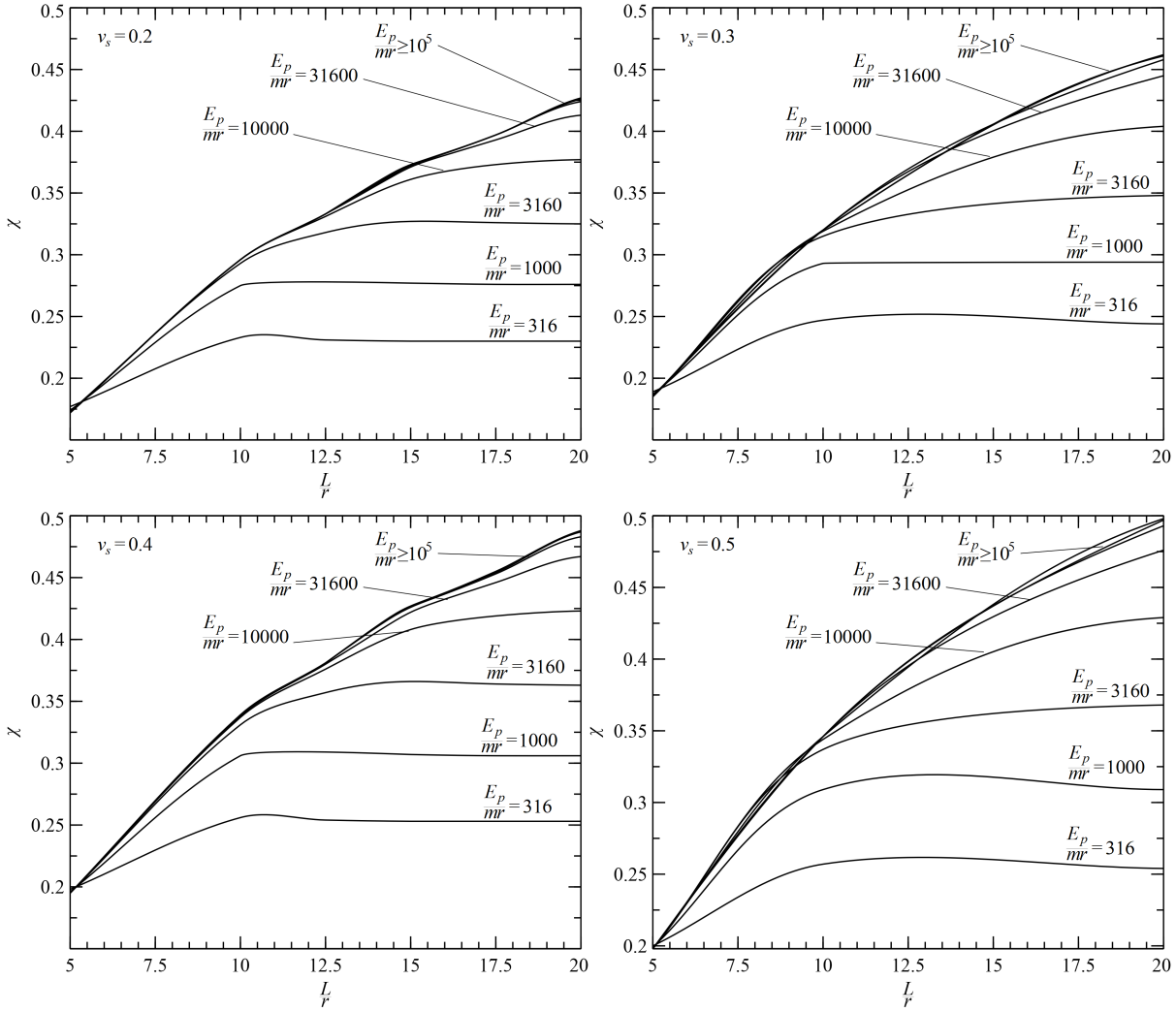

Figure 4.10: Variation of the calibration factor with respect to slenderness ratio for free-head floating piles in soil profile with linearly increasing elastic modulus

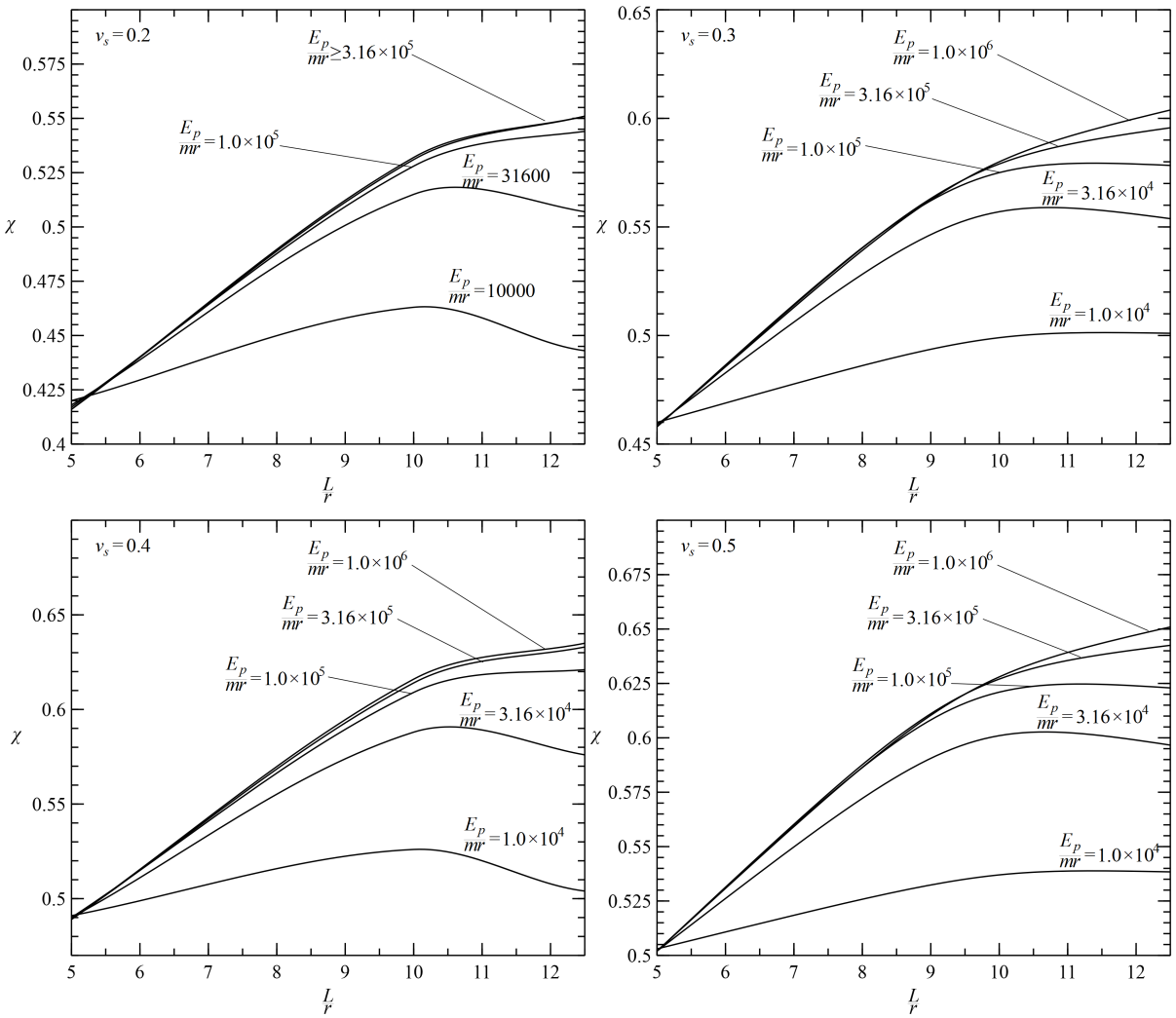

Figure 4.11: Variation of the calibration factor with respect to slenderness ratio for fixed-head floating piles in soil profile with linearly increase elastic modulus

The relationship between $\frac{L}{r}$ and χ for parabolically increasing elastic modulus is also very similar to that of the linearly increasing elastic modulus. For the range of $5 \leq \frac{L}{r} \leq 20$, plots are given showing the variation of the calibration factor with respect to the slenderness ratio for floating piles (Figures 4.12 and 4.13). Beyond this range the calibration factor gradually becomes independent of the slenderness ratio (resulting in the converging curves of Figures 4.6 - 4.9). The threshold values beyond which the calibration factor becomes independent of $\frac{L}{r}$ are given by:

$$\left(\frac{L}{r}\right)_{tr} = 3.61\left(\frac{E_p}{mr}\right)^{0.22} \tag{4.14}$$

for free-head floating piles and

$$\left(\frac{L}{r}\right)_{tr} = 4.34\left(\frac{E_p}{mr}\right)^{0.23} \tag{4.15}$$

for fixed-head floating piles. Threshold values for fixed-base piles was also found to be similar to that of floating piles.

Similarly, within this range (i.e. $5 \leq \frac{L}{r} \leq 20$,) as the relative stiffness increases the plots of the calibration factor converge to a single curve. Expressions for these convergent curves are given by:

$$\chi = (0.08 + 0.05\nu_s)\left(\frac{L}{r}\right)^{0.56} \tag{4.16}$$

for free-head piles and,

$$\chi = (0.25 + 0.18\nu_s)\left(\frac{L}{r}\right)^{0.26} \tag{4.17}$$

for fixed head piles.

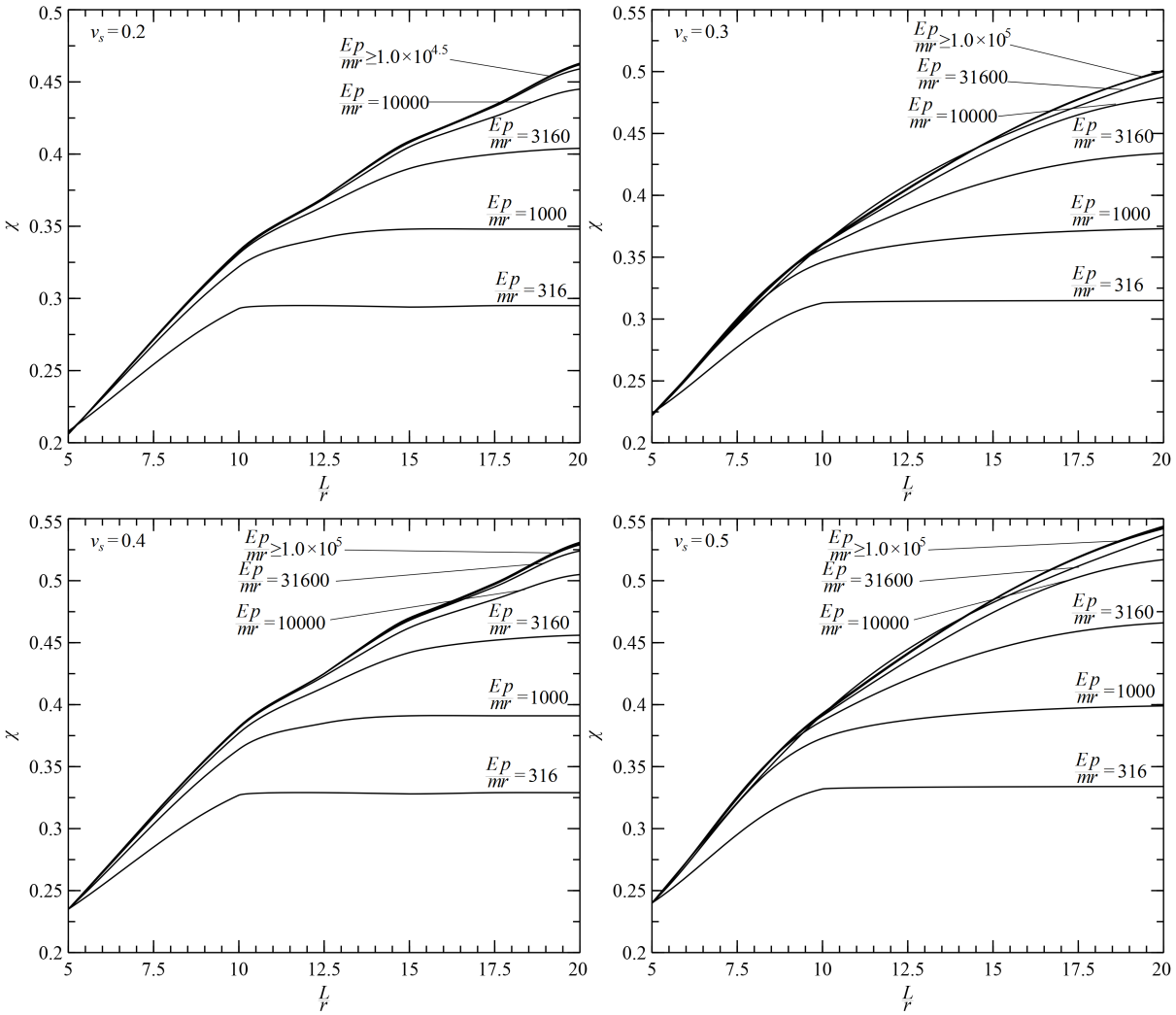

Figure 4.12: Variation of calibration factor with respect to the slenderness ratio for free-head floating piles in soil with parabolically increasing elastic modulus

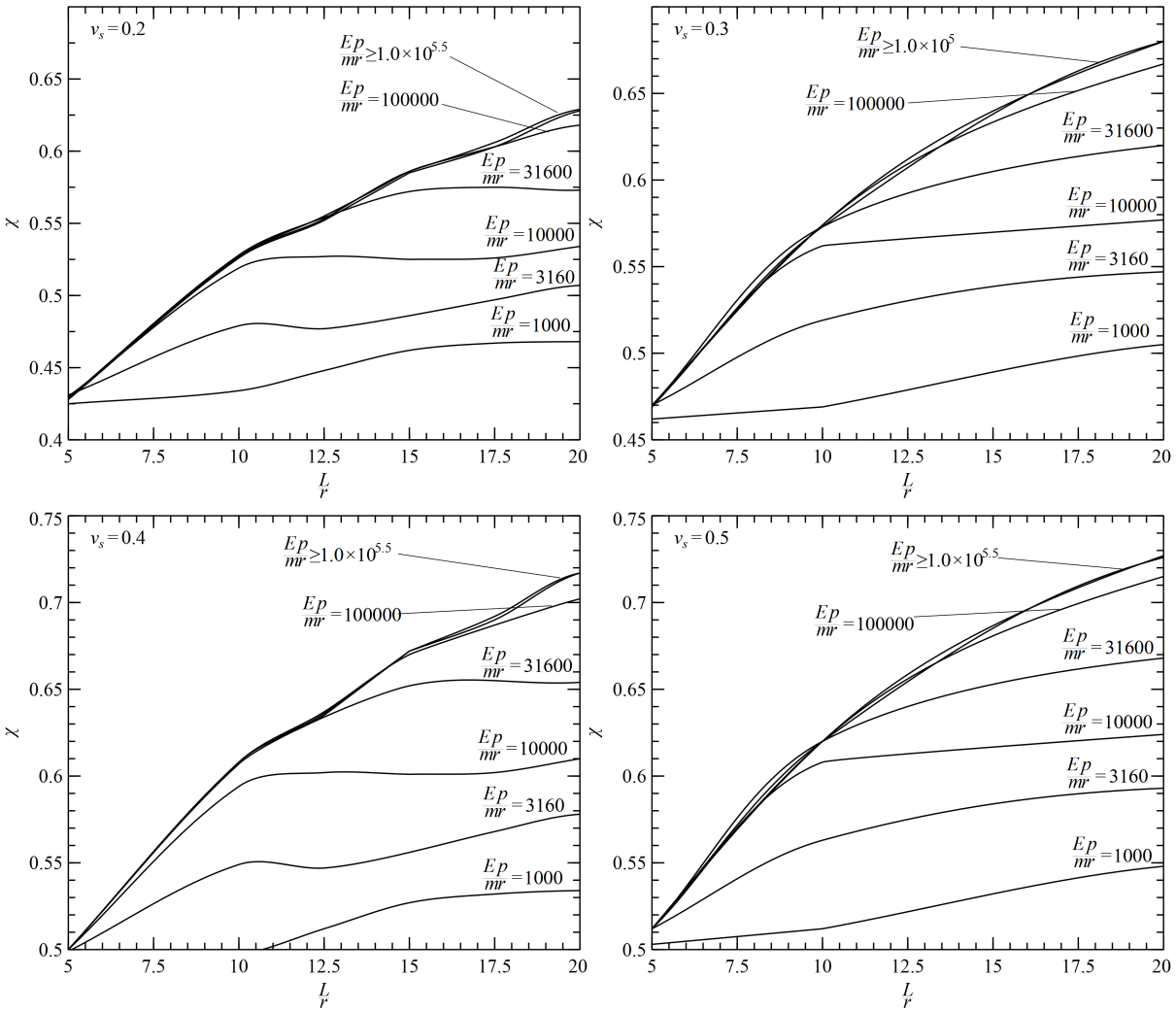

Figure 4.13: Variation of the calibration factor with respect to the slenderness ratio for fixed-head floating piles in soil with parabolically increasing elastic modulus

4.3 Effect of the soil Poisson's ratio

With respect to the calibration factor, the Poisson's ratio of the soil is the least significant. This is in line with the influence of the Poisson's ratio on the pile response reported in the literature.

Referring to the coefficients of the Poisson's ratio in (4.3), (4.4), (4.11) and (4.12), it is evident that the Poisson's ratio is relatively more influential in fixed-head piles than in free-head ones.

Figure 4.14 presents the variation of the calibration factor with respect to the Poisson's

ratio for two selected slenderness ratio values of fixed-head floating piles. The calibrations factor increases with the Poisson's ratio irrespective of other parameters; although, the largest increases are observed at high relative stiffness ratios.

It is to be noted that the threshold values for the calibration factor (Equations 4.1, 4.4, 4.9 and 4.10) are independent of the Poisson's ratio.

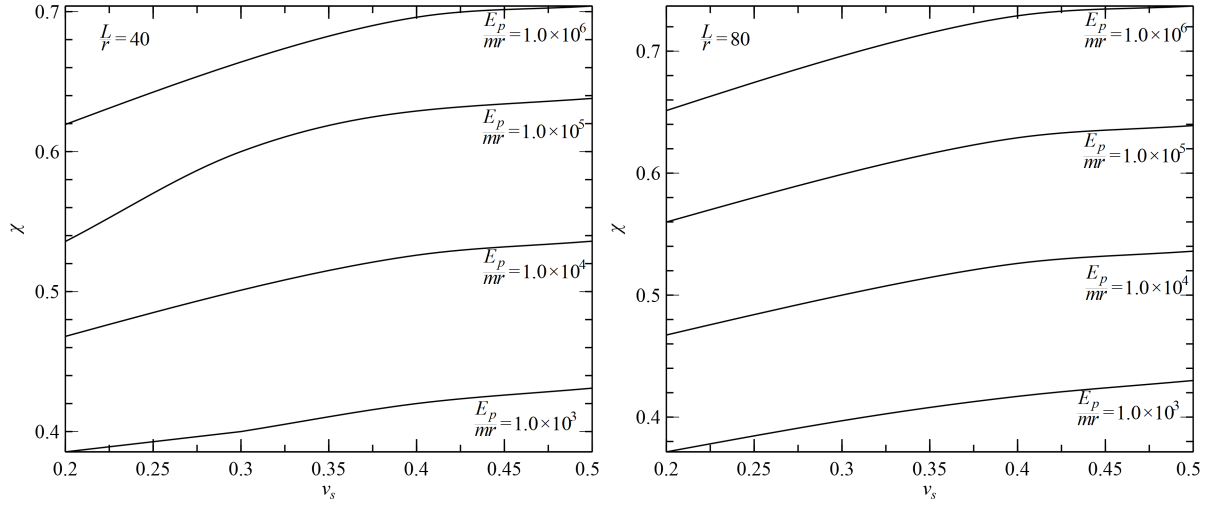

Figure 4.14: Variation of the calibration factor with respect to the soil Poisson's ratio for fixed-head floating piles in soil profile with linearly increase elastic modulus

4.4 Effect of pile end condition

The effects of the pile end conditions on the calibration factor, for the most part, have already been discussed in the previous subsections but for the sake of completeness, they are summarized here.

- The most observable effect of the pile end conditions is for the case of fixed-base short rigid piles. Such piles practically will not exhibit displacement; hence, the calibration factor increases indefinitely.
- For piles with $\frac{L}{r} \geq 60$ in soils with linearly increasing modulus and for piles with $\frac{L}{r} \geq 80$ in soils with parabolically varying modulus, the calibration factor is independent of the pile base condition.
- For a given Poisson's ratio, relative stiffness and slenderness ratio, the calibration

factor for fixed-head piles is larger than their free-head counterparts.

4.5 Comparison of calibration factor threshold values with critical slenderness ratio and critical relative stiffness

From the discussion in the previous sections, it is evident that the calibration factor mirrors the characteristics of the pile response reported in literature; specially, the pile head displacement. The calibration factor like the pile head displacement shows independence to the relative stiffness as $\frac{E_p}{mr}$ increases. Furthermore, as the slenderness ratio increases, the calibration factor like the pile head displacement, becomes independent of $\frac{L}{r}$. The boundaries where pile head displacement becomes independent of these quantities indicate critical values beyond which a pile behave as long and flexible, $\left(\frac{L}{r}\right)_{cr}$ or short and rigid $\left(\frac{E_p}{mr}\right)_{cr}$.

Figure 4.15 compares critical values reported in the literature with threshold values determined from the calibration factor for free-head floating piles embedded in soils with linearly increasing elastic modulus. It is evident that the expression for the threshold value in Equation (4.9) is similar to that of the critical (active) slenderness ratio. The threshold expression can thus be interpreted as an estimation of the critical slenderness ratio. Therefore, Equation (4.3) can be thought of as the calibration factor for long flexible free-head floating piles.

Similarly, (4.1) is compared against published expressions for the critical relative stiffness. The comparison is not as conclusive as the former, with the boundary for short rigid piles being larger than the threshold values in (4.1) by a full logarithmic cycle. The plot compares the expressions in (2.27) and (4.1). The difference between these two expressions is mainly in the coeffcients in which the coefficent in former is approximatly five times the latter.

Figure 4.16 compares the threshold values with the critical values for fixed-head floating piles in soil with linearly increasing elastic modulus. In comparing the critical relative

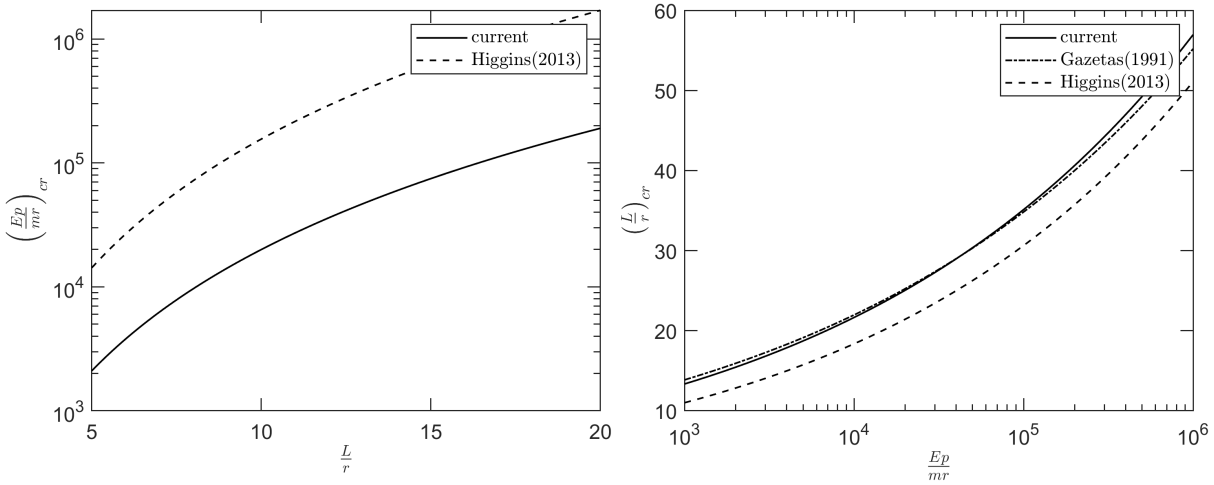

Figure 4.15: Comparison of calibration factor threshold with published expressions for critical relative stiffness (left) and critical pile length (right) for free-head floating piles in soil profile with linearly increasing elastic modulus

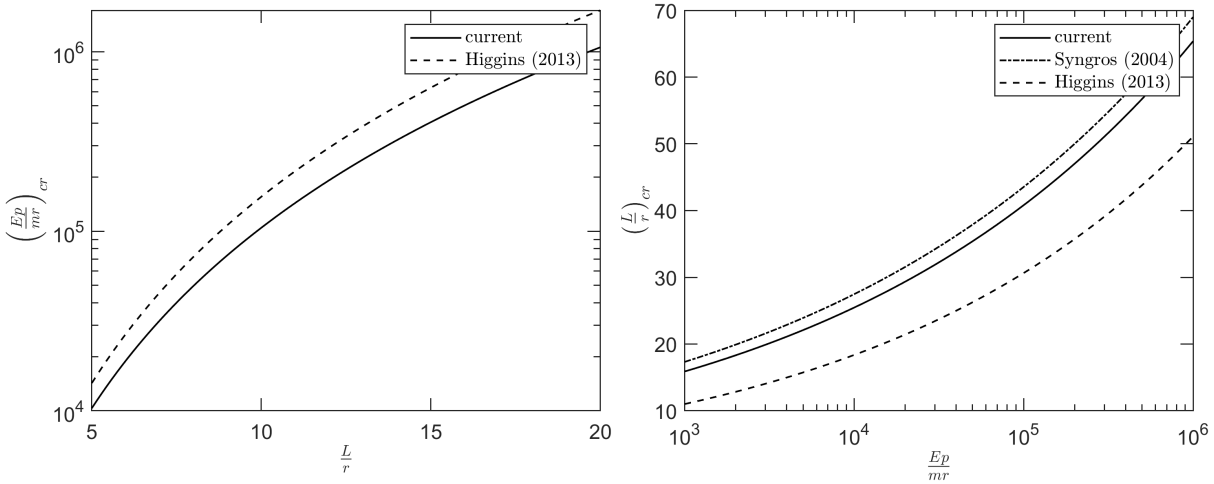

Figure 4.16: Comparison of calibration factor threshold with published expressions for critical relative stiffness (left) and critical pile length (right) for fixed-head floating piles in soil profile with linearly increase elastic modulus

stiffness presented by Higgins et al. (2013) with those of the threshold values, the curves compare well, unlike the previous case. For the threshold slenderness ratio while the plot shows more deviation across the curves, the threshold value from the current work compares well with Syngros (2004).

The comparison with Higgins et al. (2013) in both cases is less than satisfactory, especially the comparisons for critical relative stiffness for free-head piles. It is to be remembered that when validating FEM results similar difference were noted between the FEM results and normalized pile head displacements reported by the Higgins et al. (2013). But in those cases the largest differences were associated with fixed-head piles. A possible explanation

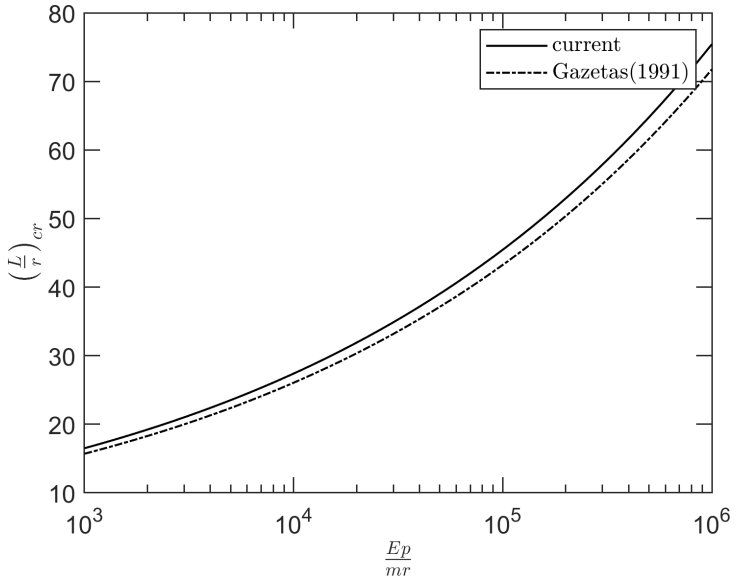

Figure 4.17: Comparison of calibration factor threshold with published expressions for critical pile length for free-head floating piles in soil profile with parabolically varying elastic modulus

put forward based on a limited FEM study pointed to the fact that the boundary distance used in the finite element modeling of Higgins et al. (2013) may not have been enough, see Section 3.4.6.

Nevertheless, one is justified in interpreting the threshold values as critical values, especially the thresholds in (4.9) and (4.10) can be considered to be estimations of the critical slenderness ratio and the associated calibration factors can be considered calibration factors for long flexible piles.

Likewise, for the case of piles embedded in soil with parabolically varying elastic modulus, the threshold slenderness ratio of free-head floating piles also compares well with the critical relative slenderness ratio reported by Gazetas (1991), see Figure 4.17.

4.6 Validation of model calibration

As pointed out above, model calibration process was conducted by equating the pile head displacement from finite element analysis to that of the beam-on-Pasternak foundation analysis. Therefore, the pile head response obtained from the calibrated models must match the finite element results. In this regard, a representative range of pile and soil

parameters from the set used to calibrate the model were selected and used to analyze the static pile responses using the two methods. Table ?? and ?? present the percentage deviation of the results of the calibrated model from the finite element analysis.

The mean deviation in all cases is below 4% while the maximum deviation reaches 10% for long flexible free-head floating piles. Whilst, the latter value is significant, over all, the mean deviations are considerably small. Therefore, one can conclude that the calibrated model predicts the pile head displacement within an average value of less than 4%.

Table 4.1: Validation of model calibration for piles embedded in soil with linearly increasing elastic modulus

Pile Type	% Min. Abs. Dev.	% Max. Abs. Dev.	% Mean Abs. Dev.
FHFB[1] $\frac{E_p}{mr} > 11.24\left(\frac{L}{r}\right)^{3.25}$	0.01	2.84	1.27
FHFB $\frac{L}{r} > 3.13\left(\frac{E_p}{mr}\right)^{0.21}$	0.49	10.45	3.53
FxHFxB $\frac{E_p}{mr} > 47.8\left(\frac{L}{r}\right)^{3.34}$	0.02	2.40	1.14
FxHFxB $\frac{L}{r} > 3.49\left(\frac{E_p}{mr}\right)^{0.21}$	0.03	5.61	1.31

Table 4.2: Validation of model calibration for piles embedded in soil with parabolically increasing elastic modulus

Pile Type	% Min. Abs. Dev.	% Max. Abs. Dev.	% Mean Abs. Dev.
FHFB $\frac{E_p}{mr} > 3.56\left(\frac{L}{r}\right)^{3.25}$	0.1	6.62	3.39
FHFB $\frac{L}{r} > 3.61\left(\frac{E_p}{mr}\right)^{0.22}$	0.02	7.23	2.86
FxHFxB $\frac{E_p}{mr} > 21.46\left(\frac{L}{r}\right)^{3.07}$	0.002	2.97	1.32
FxHFxB $\frac{L}{r} > 4.34\left(\frac{E_p}{mr}\right)^{0.23}$	0.02	3.78	1.70

Figures 4.18 and 4.19 show the displacement profiles from the finite element and beam-on-Pasternak subgrade analysis using the calibration factor obtained above. As noted, at the pile head, the two solutions are in good agreement, but the beam-on-Pasternak subgrade solution does not match the finite element solution across the full pile length. For example, in Figure 4.18 for short rigid free head piles (a) the difference at the pile base is 11.8% of the total displacement at the pile head. For long flexible free-head piles (b), the difference in displacement profile is not as significant and maximum deviation occurs at the zone of maximum curvature which implies some difference in bending moment as

[1]validation done using (4.13)

well. Direct estimation of differences in bending moment is not possible as 3D volumetric elements were used in the finite element analysis.

For short rigid fixed-head piles, Figure 4.19 (a), the difference in pile displacement is almost constant with depth . This may be due to the relatively small displacement in short fixed-head piles (note the horizontal scale). For long flexible fixed-head piles, Figure 4.19 (b), similar to their free-head counterparts, the largest difference between FEM and beam-on-Pasternak subgrade analysis occurs at the point of high curvature.

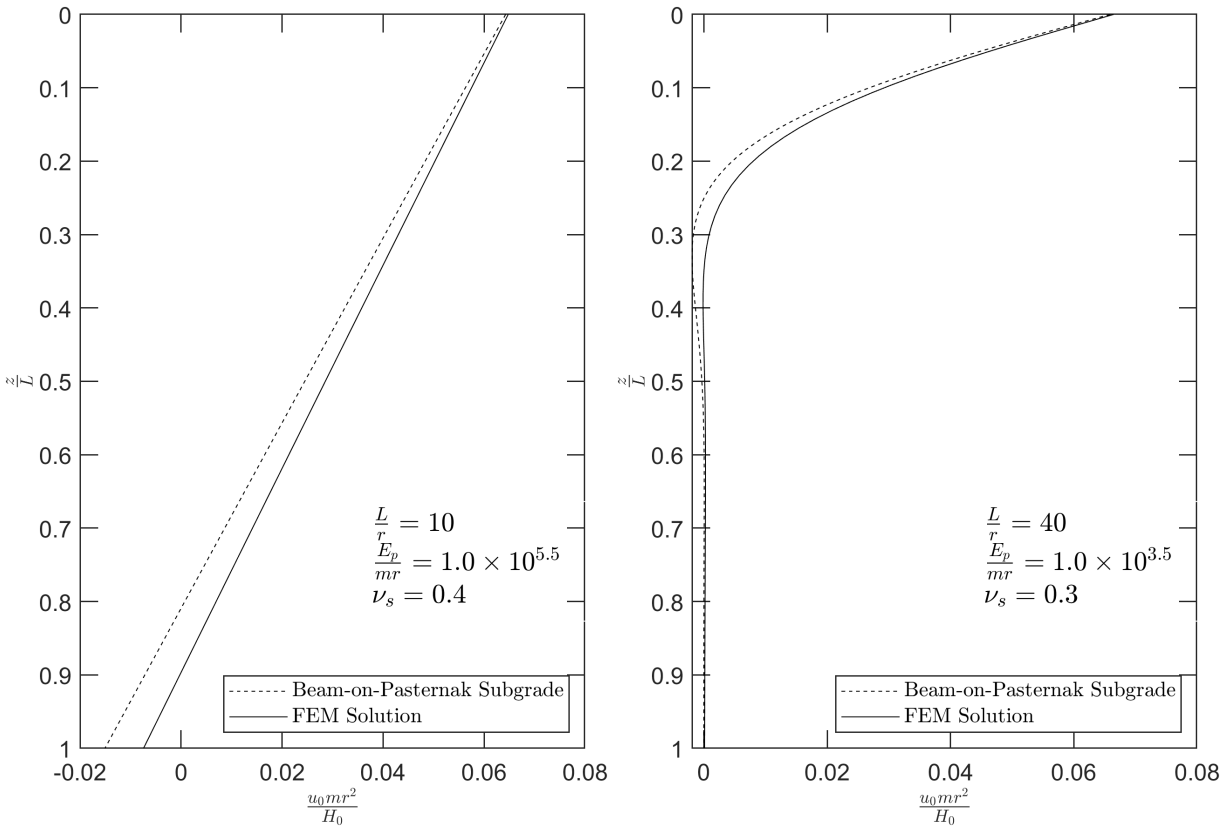

(a) Short rigid (b) long flexible

Figure 4.18: Comparison of pile displacement profile for free-head floating piles embedded in soil with linearly increasing elastic modulus

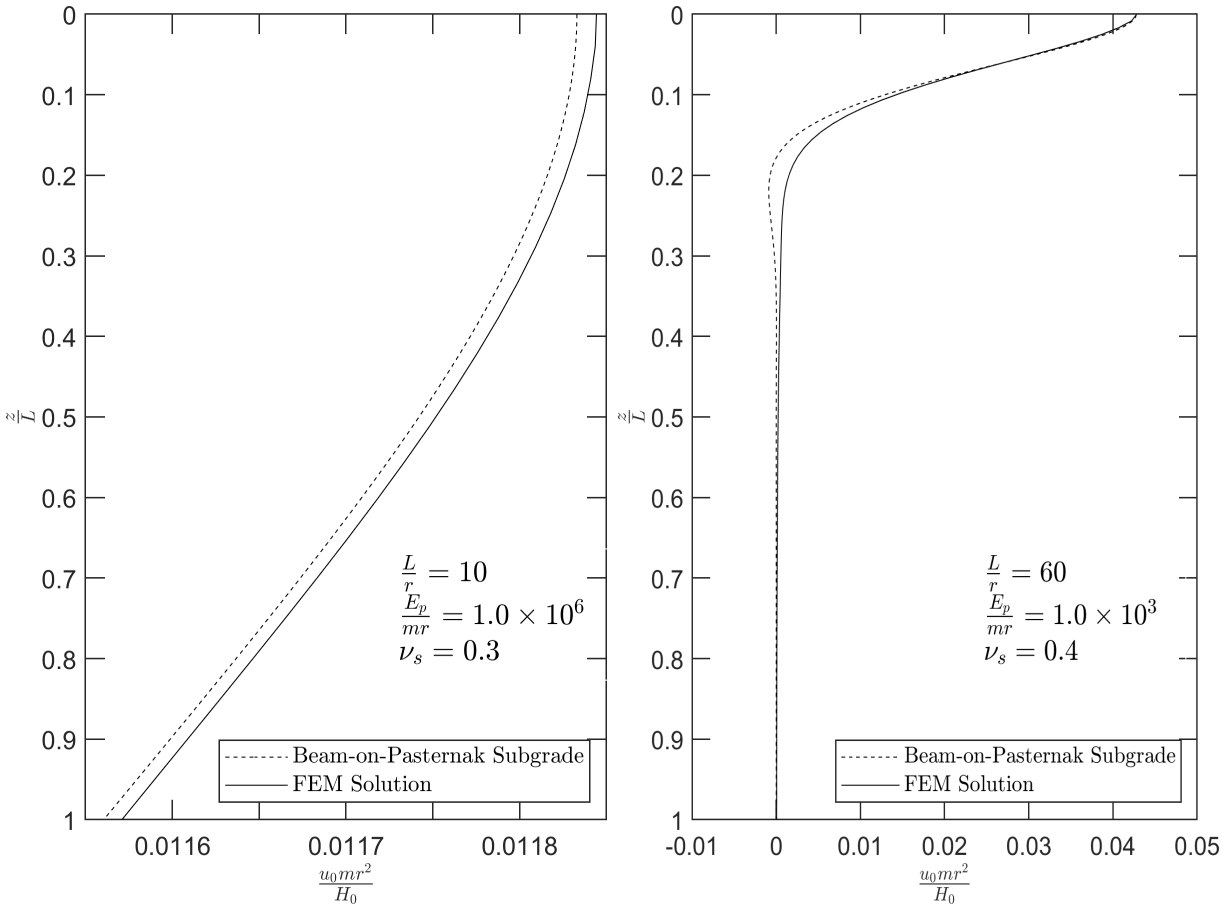

(a) Short rigid (b) long flexible

Figure 4.19: Comparison of pile displacement profile for fixed-head floating piles embedded in soil with linearly increasing elastic modulus

4.7 Calibrated subgrade parameters

Using equations developed for the calibration factors, expressions for the parameters of the Kerr-equivalent Pasternak subgrade model are given for different cases.

4.7.1 Piles embedded in soils with linearly increasing elastic modulus

4.7.1.1 Free-head floating piles

for long flexible piles, i.e. $\frac{L}{r} > 3.13 \left(\frac{E_p}{mr}\right)^{0.21}$:

$$K_p(z) = \left[\frac{0.4\nu_s + 0.67}{0.06\nu_s + 0.12} mr \left(\frac{E_p}{mr}\right)^{-0.11}\right] \frac{z}{r} \tag{4.18}$$

$$G_P(z) = \left[\frac{(2.72\nu_s + 4.56)(0.06\nu_s + 0.12)}{1 + \nu_s} mr^3 \left(\frac{E_p}{mr}\right)^{0.11}\right] \frac{z}{r} \tag{4.19}$$

and for short rigid piles, i.e. $\frac{E_p}{mr} > 11.24 \left(\frac{L}{r}\right)^{3.25}$:

$$K_p(z) = \left[\frac{0.4\nu_s + 0.67}{0.05\nu_s + 0.09} mr \left(\frac{L}{r}\right)^{-0.48}\right] \frac{z}{r} \tag{4.20}$$

$$G_P(z) = \left[\frac{(2.72\nu_s + 4.56)\,(0.05\nu + 0.09)}{1 + \nu_s} mr^3 \left(\frac{L}{r}\right)^{0.3}\right] \frac{z}{r} \tag{4.21}$$

As noted in section 4.2 for a more precise estimation, especially when $\frac{L}{r} < 10$ Equation (4.13) should be used for short rigid piles. The expressions above can be simplified for practical use by fitting a simpler expression to the terms involving the Poisson's ratio over the range of $0.2 \leq \nu_s \leq 0.5$. This gives:

for long flexible piles, i.e. $\frac{L}{r} > 3.13 \left(\frac{E_p}{mr}\right)^{0.21}$:

$$K_p(z) = \left[(0.39\nu_s + 5.61)\, mr \left(\frac{E_p}{mr}\right)^{-0.11}\right] \frac{z}{r} \tag{4.22}$$

$$G_P(z) = \left[(0.10\nu_s + 0.54)\, mr^3 \left(\frac{E_p}{mr}\right)^{0.11}\right] \frac{z}{r} \tag{4.23}$$

and for short rigid piles, i.e. $\frac{E_p}{mr} > 11.24 \left(\frac{L}{r}\right)^{3.25}$:

$$K_p(z) = \left[(0.22\nu_s + 7.46)\, mr \left(\frac{L}{r} \right)^{-0.48} \right] \frac{z}{r} \tag{4.24}$$

$$G_P(z) = \left[(0.095\nu_s + 0.41)\, mr^3 \left(\frac{L}{r} \right)^{0.3} \right] \frac{z}{r} \tag{4.25}$$

4.7.1.2 Fixed-head floating piles

for long flexible piles, i.e. $\frac{L}{r} > 3.49 \left(\frac{E_p}{mr} \right)^{0.21}$:

$$K_p(z) = \left[\frac{0.4\nu_s + 0.67}{0.11\nu_s + 0.2} mr \left(\frac{E_p}{mr} \right)^{-0.08} \right] \frac{z}{r} \tag{4.26}$$

$$G_P(z) = \left[\frac{(2.72\nu_s + 4.56)(0.11\nu_s + 0.2)}{1 + \nu_s} mr^3 \left(\frac{E_p}{mr} \right)^{0.08} \right] \frac{z}{r} \tag{4.27}$$

and for short rigid piles, i.e. $\frac{E_p}{mr} > 47.8 \left(\frac{L}{r} \right)^{3.34}$:

$$K_p(z) = \left[\frac{0.4\nu_s + 0.67}{0.26\nu_s + 0.28} mr \left(\frac{L}{r} \right)^{-0.20} \right] \frac{z}{r} \tag{4.28}$$

$$G_P(z) = \left[\frac{(2.72\nu_s + 4.56)\,(0.26\nu + 0.28)}{1 + \nu_s} mr^3 \left(\frac{L}{r} \right)^{0.20} \right] \frac{z}{r} \tag{4.29}$$

similarly, fitting simpler expressions, for long flexible piles, i.e. $\frac{L}{r} > 3.49 \left(\frac{E_p}{mr} \right)^{0.21}$:

$$K_p(z) = \left[(0.11\nu_s + 3.36)\, mr \left(\frac{E_p}{mr} \right)^{-0.08} \right] \frac{z}{r} \tag{4.30}$$

$$G_P(z) = \left[(0.21\nu_s + 0.90)\, mr^3 \left(\frac{E_p}{mr} \right)^{0.08} \right] \frac{z}{r} \tag{4.31}$$

and for short rigid piles, i.e. $\frac{E_p}{mr} > 47.8 \left(\frac{L}{r} \right)^{3.34}$:

$$K_p(z) = \left[(-0.45\nu_s + 2.34)\, mr \left(\frac{L}{r}\right)^{-0.20} \right] \frac{z}{r} \tag{4.32}$$

$$G_P(z) = \left[(0.69\nu_s + 1.27)\, mr^3 \left(\frac{L}{r}\right)^{0.20} \right] \frac{z}{r} \tag{4.33}$$

4.7.1.3 Fixed-base piles

As noted previously, the calibration factor for short rigid fixed-base piles increases indefinitely, while the calibration factors and the associated thresholds for long flexible piles are the same as those for floating piles. Thus, the expressions developed above for $\frac{L}{r} > \left(\frac{L}{r}\right)_{cr}$ can also be used for fixed-base piles embedded in soils with linearly increasing elastic modulus.

4.7.2 Piles embedded in soils with parabolically varying elastic modulus

4.7.2.1 Free-head floating piles

for long flexible piles, i.e. $\frac{L}{r} > 3.61 \left(\frac{E_p}{mr}\right)^{0.22}$:

$$K_p(z) = \left[\frac{0.4\nu_s + 0.67}{0.09\nu_s + 0.17} mr \left(\frac{E_p}{mr}\right)^{-0.10} \right] \left(\frac{z}{r}\right)^{0.5} \tag{4.34}$$

$$G_P(z) = \left[\frac{(2.72\nu_s + 4.56)(0.09\nu_s + 0.17)}{1 + \nu_s} mr^3 \left(\frac{E_p}{mr}\right)^{0.10} \right] \left(\frac{z}{r}\right)^{0.5} \tag{4.35}$$

and for short rigid piles, i.e. $\frac{E_p}{mr} > 3.56 \left(\frac{L}{r}\right)^{3.25}$:

$$K_p(z) = \left[\frac{0.4\nu_s + 0.67}{0.05\nu_s + 0.08} mr \left(\frac{L}{r}\right)^{-0.56}\right] \left(\frac{z}{r}\right)^{0.5} \tag{4.36}$$

$$G_P(z) = \left[\frac{(2.72\nu_s + 4.56)\,(0.05\nu + 0.08)}{1 + \nu_s} mr^3 \left(\frac{L}{r}\right)^{0.56}\right] \left(\frac{z}{r}\right)^{0.5} \tag{4.37}$$

likewise, fitting simpler expressions, for long flexible piles, i.e. $\frac{L}{r} > 3.61 \left(\frac{E_p}{mr}\right)^{0.22}$:

$$K_p(z) = \left[(0.19\nu_s + 3.95)\, mr \left(\frac{E_p}{mr}\right)^{-0.10}\right] \left(\frac{z}{r}\right)^{0.5} \tag{4.38}$$

$$G_P(z) = \left[(0.16\nu_s + 0.77)\, mr^3 \left(\frac{E_p}{mr}\right)^{0.10}\right] \left(\frac{z}{r}\right)^{0.5} \tag{4.39}$$

and for short rigid piles, i.e. $\frac{E_p}{mr} > 3.56 \left(\frac{L}{r}\right)^{3.25}$:

$$K_p(z) = \left[(-0.16\nu_s + 8.36)\, mr \left(\frac{L}{r}\right)^{-0.56}\right] \left(\frac{z}{r}\right)^{0.5} \tag{4.40}$$

$$G_P(z) = \left[(0.11\nu_s + 0.36)\, mr^3 \left(\frac{L}{r}\right)^{0.56}\right] \left(\frac{z}{r}\right)^{0.5} \tag{4.41}$$

4.7.2.2 Fixed-head floating piles

for long flexible piles, i.e. $\frac{L}{r} > 4.34 \left(\frac{E_p}{mr}\right)^{0.23}$:

$$K_p(z) = \left[\frac{0.4\nu_s + 0.67}{0.15\nu_s + 0.27} mr \left(\frac{E_p}{mr}\right)^{-0.07}\right] \left(\frac{z}{r}\right)^{0.5} \tag{4.42}$$

$$G_P(z) = \left[\frac{(2.72\nu_s + 4.56)(0.15\nu_s + 0.27)}{1 + \nu_s} mr^3 \left(\frac{E_p}{mr}\right)^{0.07}\right] \left(\frac{z}{r}\right)^{0.5} \tag{4.43}$$

and for short rigid piles, i.e. $\frac{E_p}{mr} > 21.46 \left(\frac{L}{r}\right)^{3.07}$:

$$K_p(z) = \left[\frac{0.4\nu_s + 0.67}{0.18\nu_s + 0.25} mr \left(\frac{L}{r}\right)^{-0.26}\right] \left(\frac{z}{r}\right)^{0.5} \tag{4.44}$$

$$G_P(z) = \left[\frac{(2.72\nu_s + 4.56)(0.18\nu_s + 0.25)}{1 + \nu_s} mr^3 \left(\frac{L}{r}\right)^{0.26}\right] \left(\frac{z}{r}\right)^{0.5} \tag{4.45}$$

similarly, fitting simpler expressions, for long flexible piles, i.e. $\frac{L}{r} > 4.34 \left(\frac{E_p}{mr}\right)^{0.23}$:

$$K_p(z) = \left[(0.07\nu_s + 2.49)\, mr \left(\frac{E_p}{mr}\right)^{-0.07}\right] \left(\frac{z}{r}\right)^{0.5} \tag{4.46}$$

$$G_P(z) = \left[(0.29\nu_s + 1.22)\, mr^3 \left(\frac{E_p}{mr}\right)^{0.07}\right] \left(\frac{z}{r}\right)^{0.5} \tag{4.47}$$

and for short rigid piles, i.e. $\frac{E_p}{mr} > 21.46 \left(\frac{L}{r}\right)^{3.07}$:

$$K_p(z) = \left[(-0.21\nu_s + 2.66)\, mr \left(\frac{L}{r}\right)^{-0.26}\right] \left(\frac{z}{r}\right)^{0.5} \tag{4.48}$$

$$G_P(z) = \left[(0.42\nu_s + 1.13)\, mr^3 \left(\frac{L}{r}\right)^{0.26}\right] \left(\frac{z}{r}\right)^{0.5} \tag{4.49}$$

4.7.2.3 Fixed-base piles

Correspondingly, the expressions developed above for $\frac{L}{r} > \left(\frac{L}{r}\right)_{cr}$ can be used for fixed base piles embedded in soil with parabolically increasing elastic modulus, while the calibration factor increases indefinitely for $\frac{E_p}{mr} > \left(\frac{E_p}{mr}\right)_{cr}$.

Chapter 5

Static Pile Response

The beam-on-Pasternak subgrade analysis (Section 3.5) is used alongside the Kerr-equivalent Pasternak subgrade model in order to initially determine the calibration factor (Chapter 4). The current chapter employs the calibrated model to evaluate the static response of a single pile in soils with linearly and parabolically increasing elastic modulus. The investigation is done for all cases of the pile end condition and for both long flexible and short rigid piles.

The primary means of representing the static pile response is through the pile head stiffness coefficients (or equivalently the pile head flexibility influence coefficients). The pile head stiffness coefficients represent the lateral load or moment required for a unit displacement or rotation at the pile head.

The pile head response may be expressed in terms of pile flexibility as:

$$u_0 = \frac{I_{HH}}{mr^2} H_0 + \frac{I_{HM}}{mr^3} M_0 \tag{5.1}$$

$$\theta_0 = \frac{I_{MH}}{mr^3} H_0 + \frac{I_{MM}}{mr^4} M_0 \tag{5.2}$$

for free-head piles and,

$$u_0 = \frac{I_{HH}}{mr^2} H_0 \tag{5.3}$$

for fixed-head piles.

where I_{HH}, I_{HM}, I_{MH}, I_{MM} are dimensionless flexibility influence factors. Note that from Betti's reciprocal theorem $I_{HM} = I_{MH}$.

Equivalently, one may also use stiffness based expressions:

$$H_0 = K_{HH} u_0 + K_{MH} \theta_0 \tag{5.4}$$

$$M_0 = K_{HM} u_0 + K_{MM} \theta_0 \tag{5.5}$$

for free-head piles and,

$$H_0 = K_{HH} u_0 \tag{5.6}$$

for fixed-head piles

where K_{HH}, K_{HM}, K_{MH}, K_{MM} are stiffness coefficients. Note that expressions (5.4) - (5.6) are can be obtained by inverting (5.1) - (5.3).

The pile head flexibility coefficients are evaluated by first computing the pile head displacement for a given pile head load H_0 with $M_0 = 0$ for evaluating $I_{HH}$and I_{MH} and for a given M_0 with $H_0 = 0$ for evaluating $I_{HM}$and I_{MH}. The pile head displacements are computed using the beam-on-Pasternak subgrade analysis and associated solution methods stated in Section 3.5. The computation is done for each 2176 combination of parameters that was used in formulating the calibration factor. This is done using MATLAB (2022) scripts. The script is made available at the author's GitHub page at https://github.com/MathewosEnd/Response-of-Laterally-Loaded-piles-in-Kerr-Equivalent-Pasternak-subgrade.

The pile head displacements are then used to compute the flexibility influence coefficients

using Equations (5.1) - (5.3). Each group of coefficients (i.e. 272 data points for pile end condition and non-homogeneity type) are used to formulate expression through the use of curve fitting. The curve fitting is done using MATLAB's curve fitting toolbox.

In the discussion to follow, the best fit expressions are presented. Furthermore, the expressions are inverted to formulate stiffness coefficients. It should be emphasized that restrictions on the applicability of the expressions developed for the calibration factors in terms of long and short piles (i.e., critical relative stiffness and critical slenderness ratio) are also applicable to the expressions developed in this section. For examples, for free head floating piles in soil with linearly increasing elastic modulus, using expressions (4.18) and (4.19) developed for $\frac{L}{r} > \left(\frac{L}{r}\right)_{tr} \left(= 3.13 \left(\frac{E_p}{mr}\right)^{0.21}\right)$ would result in pile head responses independent of the pile slenderness ratio and pile base conditions. Since, as demonstrated in section 4.5, the threshold for applicability of this expression does also represent the critical pile slenderness ratio delineating long flexible piles from transitional and short rigid piles.

5.1 Piles Embedded in soil with linearly increasing elastic modulus

5.1.1 Free-head floating Piles

The solution for the governing deferential equation is found using numerical methods. The governing equation was solved for a range of parameters and the pile head flexibility influence factors were determined through the use of curve fitting. The influence factors are given by:

$$I_{HH} = (1.003 - 0.03\nu_s)\left(\frac{E_p}{mr}\right)^{-0.34} \tag{5.7}$$

$$I_{MH} = (0.96 - 0.02\nu_s)\left(\frac{E_p}{mr}\right)^{-0.56} \tag{5.8}$$

$$I_{HM} = (1.03 - 0.02\nu_s)\left(\frac{E_p}{mr}\right)^{-0.56} \tag{5.9}$$

$$I_{MM} = (1.55 - 0.02\nu_s)\left(\frac{E_p}{mr}\right)^{-0.78} \tag{5.10}$$

for long flexible piles, i.e. $\frac{L}{r} > 3.13\left(\frac{E_p}{mr}\right)^{0.21}$ and

$$I_{HH} = (1.03 + 0.01\nu_s)\left(\frac{L}{r}\right)^{-1.22} \tag{5.11}$$

$$I_{MH} = (1.17 - 0.007\nu_s)\left(\frac{L}{r}\right)^{-2.17} \tag{5.12}$$

$$I_{HM} = (1.19 - 0.002\nu_s)\left(\frac{L}{r}\right)^{-2.18} \tag{5.13}$$

$$I_{MM} = (1.51 - 0.02\nu_s)\left(\frac{L}{r}\right)^{-3.11} \tag{5.14}$$

for short rigid piles, i.e. $\frac{E_p}{mr} > 11.24\left(\frac{L}{r}\right)^{3.25}$.

Expressions (5.11) - (5.14) are based on the more precise equation for the calibration factor in Equation (4.13). As is evident, the Poisson's ratio has a negligible effect (of the order of 1.5%) on the pile head flexibility and can justifiably be neglected from the computation.

As a first form of validation I_{MH} and I_{HM} are compared, it is found that for $\frac{L}{r} > 3.13\left(\frac{E_p}{mr}\right)^{0.21}$ (long flexible piles) the deviation between the two is 7.2%. It should be noted that the deviation in the corresponding terms in Higgins et al. (2013) and Basu and Higgins (2011) work is of the order of 6%. Hence, comparatively, the two terms (i.e. I_{MH} and I_{HM}) are within acceptable margins. Similarly, the difference in I_{MH} and I_{HM} for $\frac{E_p}{mr} > 11.24\left(\frac{L}{r}\right)^{3.25}$ is a maximum of 1.3%.

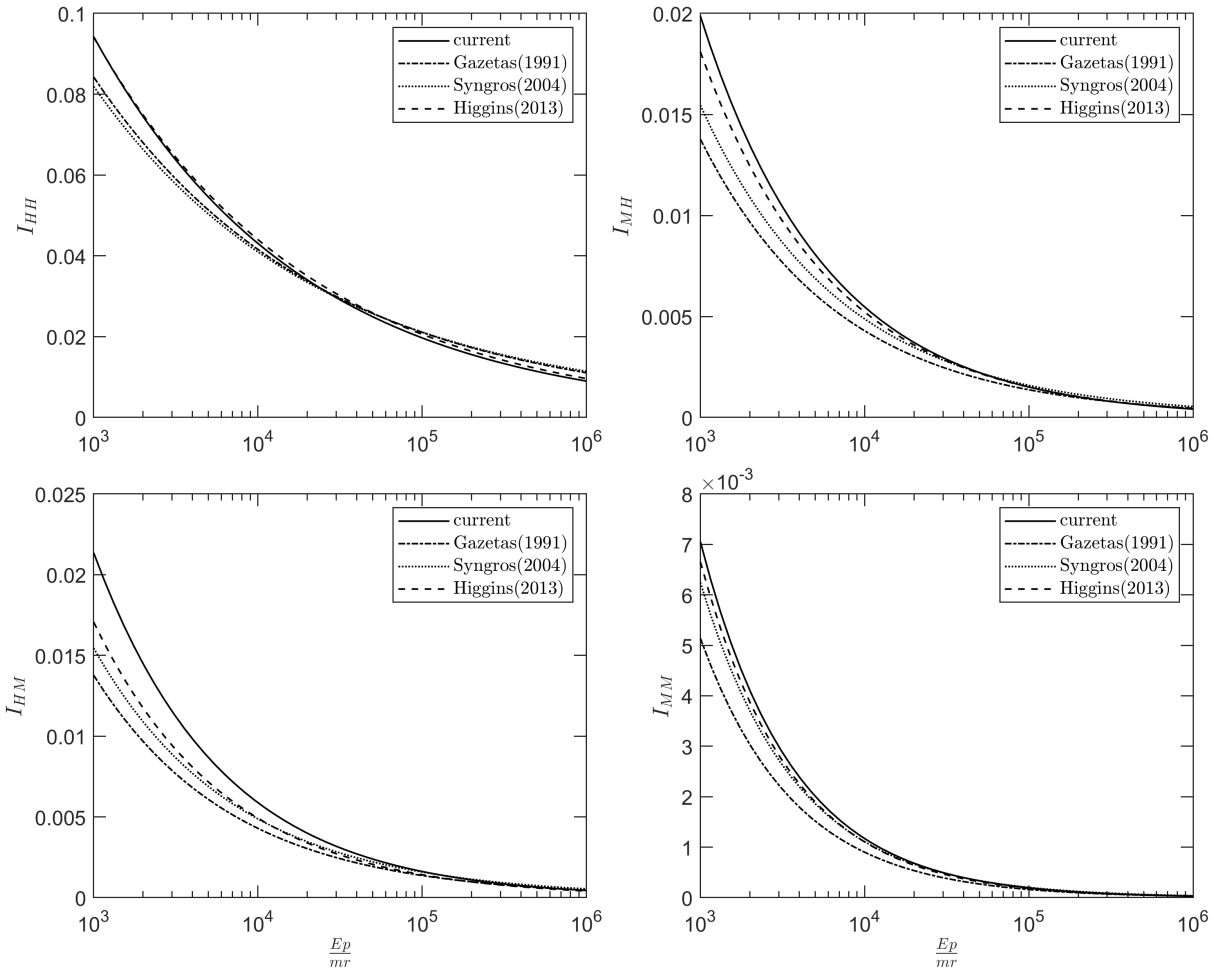

Figure 5.1: Comparison of influence factors for free-head floating long flexible piles embedded in soil with linearly increasing elastic modulus

Figure 5.1 presents the current influence factors along with those proposed in the literature for $\frac{L}{r} > 3.13\left(\frac{E_p}{mr}\right)^{0.21}$ (long flexible piles). The influence factors compare well with those of Higgins et al. (2013), while generally being larger than those proposed by Gazetas (1991) and Syngros (2004). A larger influence factor implies greater pile head displacement. Thus, the proposed influence factors may be thought of as being comparatively on the conservative side. The largest deviations are seen for smaller $\frac{E_p}{mr}$ and for the cross swaying-rocking flexibility influence factors.

Comparison of the influence factors obtained with those published in the literature for short rigid piles $\left(\frac{E_p}{mr} > 11.24\left(\frac{L}{r}\right)^{3.25}\right)$ is presented in Figure 5.2. In all cases, the current factors are larger than those by Higgins et al. (2013). The largest deviations are noted for lower end of the slenderness ratio with the most significant differences being for I_{MM}. Such a difference between the current work and Higgins et al. (2013) was also observed in

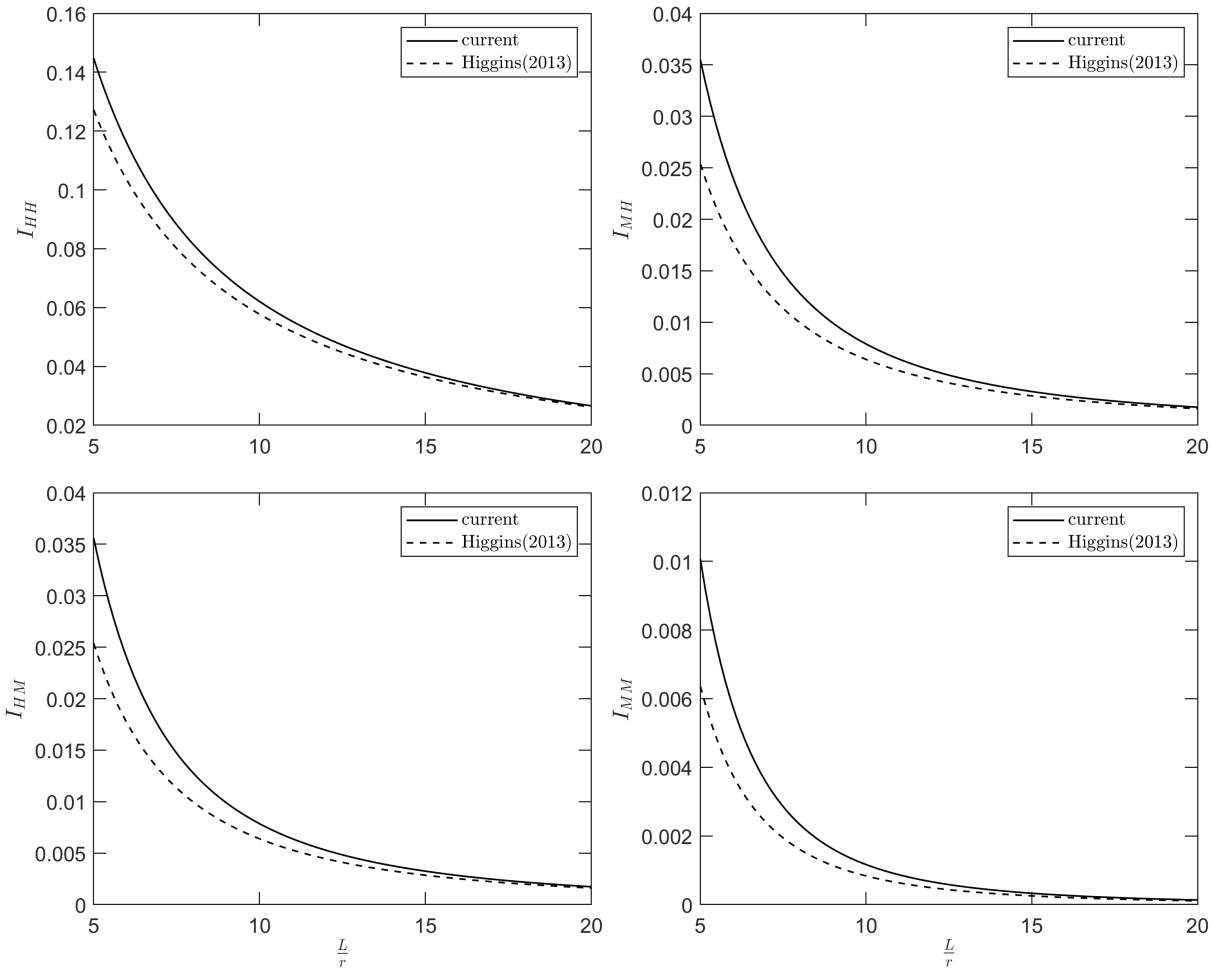

Figure 5.2: Comparison of influence factors for free-head floating short rigid piles embedded in soil with linearly increasing elastic modulus

validating finite element analysis results, where a possible explanation is given (Section 3.4.6).

Inverting the expressions in (5.7) - (5.10) and (5.11) - (5.14), one obtains, the pile head stiffness coefficients as follows:

$$\frac{K_{HH}}{mr^2} = (0.097\nu_s + 2.74)\left(\frac{E_p}{mr}\right)^{0.34} \tag{5.15}$$

$$\frac{K_{MH}}{mr^3} = (0.052\nu_s + 1.82)\left(\frac{E_p}{mr}\right)^{0.56} \tag{5.16}$$

$$\frac{K_{HM}}{mr^3} = (0.046\nu_s + 1.70)\left(\frac{E_p}{mr}\right)^{0.56} \tag{5.17}$$

$$\frac{K_{MM}}{mr^4} = (0.031\nu_s + 1.77)\left(\frac{E_p}{mr}\right)^{0.78} \tag{5.18}$$

for long flexible piles, i.e. $\frac{L}{r} > 3.13\left(\frac{E_p}{mr}\right)^{0.21}$ and

$$\frac{K_{HH}}{mr^2} = (-0.40\nu_s + 9.26)\left(\frac{L}{r}\right)^{1.22} \tag{5.19}$$

$$\frac{K_{MH}}{mr^3} = (-0.23\nu_s + 7.30)\left(\frac{L}{r}\right)^{2.175} \tag{5.20}$$

$$\frac{K_{HM}}{mr^3} = (-0.26\nu_s + 7.18)\left(\frac{L}{r}\right)^{2.175} \tag{5.21}$$

$$\frac{K_{MM}}{mr^4} = (-0.13\nu_s + 6.32)\left(\frac{L}{r}\right)^{3.11} \tag{5.22}$$

for short rigid piles, i.e. $\frac{E_p}{mr} > 11.24\left(\frac{L}{r}\right)^{3.25}$

5.1.2 Fixed-head floating piles

Using Equations (4.26) - (4.29) with the corresponding boundary value problem expressions, the pile head flexibility influence factors was obtained as follows:

$$I_{HH} = (0.50 - 0.02\nu_s)\left(\frac{E_p}{mr}\right)^{-0.35} \tag{5.23}$$

for long flexible piles, i.e. $\frac{L}{r} > 3.49\left(\frac{E_p}{mr}\right)^{0.21}$ and,

$$I_{HH} = (0.40 - 0.04\nu_s)\left(\frac{L}{r}\right)^{-1.54} \tag{5.24}$$

for short rigid piles, i.e. $\frac{E_p}{mr} > 47.8\left(\frac{E_p}{mr}\right)^{3.34}$

Figure 5.3 presents comparison of the current I_{HH} with that proposed by Higgins et al. (2013) for short rigid fixed-head piles, Similar to free-head piles, the influence factor in this case is larger than the one provided by Higgins et al. (2013). Possible explanation

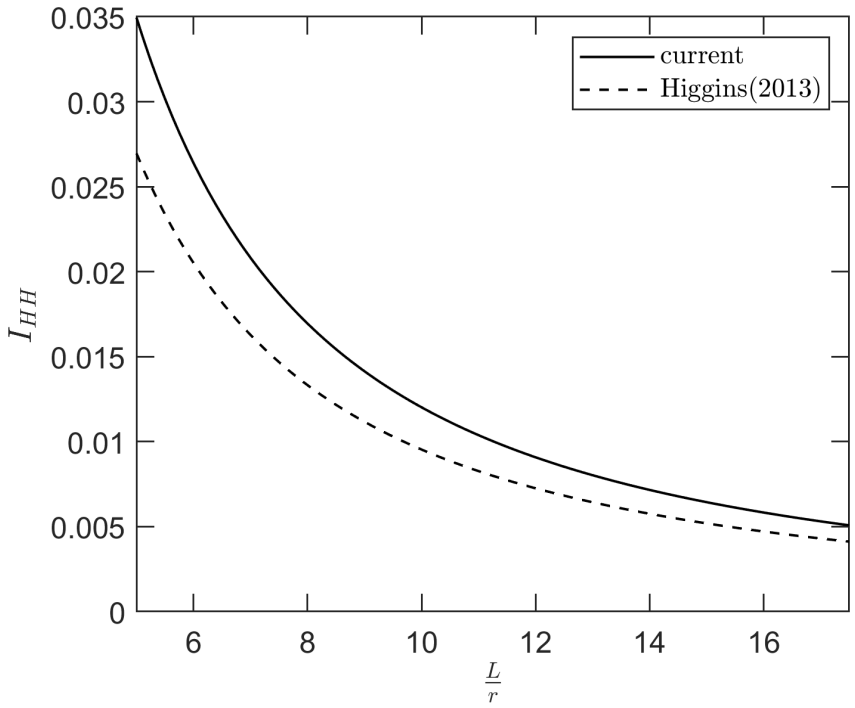

Figure 5.3: Comparison of influence factors for fixed-head floating short rigid piles embedded in soil with linearly increasing elastic modulus

for such a difference is given in Section 3.4.6. Figure 5.4 shows a comparisons of I_{HH} for long flexible fixed head piles. The curve fit equation from this work matches that of Higgins et al. (2013) very well while the solution by Syngros (2004) a significantly higher flexibility.

Inverting (5.23) and (5.24), the stiffness coefficients are obtained as follows:

$$\frac{K_{HH}}{mr^2} = (0.08\nu_s + 2.0)\left(\frac{E_p}{mr}\right)^{0.35} \tag{5.25}$$

for long flexible piles, i.e. $\frac{L}{r} > 3.49\left(\frac{E_p}{mr}\right)^{0.21}$ and,

$$\frac{K_{HH}}{mr^2} = (0.27\nu_s + 2.5)\left(\frac{L}{r}\right)^{1.54} \tag{5.26}$$

for short rigid piles, i.e $\frac{E_p}{mr} > 47.8\left(\frac{E_p}{mr}\right)^{3.34}$

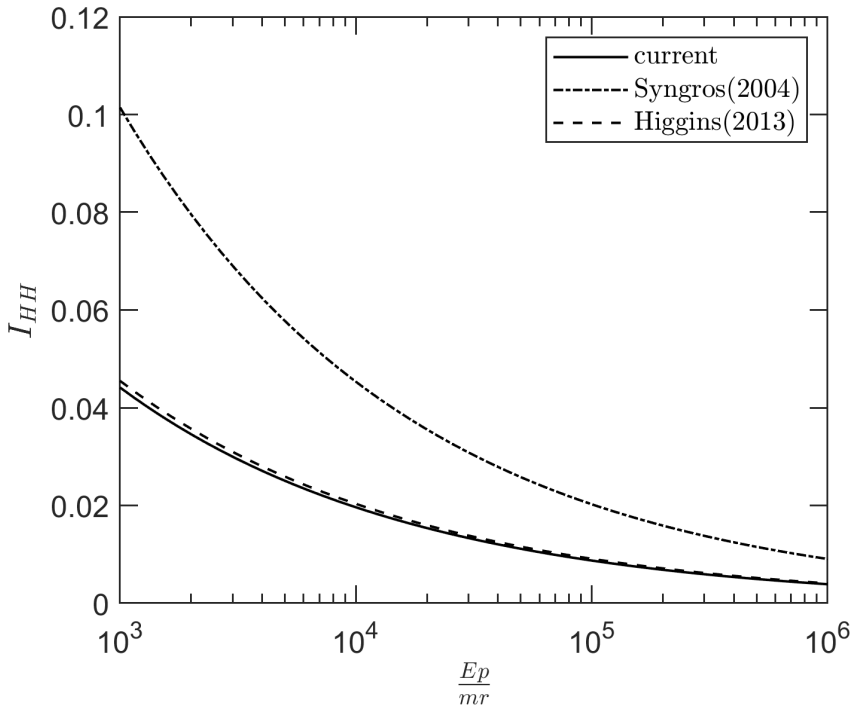

Figure 5.4: Comparison of influence factors for fixed-head floating long flexible piles embedded in soil with linearly increasing elastic modulus

5.1.3 Fixed-base piles

As was noted in previous sections, the calibration factors for long flexible fixed-base piles were practically identical to those of their floating counter parts. Similarly, the pile head flexibility and stiffness influence factors are identical to the corresponding floating-base piles. Hence, the expressions for floating piles obtained above are applicable to fixed-base piles. It should also be noted that the influence factors for short rigid fixed-base piles are extremely small and of negligible magnitude, as such piles do exhibit minimal displacement by virtue of their base fixity and pile rigidity. Equivalently, the pile head stiffness coefficients are infinitely large for such piles.

5.2 Piles embedded in soil with parabolically increasing elastic modulus

The static head response of piles embedded in soils with parabolically increasing elastic modulus is formulated in the same manner as the linearly increasing modulus. Expres-

sions for free-head floating piles and fixed-head floating piles are provided through curve fitting. Similar to the linearly increasing elastic modulus, the flexibility influence factor for fixed-base piles is practically identical to free-base piles.

5.2.1 Free-head floating piles

The governing equation was solved, using numerical methods, for a range of parameters and the pile head flexibility influence factors were determined through the use of curve fitting. The influence factors are given by:

$$I_{HH} = (0.90 - 0.01\nu_s)\left(\frac{E_p}{mr}\right)^{-0.27} \tag{5.27}$$

$$I_{MH} = (0.85 - 0.01\nu_s)\left(\frac{E_p}{mr}\right)^{-0.51} \tag{5.28}$$

$$I_{HM} = (0.95 - 0.003\nu_s)\left(\frac{E_p}{mr}\right)^{-0.52} \tag{5.29}$$

$$I_{MM} = (1.48 - 0.006\nu_s)\left(\frac{E_p}{mr}\right)^{-0.76} \tag{5.30}$$

for long flexible piles, i.e. $\frac{L}{r} > 3.61\left(\frac{E_p}{mr}\right)^{0.22}$ and

$$I_{HH} = (0.88 + 0.04\nu_s)\left(\frac{L}{r}\right)^{-0.89} \tag{5.31}$$

$$I_{MH} = (1.03 - 0.02\nu_s)\left(\frac{L}{r}\right)^{-1.83} \tag{5.32}$$

$$I_{HM} = (1.08 - 0.03\nu_s)\left(\frac{L}{r}\right)^{-1.84} \tag{5.33}$$

$$I_{MM} = (1.47 - 0.01\nu_s)\left(\frac{L}{r}\right)^{-2.77} \tag{5.34}$$

for short rigid piles, i.e. $\frac{E_p}{mr} > 3.56\left(\frac{L}{r}\right)^{3.25}$.

For free-head piles in soil with parabolically increasing modulus, Gazetas (1991) provided

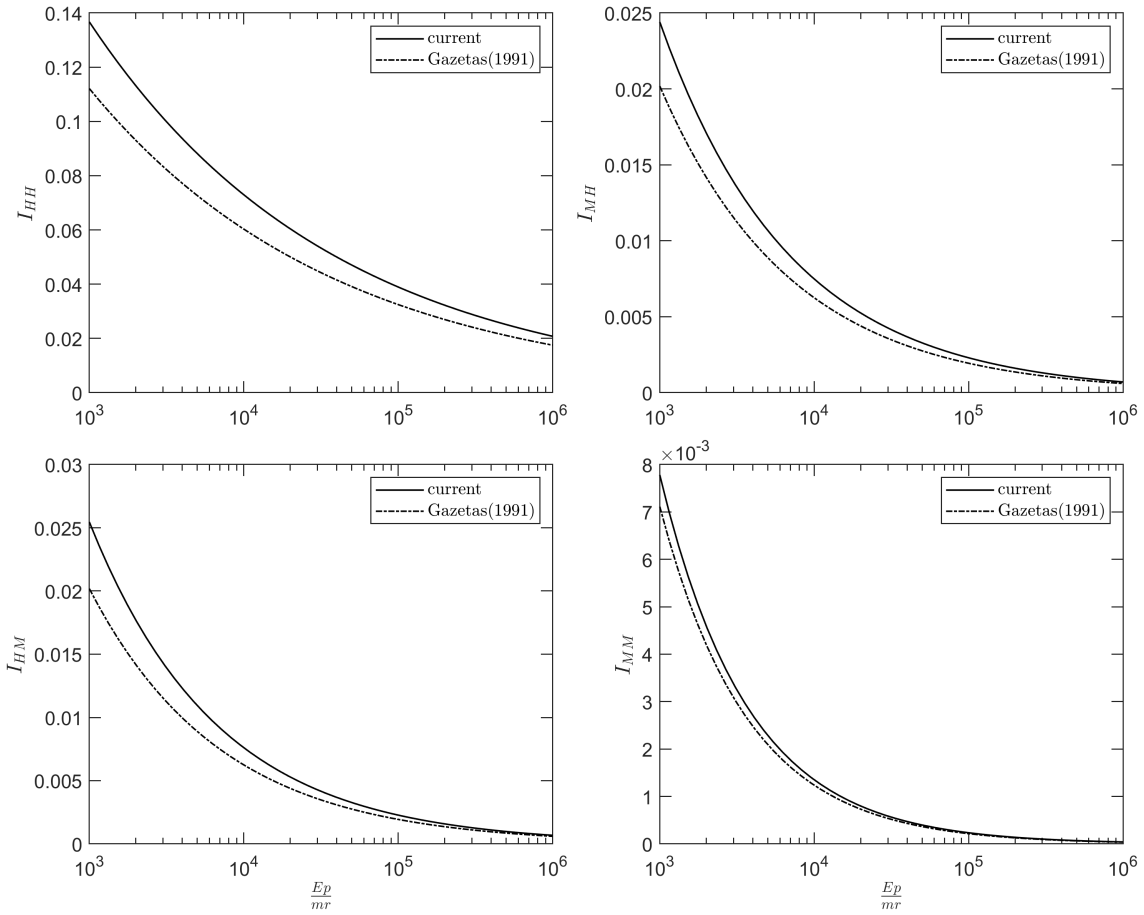

Figure 5.5: Comparison of influence factors for free-head floating long flexible piles embedded in soil with Parabolically increasing elastic modulus

expressions for the pile head stiffness (see Section 2.1.3). Figure 5.5 compares flexibility influence factors given above and those obtained by inverting Gazetas (1991) equations. Once again, the flexibility influence factors obtained in this work are found to be larger than those by Gazetas (1991). With the largest deviation occurring as $\frac{E_p}{mr}$ decreases and being significant for the cross swaying-rocking influence factor.

Inverting equations (5.27) - (5.30) and (5.31) - (5.34) one obtains, the pile head stiffness coefficients as follows:

$$\frac{K_{HH}}{mr^2} = (-0.01\nu_s + 2.82)\left(\frac{E_p}{mr}\right)^{0.27} \tag{5.35}$$

$$\frac{K_{MH}}{mr^3} = (0.08\nu_s + 1.81)\left(\frac{E_p}{mr}\right)^{0.51} \tag{5.36}$$

$$\frac{K_{HM}}{mr^3} = (0.08\nu_s + 1.62)\left(\frac{E_p}{mr}\right)^{0.52} \tag{5.37}$$

$$\frac{K_{MM}}{mr^4} = (-0.05\nu_s + 1.72)\left(\frac{E_p}{mr}\right)^{0.76} \tag{5.38}$$

for long flexible, i.e. $\frac{L}{r} > 3.61\left(\frac{E_p}{mr}\right)^{0.22}$ and

$$\frac{K_{HH}}{mr^2} = (-3.23\nu_s + 7.9)\left(\frac{L}{r}\right)^{0.895} \tag{5.39}$$

$$\frac{K_{MH}}{mr^3} = (-2.46\nu_s + 5.8)\left(\frac{L}{r}\right)^{1.825} \tag{5.40}$$

$$\frac{K_{HM}}{mr^3} = (-2.31\nu_s + 5.53)\left(\frac{L}{r}\right)^{1.835} \tag{5.41}$$

$$\frac{K_{MM}}{mr^4} = (-1.76\nu_s + 4.74)\left(\frac{L}{r}\right)^{2.775} \tag{5.42}$$

for short rigid piles, i.e. $\frac{E_p}{mr} > 3.56\left(\frac{L}{r}\right)^{3.25}$.

5.2.2 Fixed-head floating piles

The pile head flexibility influence factors for fixed-head floating piles are given by:

$$I_{HH} = (0.49 - 0.007\nu)\left(\frac{E_p}{mr}\right)^{-0.29} \tag{5.43}$$

for long flexible piles, i.e. $\frac{L}{r} > 4.34\left(\frac{E_p}{mr}\right)^{0.23}$ and,

$$I_{HH} = (0.33 - 0.01\nu_s)\left(\frac{L}{r}\right)^{-1.05} \tag{5.44}$$

for short rigid piles, i.e. $\frac{E_p}{mr} > 21.46\left(\frac{L}{r}\right)^{3.07}$.

Similarly, inverting (5.43) and (5.44), the piles head stiffness factors are obtained as follows:

$$\frac{K_{HH}}{mr^2} = (0.03\nu_s + 2.04)\left(\frac{E_p}{mr}\right)^{0.29} \tag{5.45}$$

for long flexible piles, i.e. $\frac{L}{r} > 4.34\left(\frac{E_p}{mr}\right)^{0.23}$and,

$$\frac{K_{HH}}{mr^2} = (0.09\nu_s + 3.03)\left(\frac{L}{r}\right)^{1.05} \tag{5.46}$$

for short rigid piles, i.e. $\frac{E_p}{mr} > 21.46\left(\frac{L}{r}\right)^{3.07}$.

5.2.3 Fixed-base piles

Similar to the case of piles embedded in soil with linearly increasing case, the pile head flexibility influence factors for long flexible fixed-base piles are practically identical to those of their floating counterparts. Hence, the expressions for floating piles obtained above are applicable to fixed-base piles. It should also be noted that the influence factors for short rigid fixed-base piles are extremely small and of negligible magnitude, as such piles do exhibit minimal displacement by virtue of their base fixity and pile rigidity. Correspondingly, the pile head stiffness coefficients are of infinite magnitude for such piles.

Overall, based on the comparisons done above the following, observations are summarized

- For long flexible piles embedded in linearly increasing soil irrespective of pile end conditions, expressions obtained in the current work compare well with published results, while being generally larger in magnitude. For long flexible piles embedded in parabolically increasing soil comparisons are limited to the work by Gazetas (1991). In this case, the differences between the expressions obtained in the current work and Gazetas (1991) are in line with the differences observed for the linearly increasing case.

- For short rigid piles (comparisons were done only for the linearly increasing case), expressions obtained in the current work with those from Higgins et al. (2013) show some differences, especially as the slenderness ratio decreases. A possible reason for such a deviation is as given in Section 3.4.6.

5.3 Effect of shear interaction

The Kerr-equivalent Pasternak-type continuum model (Worku 2014) takes directly into consideration shear transfer in the soil mass. In a mechanical form, such a shear transfer is represented by the shear element, which introduces interaction between spring elements. Such a formulation provides an opportunity to investigate the effect of soil shear by simply neglecting or including the shear term.

The normalized pile displacement $\left(I_{HH} = \frac{u_0 m r^2}{H_0}\right)$ are compared with and without the shear term for short rigid, intermediate and long flexible piles along with results from finite element analysis for piles in soil with linearly increasing elastic modulus, see Figures 5.6 and 5.7. For free head piles, the response obtained with the shear term included, closely resembles the finite element analysis result, since the the model was calibrated by equating the pile head displacement. Neglecting the shear term results in overestimation of the pile head displacement and overall results in a larger displacement profile which is most noticeable for short rigid piles. As pile length increases and the pile becomes long and flexible, irrespective of pile head condition, the effect of shear interaction is less significant.

For short rigid fixed-head piles, the pile response obtained by neglecting the shear term

seems to agree better with the response from FEM (see Figure 5.7). But it is to be noted that the scale at which these differences are occurring is comparatively very small and negligible (note the displacement axis in the plot).

To further investigate the effect of shear interaction, the calibrated Kerr-equivalent Pasternak-type continuum model is compared with a one-parameter Winkler model. The one-parameter Winkler-type model is characterized by (5.47) and is obtained by neglecting the vertical shear stress components τ_{xz} and τ_{yz} (Worku 2010; Worku 2013). The model is, however, calibrated first, similar to the Kerr-equivalent Pasternak model.

$$K_w = \frac{E_s}{(1 - 0.4\nu_s)\,\chi_W} \tag{5.47}$$

Comparison of the two models alongside finite element results for piles embedded in soil with linearly increasing elastic modulus are given in Figures 5.8 and 5.9. For free-head piles, since both models were calibrated by equating the pile head displacement to that obtained from FEM, they compare well with the pile head displacement from FEM. On the other hand, the overall displacement profile for short and intermediate length piles, obtained from the calibrated one-parameter model deviates from the FEM result by a comparatively larger margin than the current model. For relatively longer piles, irrespective of pile head condition, such a difference is not that observable.

For short rigid fixed-head piles, as noted before any difference perceived happens over a very small scale that the deviation between the results of the two models and the FEM are negligible, see Figure 5.9.

Comparing bending moment in the pile, the results between the two methods are very similar. Further, the location of the maximum bending moment for free-head piles using both models is approximately the same (see Figure 5.10). It should also be remembered that in verifying the model calibration (Section 4.6), the Kerr-equivalent Pasternak model deviated from the FEM solution at regions of high curvature.

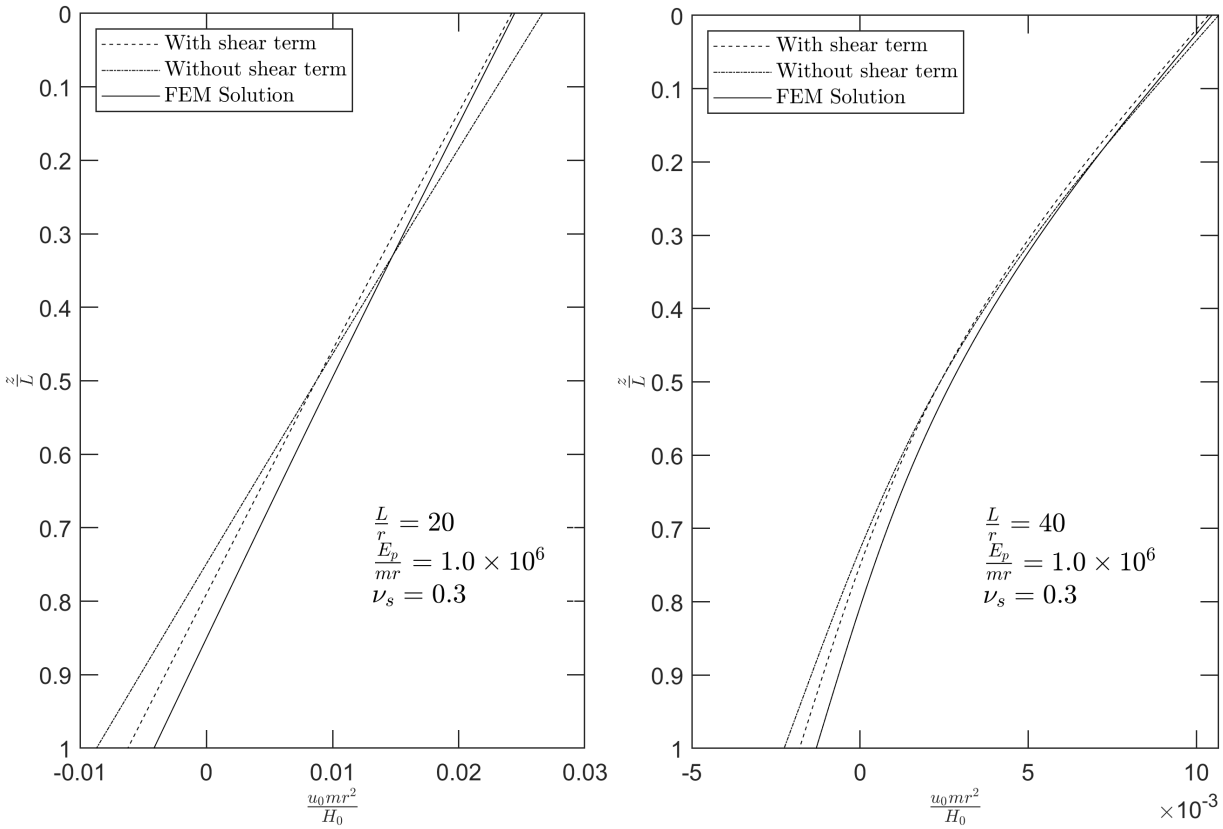

(a) Short rigid pile

(b) Intermediate length pile

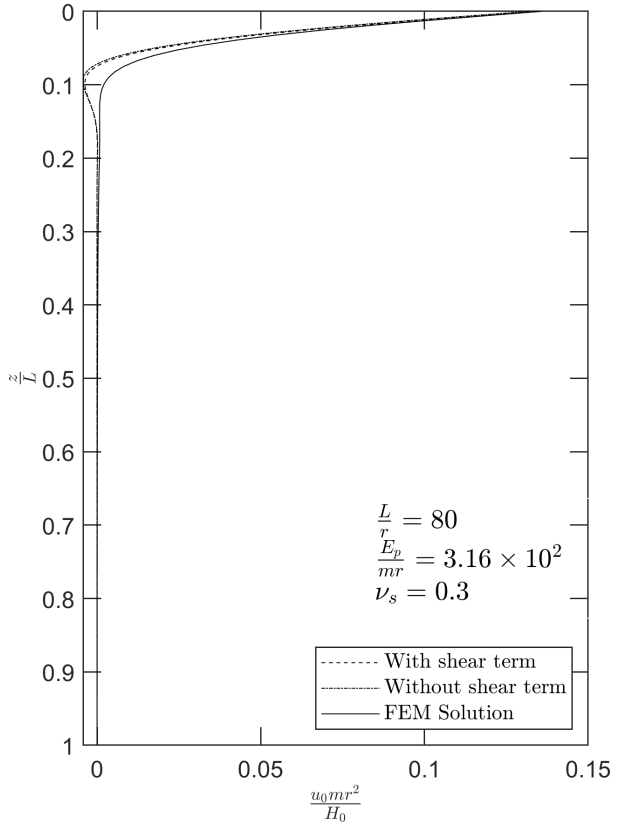

(c) Long flexible pile

Figure 5.6: Effect of shear term for free-head free-base piles in soil with linearly increasing elastic modulus

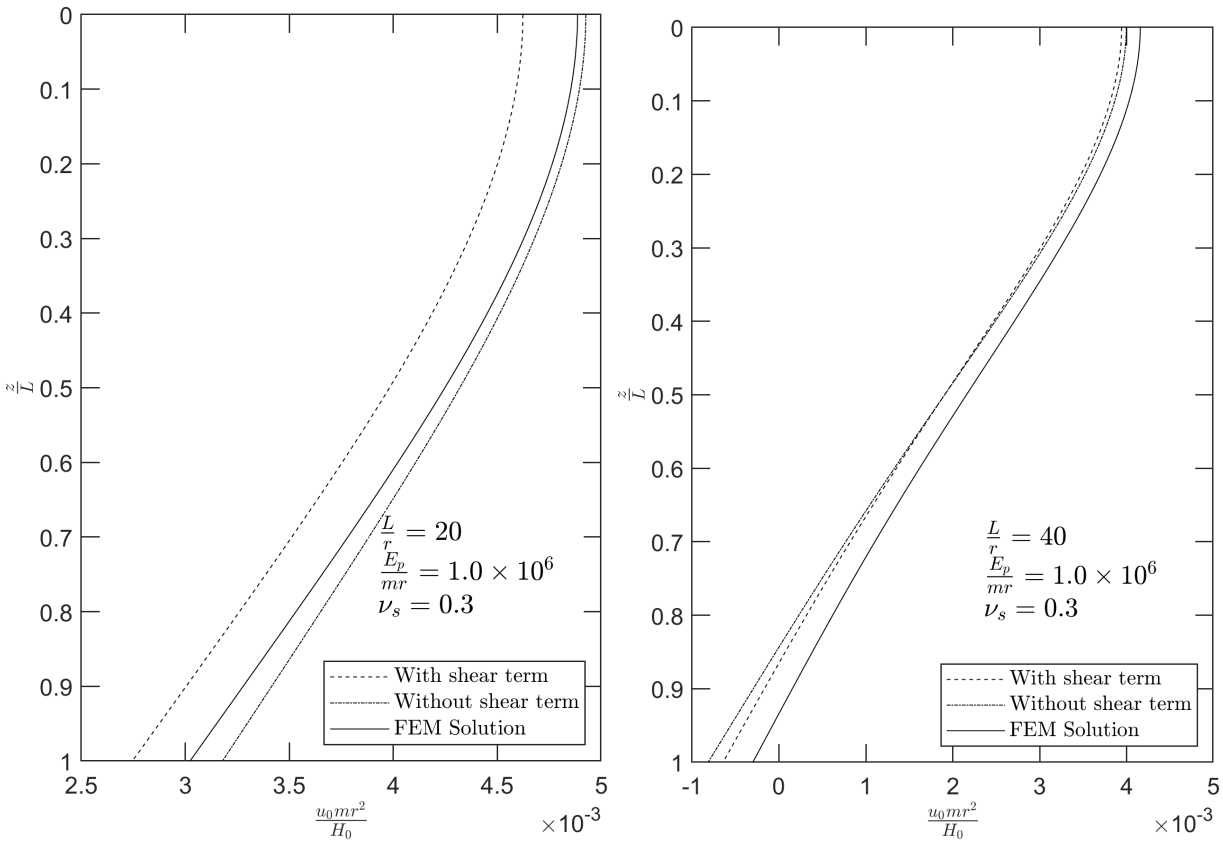

(a) Short rigid piles

(b) Intermediate pile

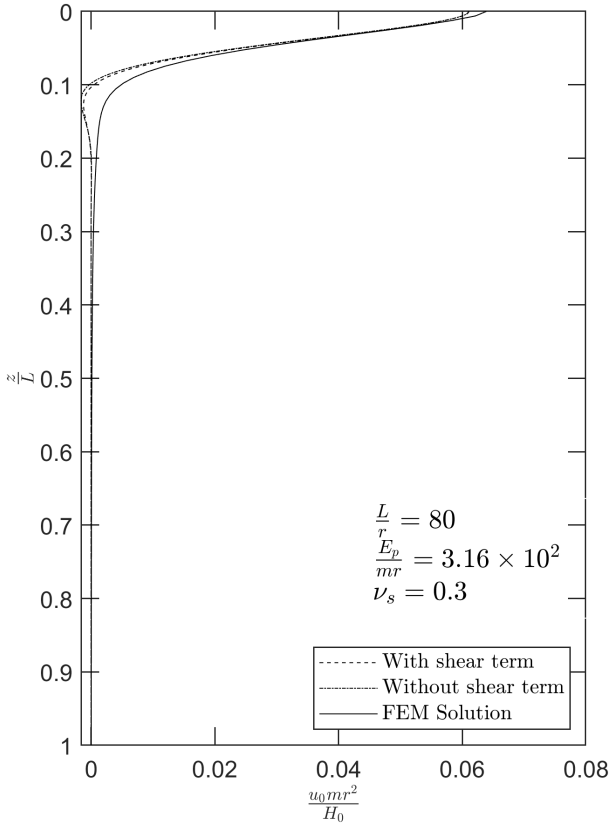

(c) Long flexible pile

Figure 5.7: Effect of shear term for fixed-head free-base piles in soil with linearly increasing elastic modulus

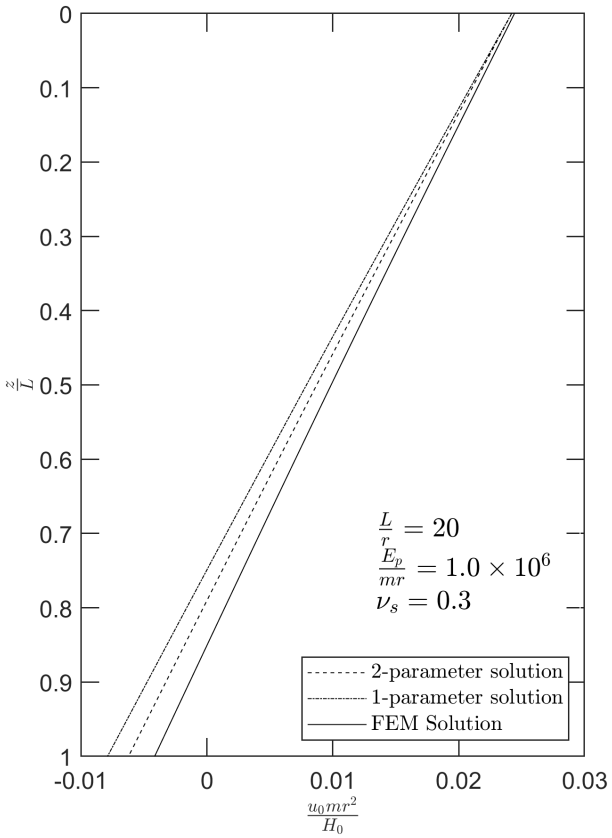

(a) Short rigid piles

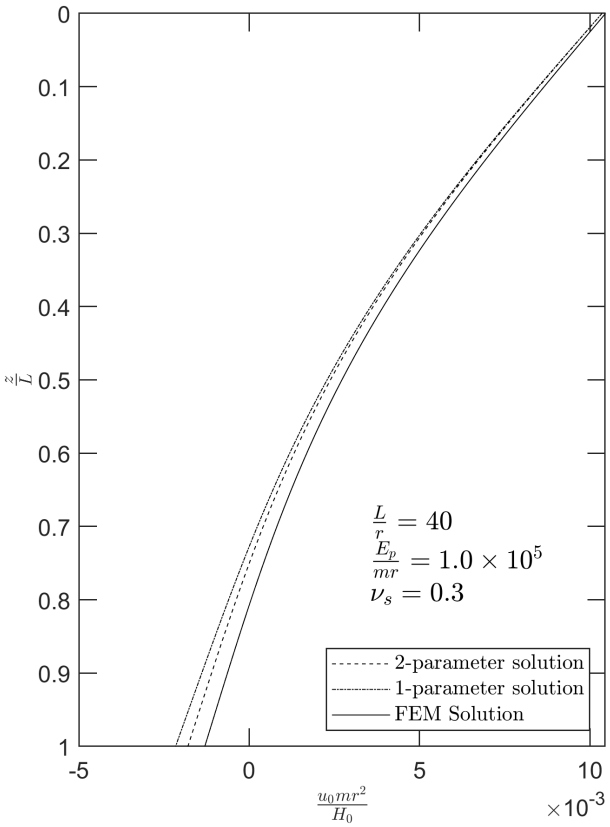

(b) Intermediate length pile

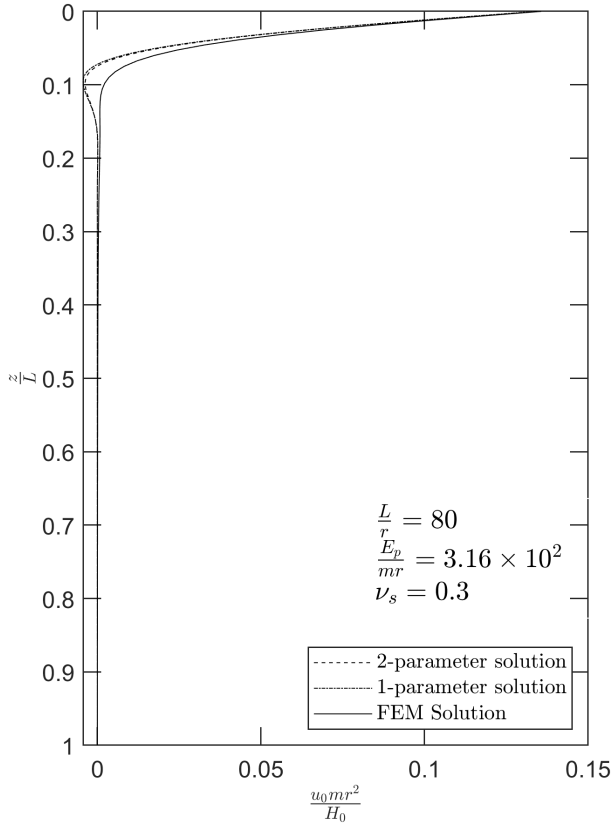

(c) Long flexible pile

Figure 5.8: Comparison of Kerr-equivalent Pasternak model and Winkler model for free-head free-base piles in soil with linearly increasing elastic modulus

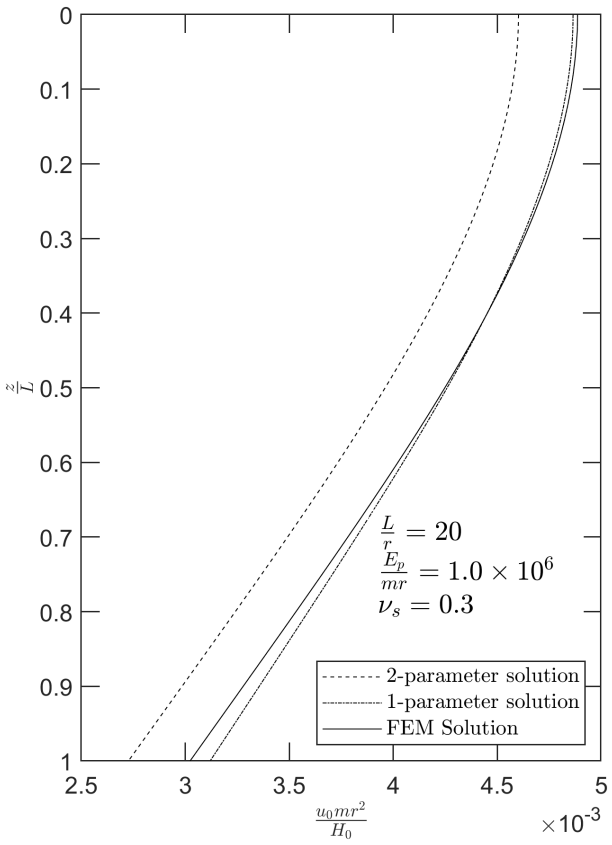

(a) Short rigid pile

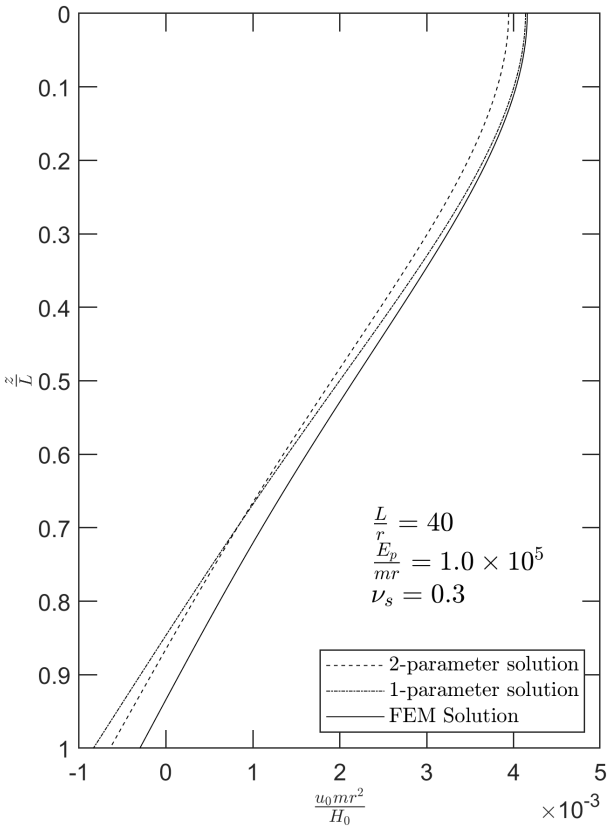

(b) Intermediate length pile

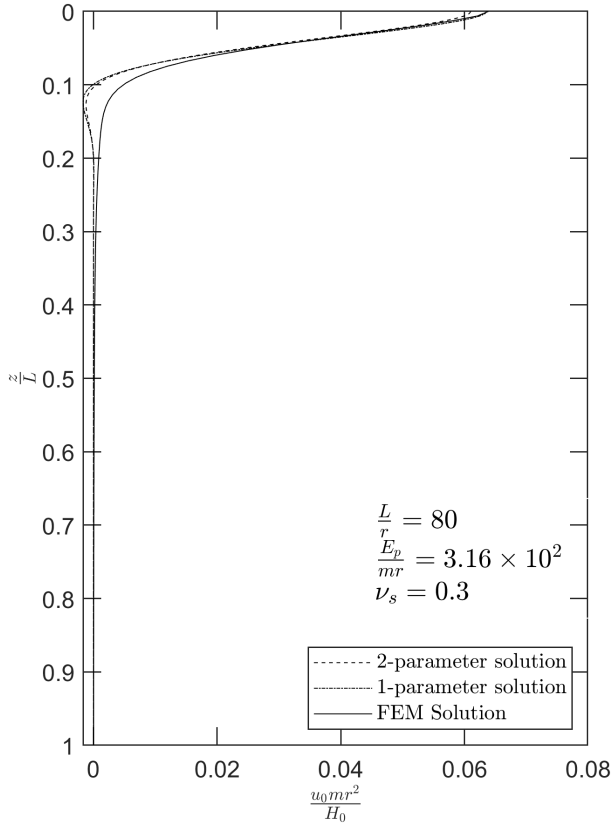

(c) Long flexible pile

Figure 5.9: Comparison of Kerr-equivalent Pasternak model and Winkler model for fixed-head free-base piles in soil with linearly increasing elastic modulus

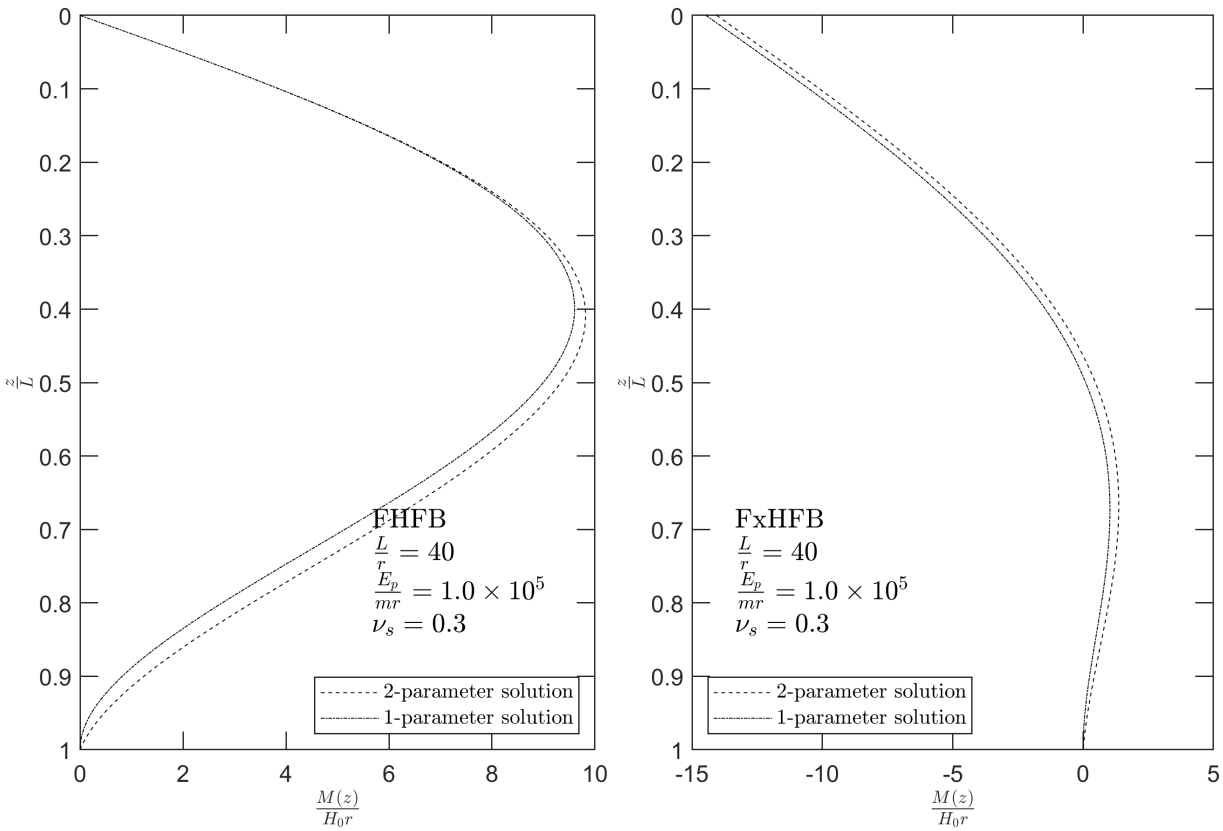

(a) Free-head pile

(b) Fixed-head pile

Figure 5.10: Comparison of bending moment from Kerr-equivalent Pasternak model and Winkler model for piles in soil with linearly increasing elastic modulus

Based on the above discussion the following may be concluded:

- For short rigid free-head piles, neglecting shear interaction results in overestimation of the pile head displacement and overall displacement profile is overestimated as well.
- For long flexible free-head and fixed-head piles the effect of shear interaction is less significant.
- The results of the calibrated Kerr-equivalent Pasternak-type continuum model are relatively more representative of the finite element solution compared to the calibrated one-parameter Winkler-type model. The exception to this is short rigid fixed-head piles but as has been pointed out, the scale of the displacements in such cases is very small and the differences are negligible.

Chapter 6

Dynamic Analysis — Inertial Interaction

An approximate energy based method outlined in Section 3.6 is used along with the calibrated Kerr-equivalent Pasternak-type continuum subgrade model, to determine the components of the pile head impedance function and damping for long piles $\left[\frac{L}{r} \geq \left(\frac{L}{r}\right)_{cr}\right]$ over the range of relevant parameters set out in Section 3.3. As the subgrade model is calibrated against static finite element analysis, it is frequency independent. In regards to the dynamic material properties, a typical value of $\beta_s = 0.05$ is used (Gazetas 1991) and $\beta_p = 0$ is assumed, since most analysis, which these results are to be compared with do not include the material damping of the pile. The range of normalized frequency (a_{0r}) used at $z = r$ is limited to the range of applicability of c_r provided by Karatzia and Mylonakis (2017).

As discussed in section 3.6, the pile head impedance is given by Novak (1974) and Gazetas (1991):

$$\mathcal{K}_{\mathrm{x}} = K_x + iC_x \tag{6.1}$$

where the real part K_x represents the dynamic pile head stiffness and C_x the pile head equivalent damping coefficient. The dynamic piles head stiffness using the approximate energy formulation is given by (see Section 3.6):

$$K_{ij} = E_p I_p \int_0^L \varphi_i'' \varphi_j'' dz - \int_0^L G_p(z) \varphi_i' \varphi_j' dz + \int_0^L k_p(z) \varphi_i \varphi_j dz - m\omega^2 \int_0^L \varphi_i \varphi_j dz \tag{6.2}$$

Using the definition of the equivalent damping ratio, it was shown that the equivalent damping ratio at the pile head can be expressed as (see Section 3.6) :

$$\beta_{ij} = \beta_p w_{ij}^p + \beta_s w_{ij}^s + \beta_{ij}^r \tag{6.3}$$

where, using the approximate energy formulation

$$w_{ij}^p = \frac{E_p I_p \int_0^L \varphi_i'' \varphi_j'' dz}{K_{ij}} \tag{6.4}$$

$$w_{ij}^s = \frac{\left[- \int_0^L G_p(z) \varphi_i' \varphi_j' dz + \int_0^L k_p(z) \varphi_i \varphi_j dz \right]}{K_{ij}} \tag{6.5}$$

$$\beta_{ij}^r = \frac{\omega \int_0^L c_r(z) \varphi_i \varphi_j dz}{2K_{ij}} \tag{6.6}$$

In the above expressions, w_{ij}^p and w_{ij}^s are weights that specify the contribution of the pile and soil material damping, while β_{ij}^r is the radiation damping ratio. It was also noted that $w_{ij}^p + w_{ij}^s = 1$, if the inertial contribution of the pile is neglected (i.e. the last term in 6.2). The pile inertial contribution is generally neglected in seismic analysis where excitation frequencies are limited (Karatzia and Mylonakis 2017).

Based on the above discussion, to fully specify the dynamic pile head response, one needs to evaluate the stiffness, K_{ij}, one of the weight functions, w_{ij}^p or w_{ij}^s, and the radiation damping ratio, β_{ij}^r.

For the current work, to evaluate the stiffness, the weight functions and radiation damping ratio are evaluated numerically as outlined in Section 3.6. This is done for each of 2176 parameter combinations. For each different groups (i.e. 272 data sets for each pile end condition and soil non-homogeneity), the three parameters are evaluated and the effects of the various relevant parameters set out in Section 3.3 investigated, and curve

fit expressions are provided, when necessary.

6.1 Dynamic pile head stiffness

Figure 6.1 presents the variation of dynamic pile head stiffness with relative pile-soil stiffness for free head piles embedded in soil with linearly increasing elastic modulus and $\nu_s = 0.4$, $a_{0r} = 0.5$. Results from the current method compare well with those found in the literature. For example, the deviation in the swaying stiffness (K_{HH}) between the current method and Syngros (2004) is of the order of 10%. Note that for piles embedded in soils with linearly increasing elastic modulus, the dynamic pile head stiffness computed are consistently larger than those found in the literature, especially, Gazetas (1991). Figure 6.1 also shows the current method with the inertial term (last term in 3.45) included and that static stiffness formulated in (5.15) - (5.18). The dynamic pile head stiffness's from the current method are similar to the static pile head stiffness proposed in (5.15) - (5.18) with a maximum difference of less than 10%.

Figure 6.2 shows the variation of dynamic pile head stiffness with normalized frequency (a_{0r}) for free head piles embedded in soil with linearly increasing elastic modulus, $\nu_s = 0.4$ and $E_p/mr = 10^4$. For all practical purposes, the dynamic pile head stiffness found by ignoring the inertial term can be considered independent of the excitation frequency. On the other hand, as the inertial term explicitly involves frequency, including it introduces dependence on a_{0r}. The maximum deviation between pile head stiffness terms with and without the inertia term increases with frequency and is about 16% for $E_p/mr = 10^4$, although it grows to about 32% for $E_p/mr = 10^6$. Not withstanding this, it should be noted that Karatzia and Mylonakis (2012) state for frequency ranges in a typical seismic loading the dynamic pile head stiffness can be adequately approximated by static ones. Similarly, Gazetas (1991) reported the ratio of the static and dynamic pile head stiffness in seismic action as unity based on a more rigorous finite element analysis for homogenous, linearly and parabolically increasing soil profiles.

The dynamic pile head stiffness for piles in parabolically increasing elastic soil also exhibits similar trends. Although in this case the current solutions are lower than those provided

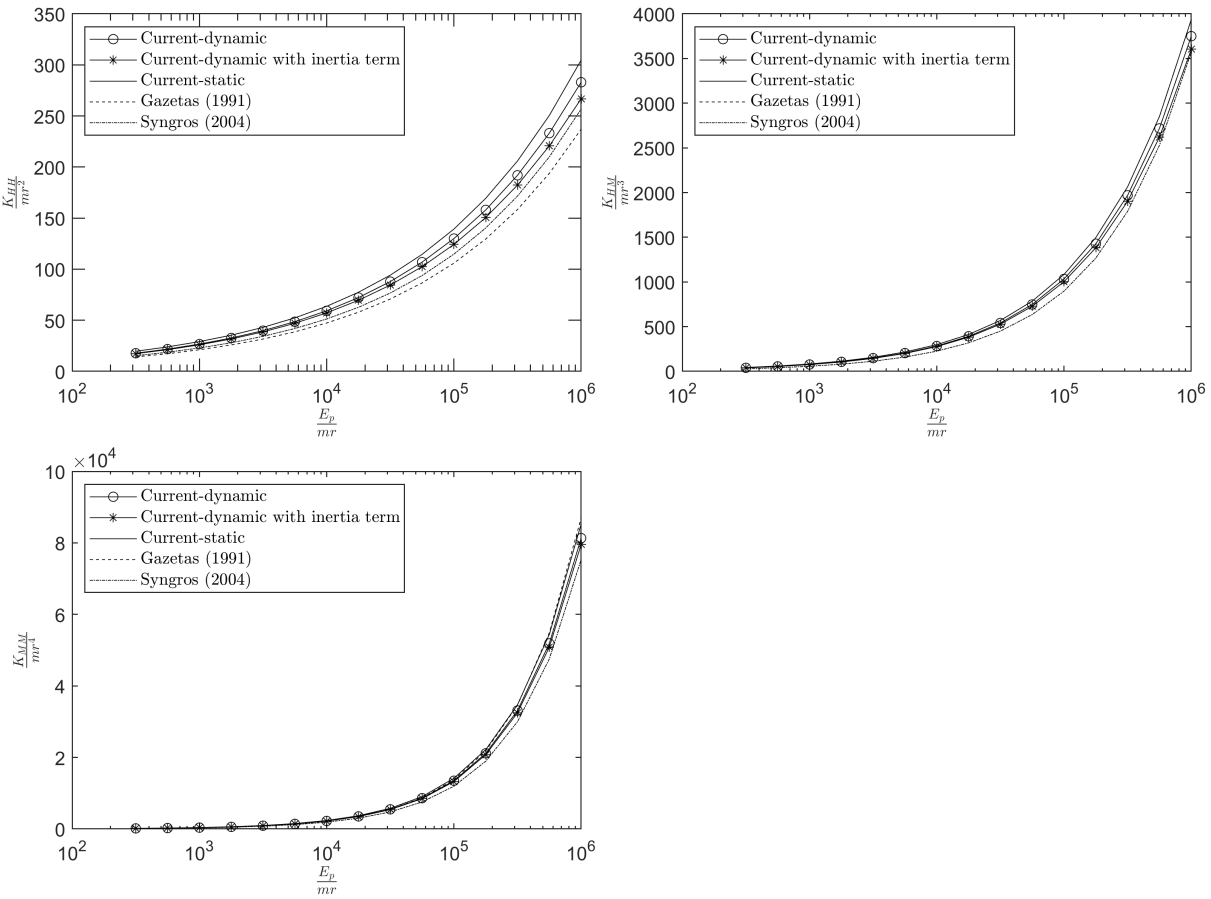

Figure 6.1: Variation of dynamic pile head stiffness with relative pile-soil stiffness for free-head piles embedded in soil with linearly increasing elastic modulus, $\nu_s = 0.4$ and $a_{0r} = 0.5$

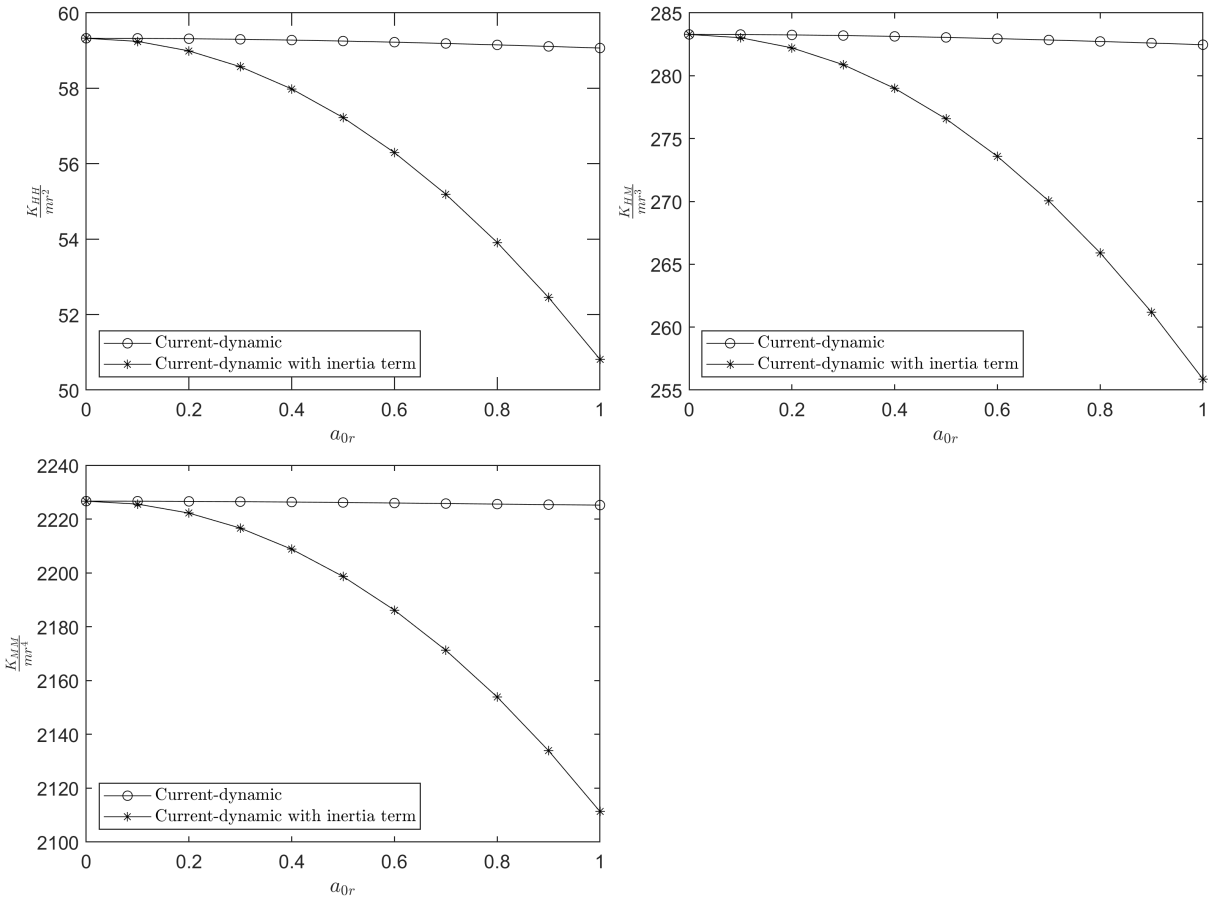

Figure 6.2: Variation of dynamic pile head stiffness with normalized frequency (a_{0r}) for free-head piles embedded in soil with linearly increasing elastic modulus, $\nu_s = 0.4$ and $E_p/mr = 10^4$

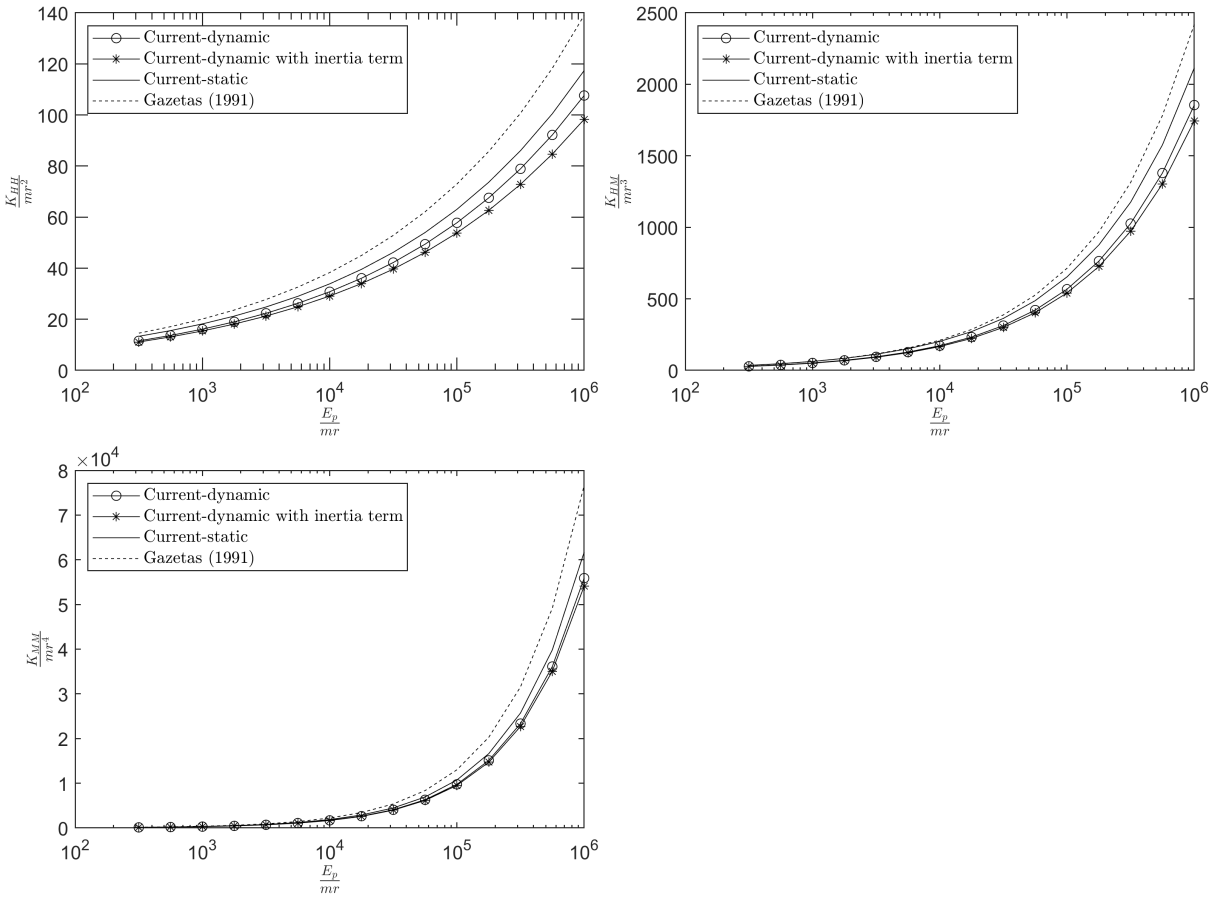

Figure 6.3: Variation of dynamic pile head stiffness with relative pile-soil stiffness for free-head piles embedded in soil with parabolically increasing elastic modulus, $\nu_s = 0.4$ and $a_{0r} = 0.5$

by Gazetas (1991) (see Figures 6.3 and 6.4).

Figure 6.5 presents the variation of dynamic pile head stiffness along with other published works for fixed-head piles. Unlike the free-head case the static and dynamic pile head stiffness vary. The differences between the two cases is approximately 60% for both types of inhomogeneities investigated. This difference also explains the deviation observed in Figure 5.4 (Section 5.1.2) where the static stiffness compared well with Higgins et al. (2013) work which is based on a static finite element analysis while showed some deviation from Syngros (2004) analysis which is based on dynamic analysis.

Similarly, comparing the dynamic pile head stiffness with and without the pile inertia term, it is observed that at higher frequencies the inertia term does influence the pile head stiffness.

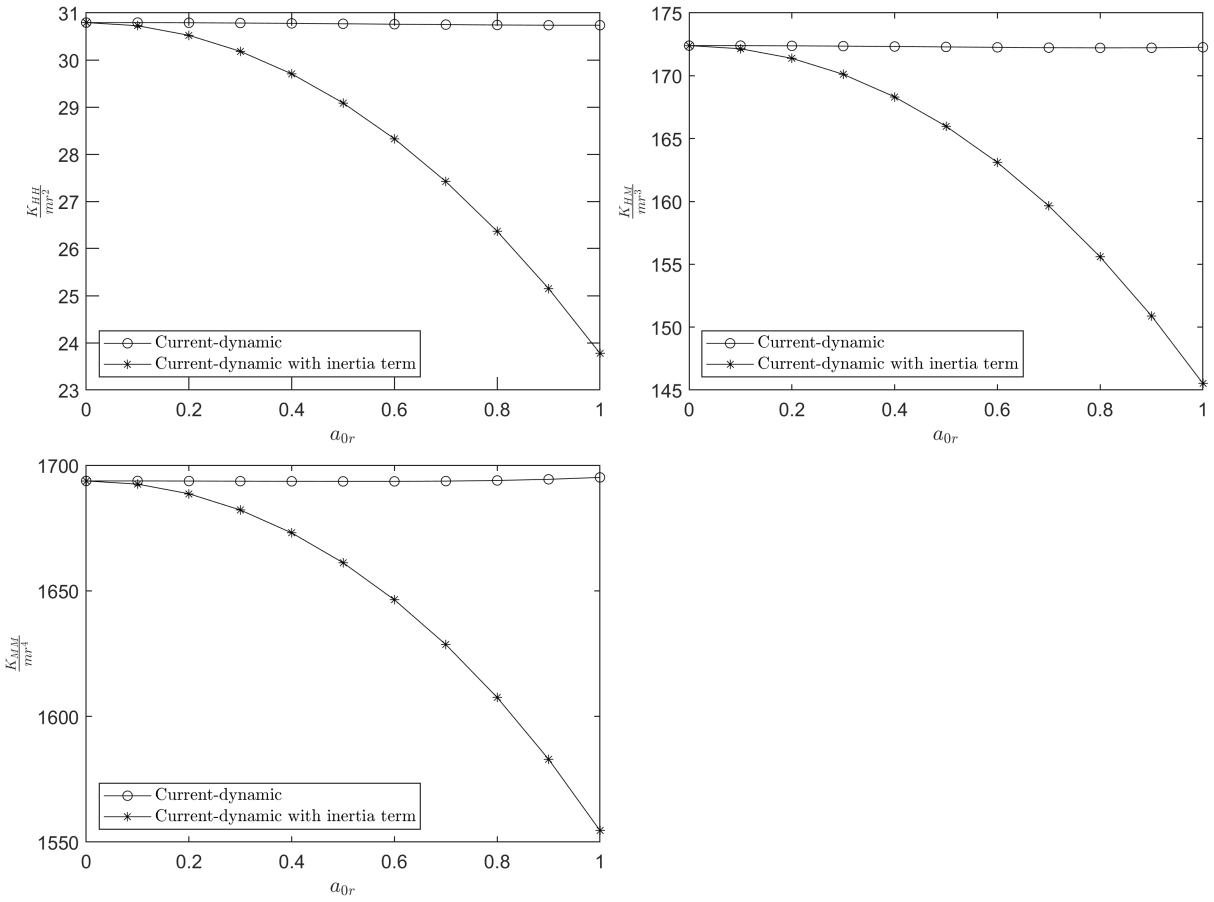

Figure 6.4: Variation of dynamic pile head stiffness with normalized frequency (a_{0r}) for free-head piles embedded in soil with parabolically increasing elastic modulus, $\nu_s = 0.4$ and $^{E_p}/_{mr} = 10^4$

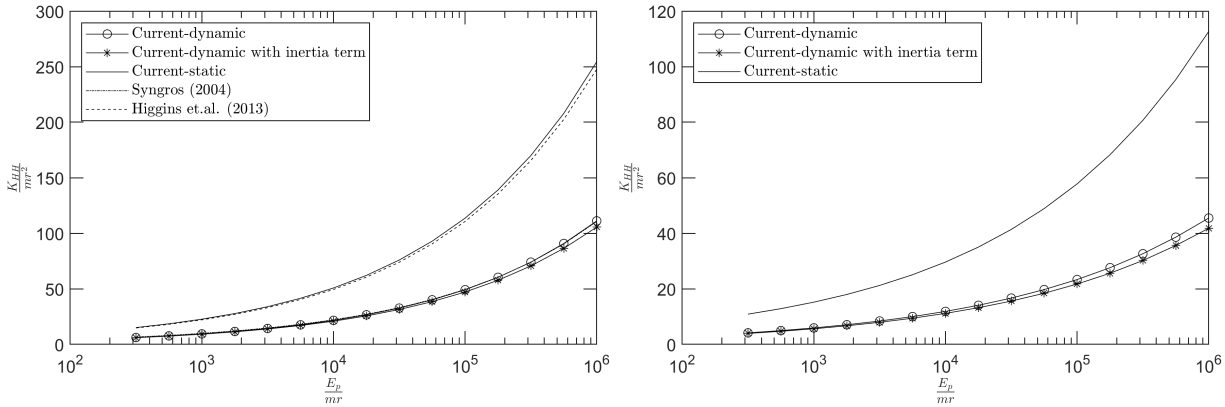

(a) Linearly increasing stiffness (b) Parabolically increasing stiffness

Figure 6.5: Variation of dynamic pile head stiffness with relative pile-soil stiffness for fixed-head piles, $\nu_s = 0.35$ and $a_{0r} = 0.5$

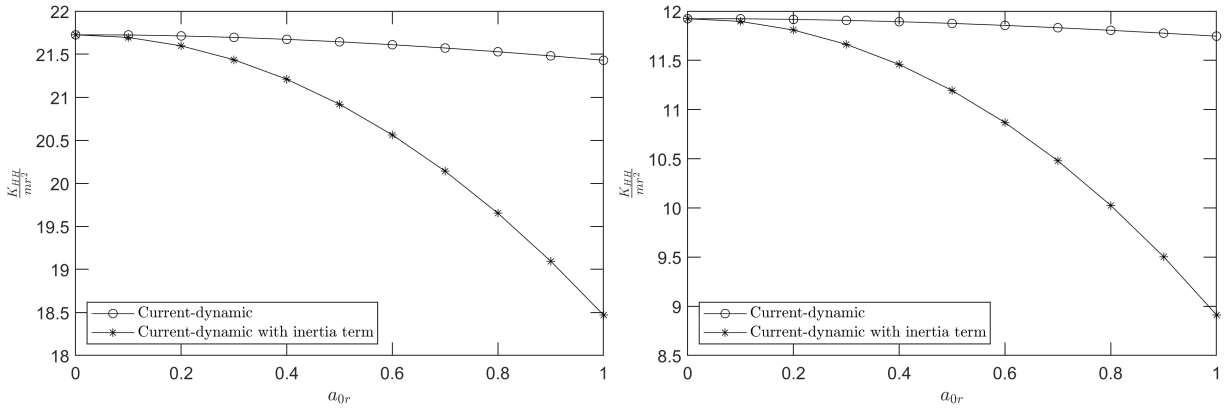

(a) Linearly increasing stiffness (b) Parabolically increasing stiffness

Figure 6.6: Variation of dynamic pile head stiffness with normalized frequency (a_{0r}) for fixed-head piles, $\nu_s = 0.4$ and $^{E_p}/_{mr} = 10^4$

6.2 Pile head damping

The pile head damping is expressed using the pile head dashpot coefficient or equivalently the pile head damping ratio computed from (3.46) and (3.47), respectively. The damping ratio is used for this work. For this purpose, one has to evaluate one of the weighing factors w_{ij}^p or w_{ij}^s and the radiation damping ratio β_{ij}^r using equations (3.48) - (3.50). As noted in the previous sections, the integrals are evaluated numerically. The analysis is done for a range of parameters defined in section 3.3. Additionally, the normalized frequency parameter, a_{0r}, was set to vary over the range of $a_{0r} = 0.0 - 1.0$.

The effect of each parameter on the pile head damping parameters is discussed as follows.

6.2.1 Effect of Poisson's ratio

The Poisson's ratio is found to have the least significance to the material damping weighting factors and radiation damping ratio for both free head and fixed head piles. For example, Figures 6.7 and 6.8 show the variation of the hysteretic soil damping weight factor and radiation damping ratio with the Poisson's ratio, respectively, for $E_p/mr = 10^4$ and $a_{0r} = 0.5$. Overall the variation of w_{ij}^s with Poisson's ratio with respect to the mean value is less than 5%. The same is true for β_{ij}^r with the exception of fixed-head piles in soil with linearly increasing modulus, where the variation increases to 10%. For both damping parameters, it is evident that the Poisson's ratio has negligible effect.

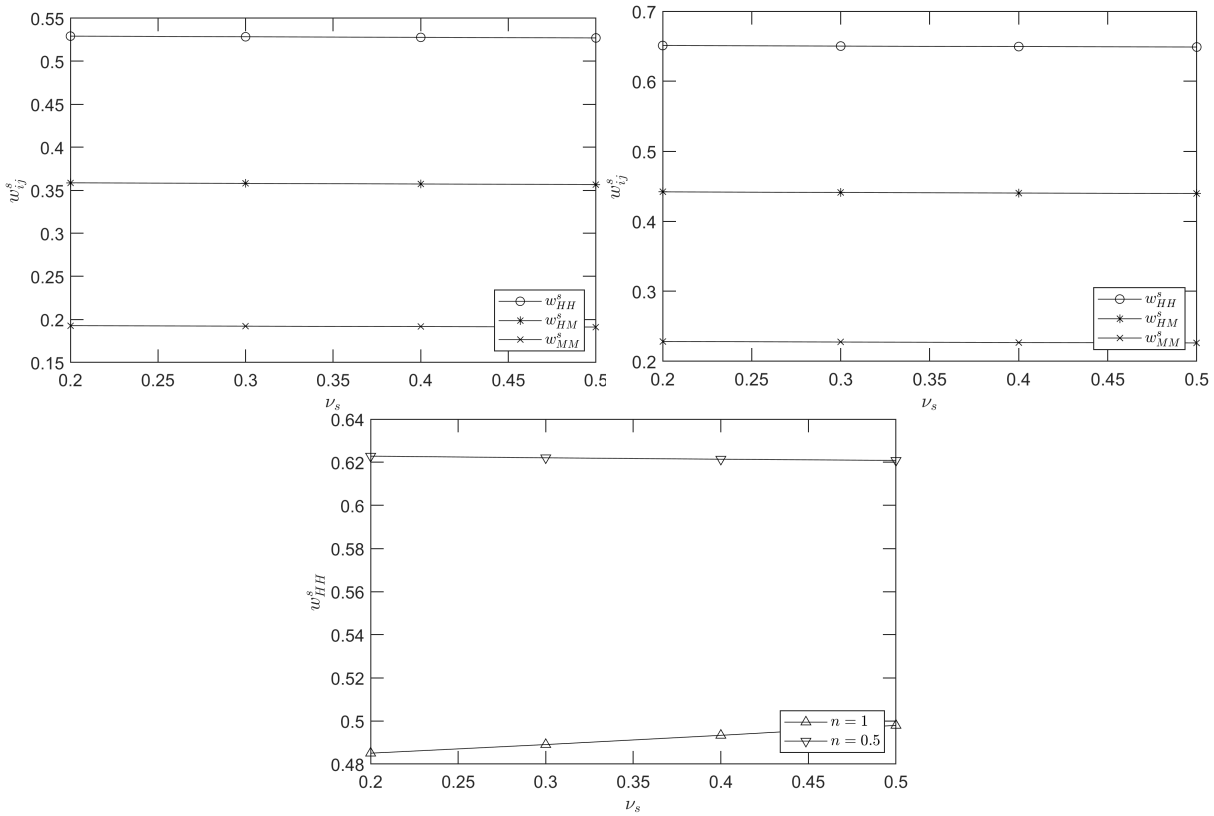

Figure 6.7: Variation of w_{ij}^s with Poisson's ratio for $E_p/mr = 10^4$ and $a_{0r} = 0.5$ (top: free-head pile, left $n = 1$ and right $n = 0.5$, bottom: fixed-head pile)

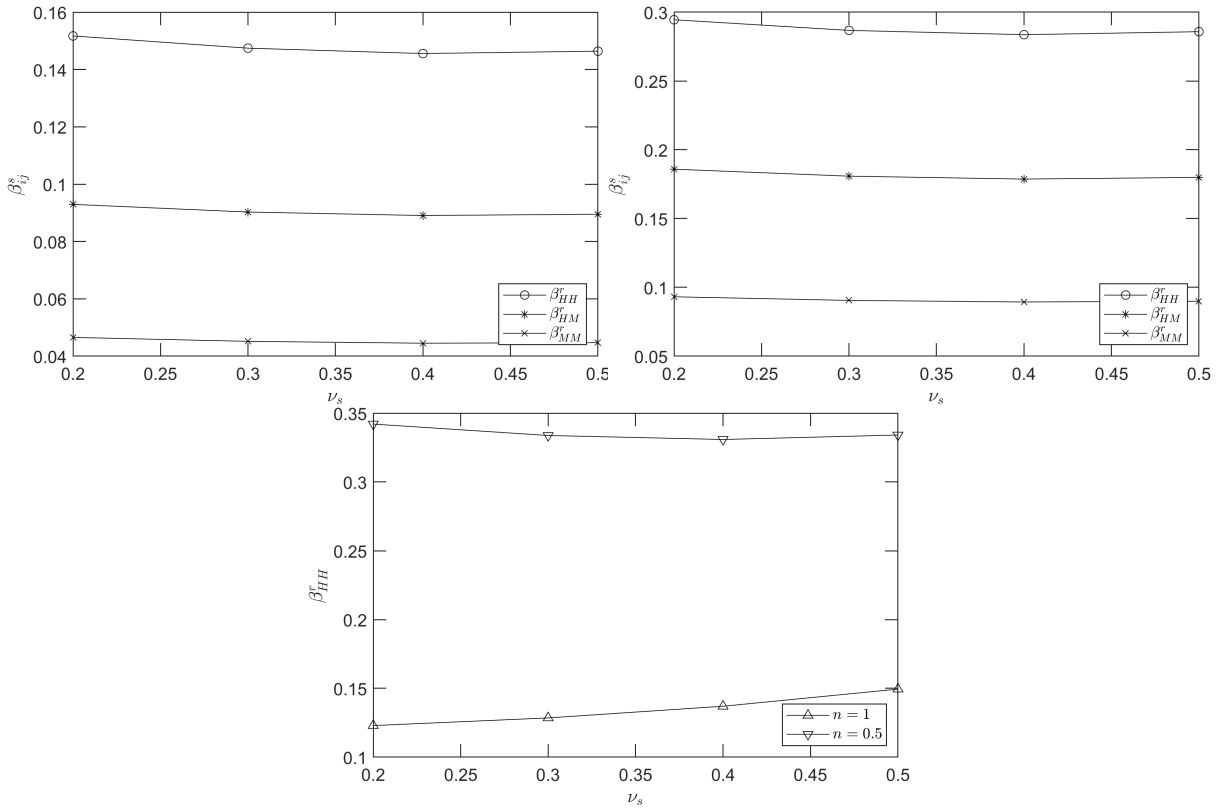

Figure 6.8: Variation of β^r_{ij} with Poisson's ratio for $E_p/mr = 10^4$ and $a_{0r} = 0.5$ (top: free-head pile, left $n = 1$ and right $n = 0.5$, bottom: fixed-head pile)

6.2.2 Effect of relative stiffness

Referring to Figures 6.9 - 6.11 the relative stiffness has a limited influence over the hysteretic soil damping weight factor, w^s_{ij}. In general, the deviation of the individual w^s_{ij} from the mean value with respect to the relative stiffness is less than 5%, with the largest deviations occurring for the rocking mode.

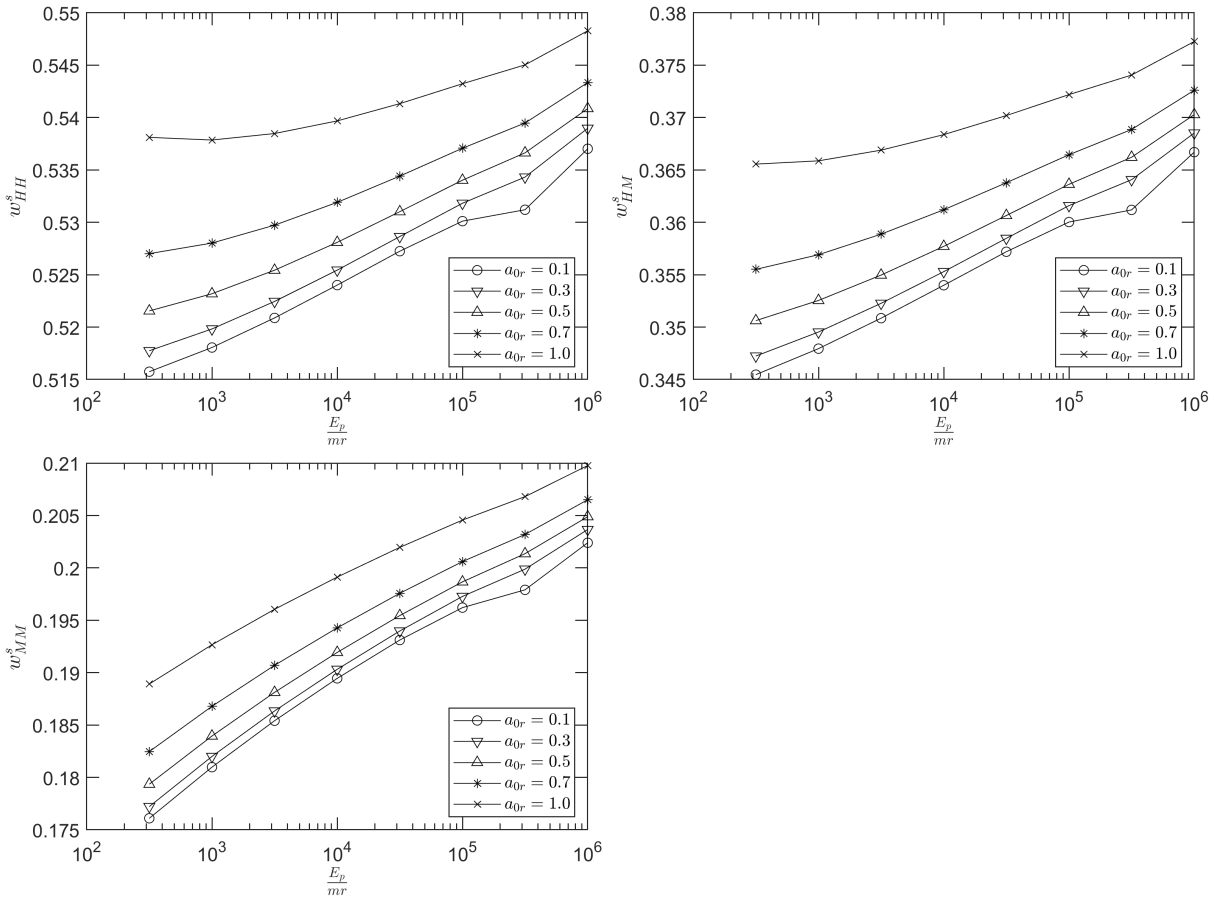

Figure 6.9: Variation of w^s_{ij} with relative stiffness for free-head piles in soil with linearly increasing elastic modulus (results averaged over Poisson's ratio)

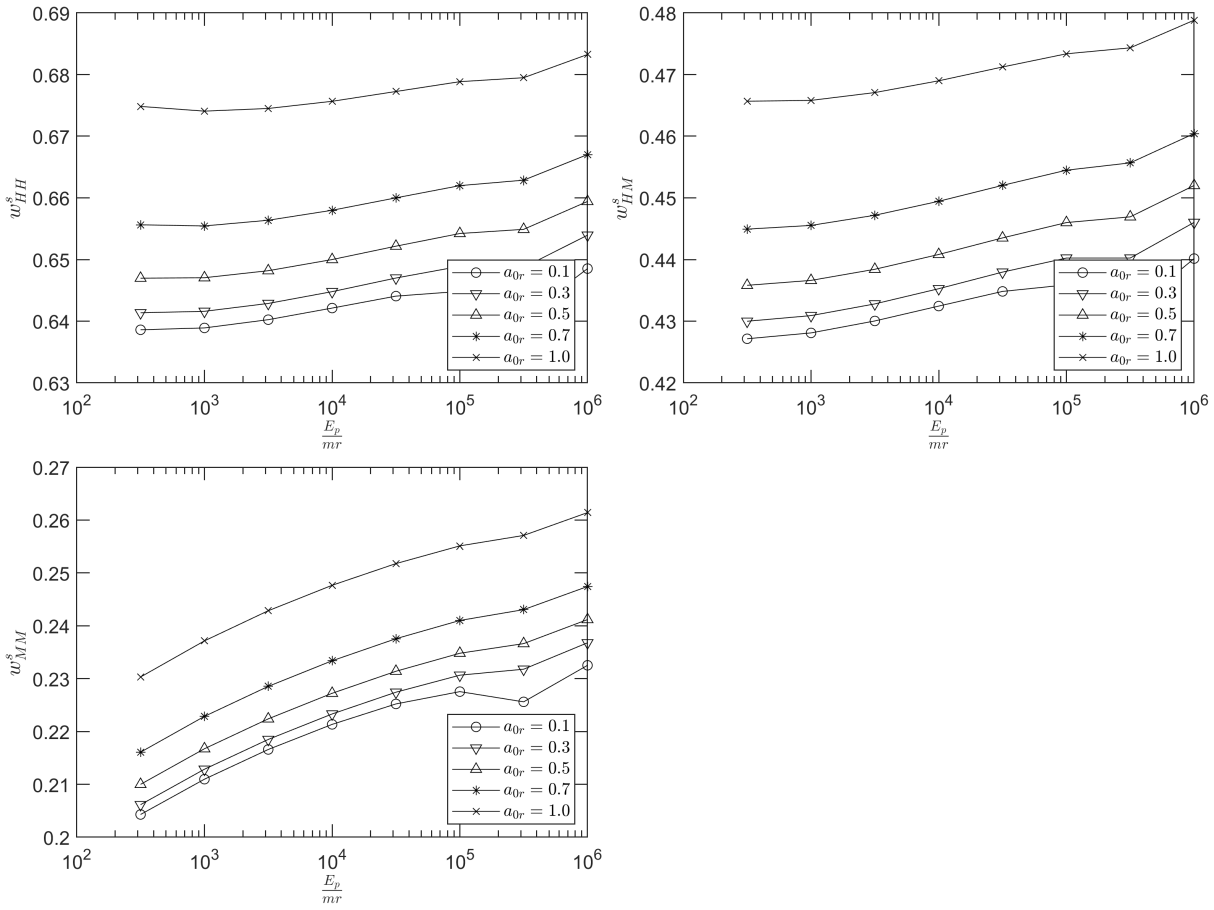

Figure 6.10: Variation of w^s_{ij} with relative stiffness for free-head piles in soil with parabolically increasing elastic modulus (results averaged over Poisson's ratio)

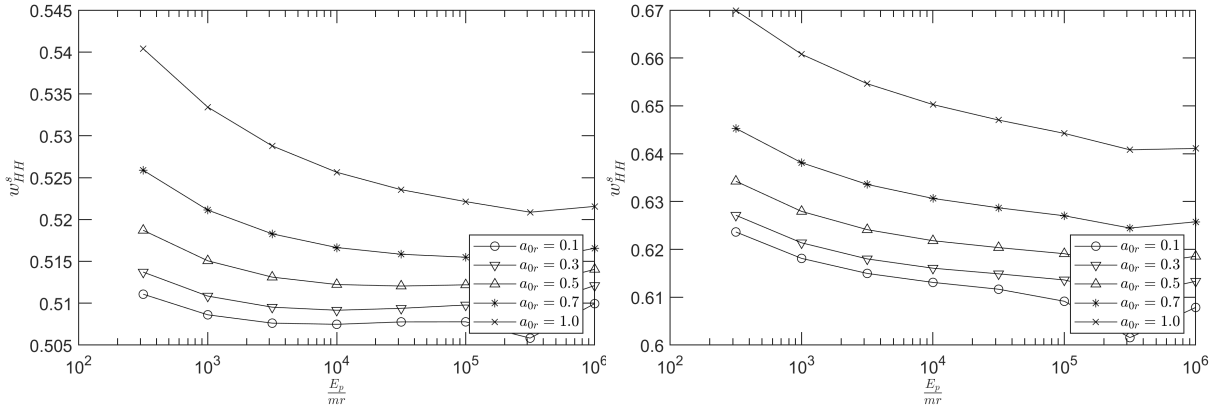

Figure 6.11: Variation of w^s_{ij} with relative stiffness for fixed-head piles with $a_{0r} = 0.5$ (left: $n = 1$, right: $n = 0.5$, results averaged over Poisson's ratio)

On the other hand, the radiation damping ratios, β^r_{ij}, increase with the relative stiffness irrespective of the form of non-homogeneity and pile head condition. The trend is most pronounced at the higher end of the excitation frequency range investigated (see Figures 6.12 - 6.14). Comparing free-head piles (Figure 6.12 and 6.13) to fixed-head (Figure

6.14) ones, the effect of $\frac{E_p}{mr}$ is relatively more marked for free-head piles.

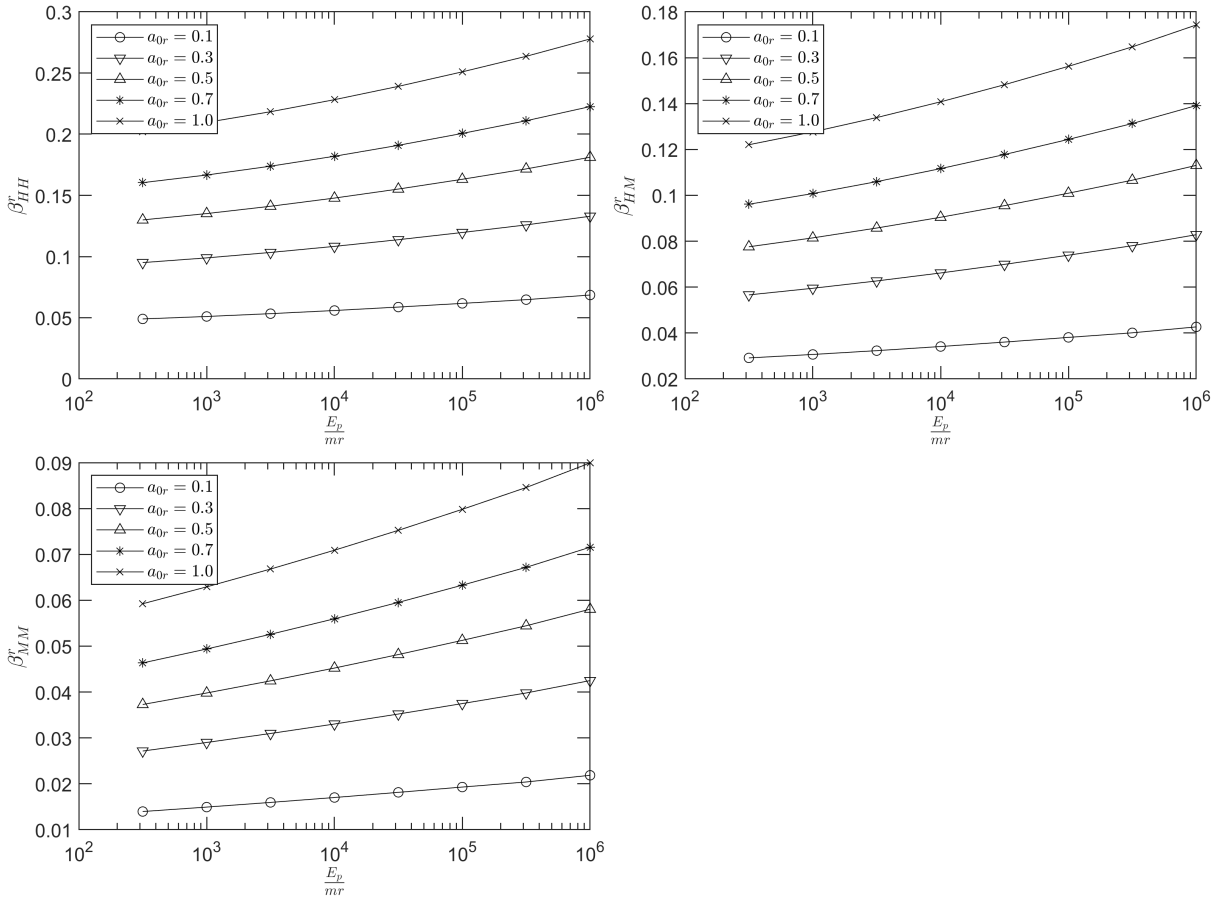

Figure 6.12: Variation of β^r_{ij} with relative stiffness for free-head piles in soil with linearly increasing elastic modulus (results averaged over Poisson's ratio)

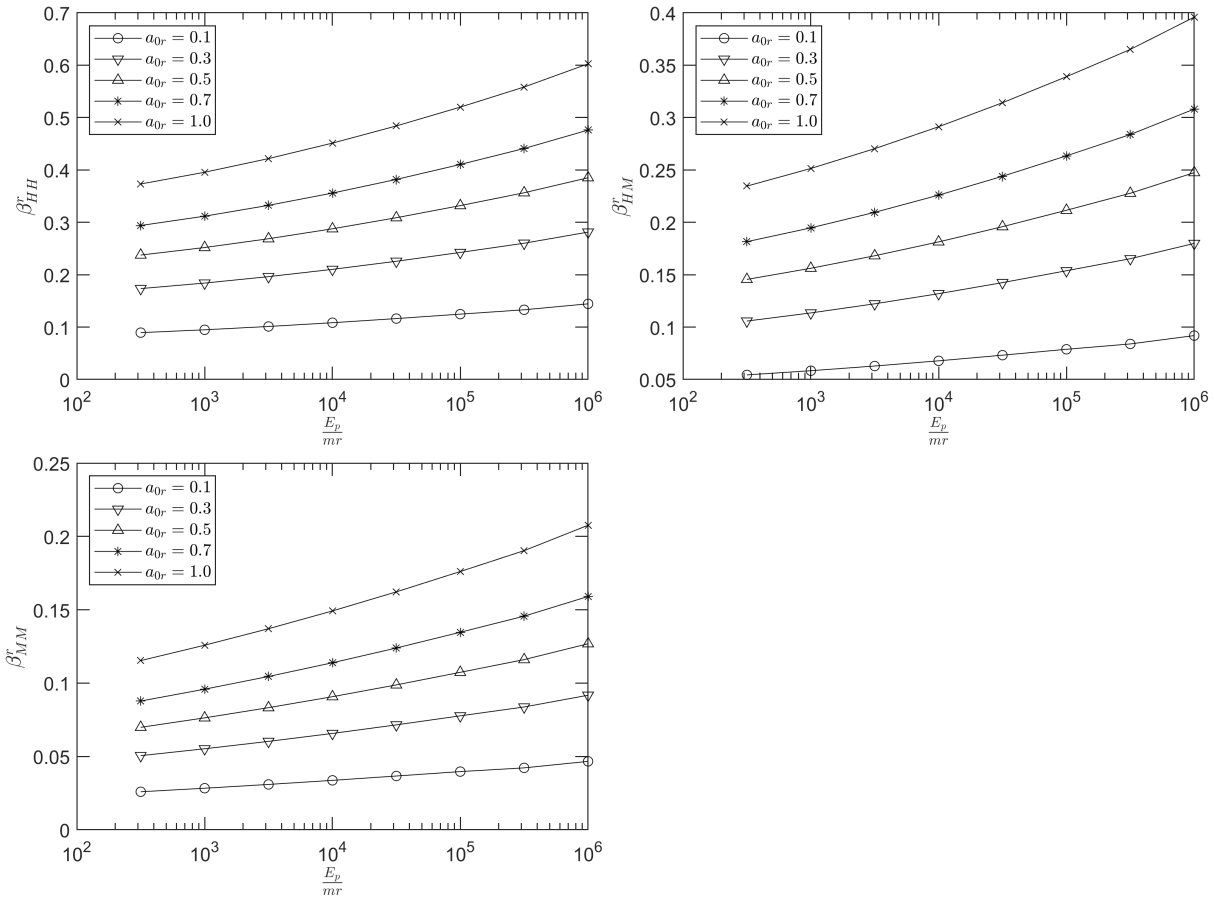

Figure 6.13: Variation of β^r_{ij} with relative stiffness for free-head piles in soil with parabolically increasing elastic modulus (results averaged over Poisson's ratio)

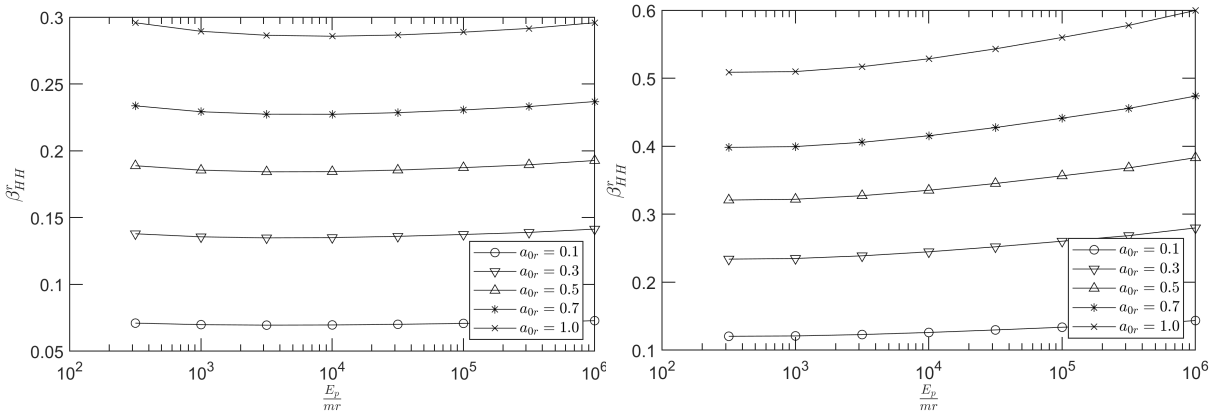

Figure 6.14: Variation of β^r_{ij} with relative stiffness for fixed-head piles (left: $n = 1$, right: $n = 0.5$, results averaged over Poisson's ratio)

6.2.3 Effect of excitation frequency

Similar to the Poisson's ratio and relative stiffness, the influence of the excitation frequency on the material damping weight factor is negligible (See Figures 6.15 - 6.17). In

the figures, it may appear that excitation frequency may have an influence but note the scale of the ordinate which is very small.

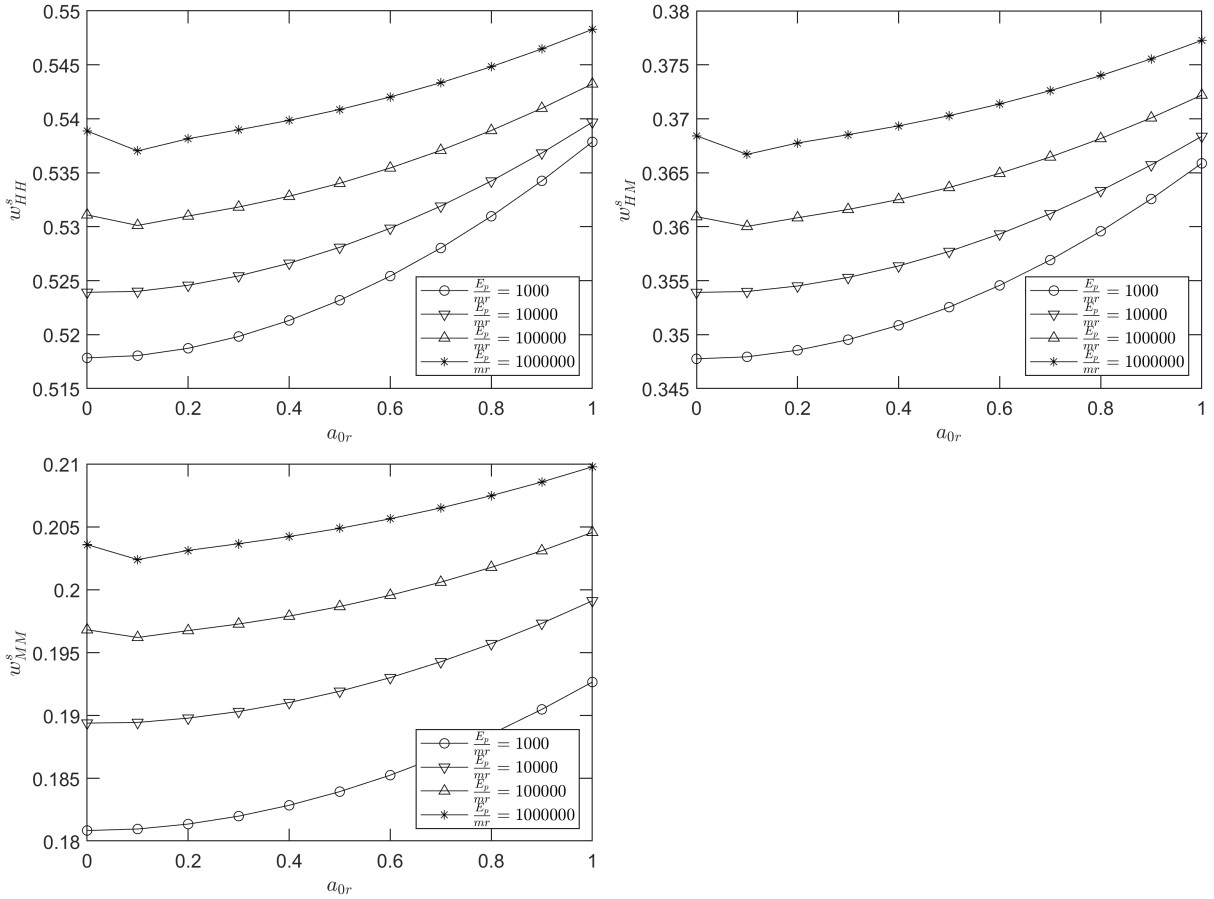

Figure 6.15: Variation of w^s_{ij} with normalized frequency for free-head piles in soil with linearly increasing elastic modulus (results averaged over Poisson's ratio)

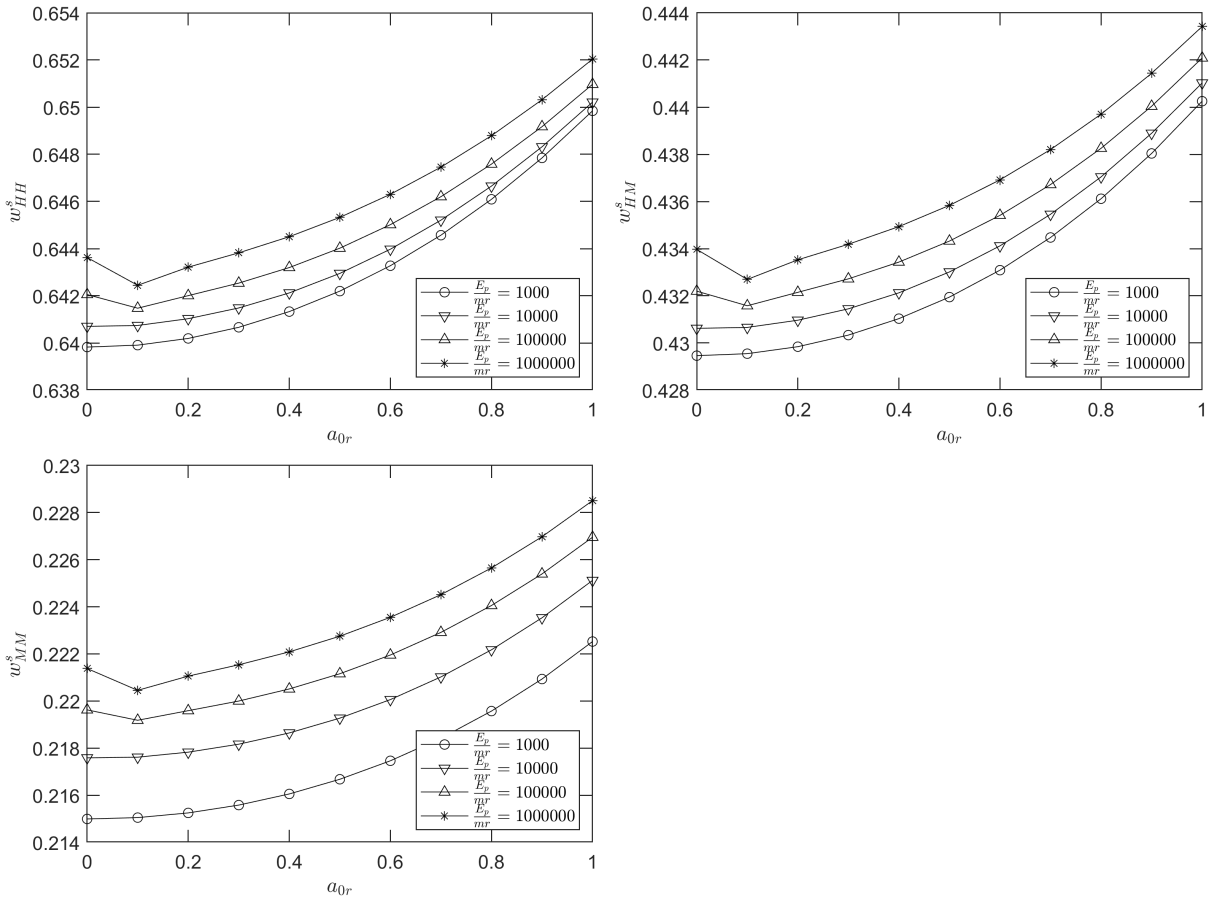

Figure 6.16: Variation of w^s_{ij} with normalized frequency for free-head piles in soil with parabolically increasing elastic modulus (results averaged over Poisson's ratio)

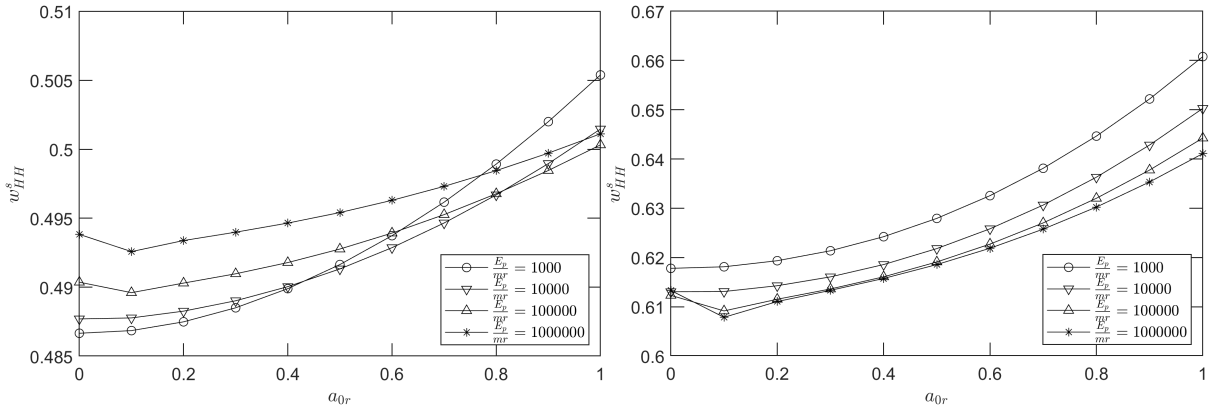

Figure 6.17: Variation of w^s_{ij} with normalized frequency for fixed-head piles (left: $n = 1$, right: $n = 0.5$, results averaged over Poisson's ratio)

On the contrary, the radiation damping coefficient shows appreciable change with respect to the normalized excitation frequency. Referring to Figures 6.18 - 6.20, the radiation damping coefficient increases with the excitation frequency. Relatively, the frequency is the most dominant parameter governing the variation of radiation damping as could be

expected.

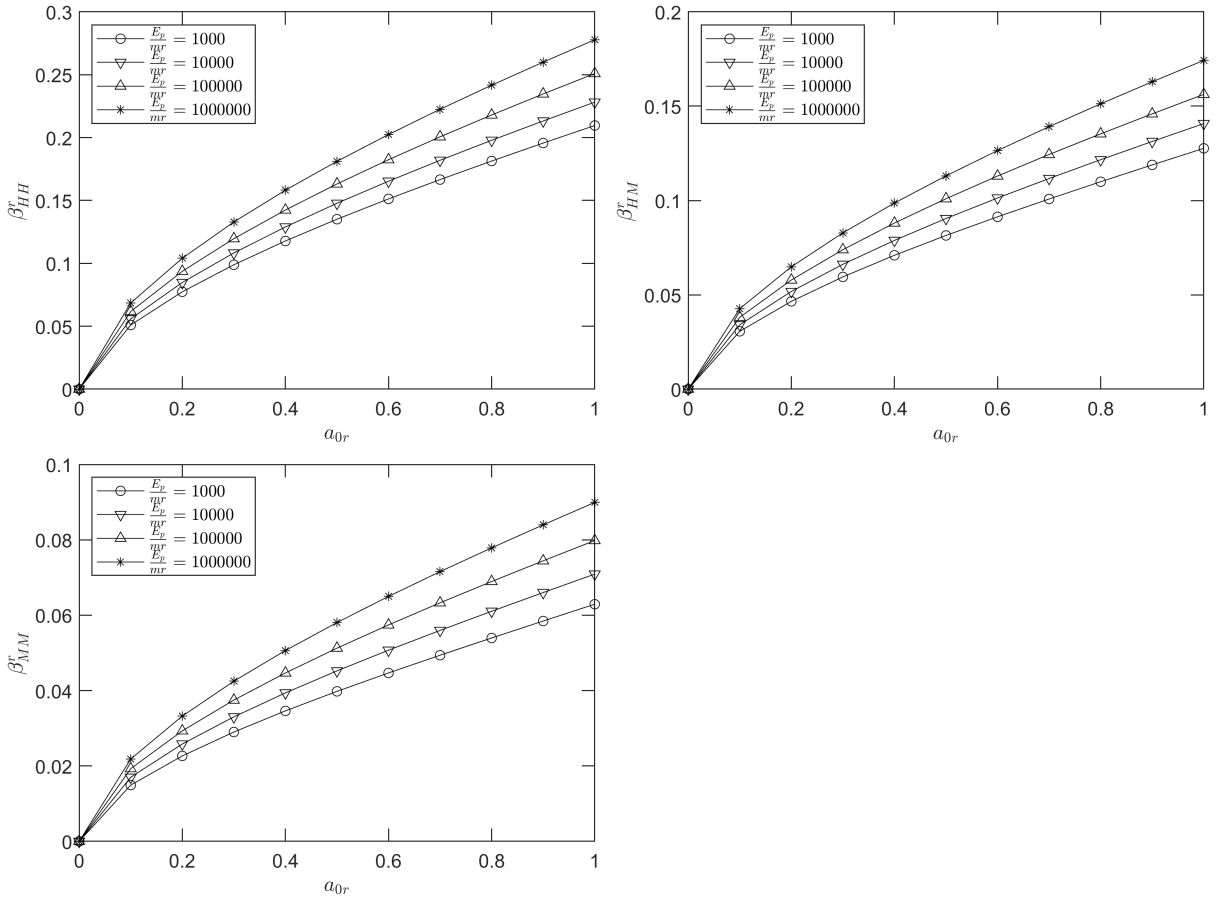

Figure 6.18: Variation of β^r_{ij} with normalized frequency for free-head piles in soil with linearly increasing elastic modulus (results averaged over Poisson's ratio)

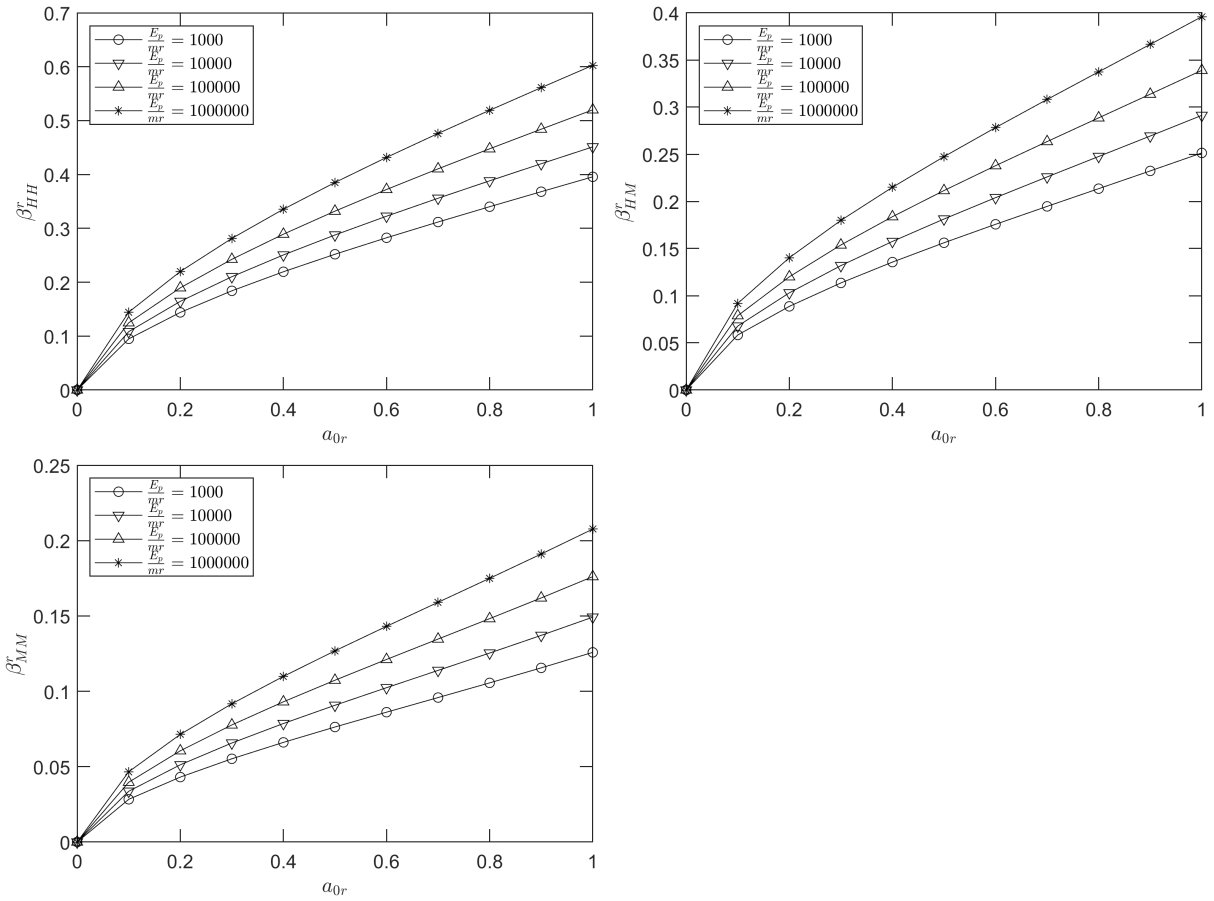

Figure 6.19: Variation of β^r_{ij} with normalized frequency for free-head piles in soil with parabolically increasing elastic modulus (results averaged over Poisson's ratio)

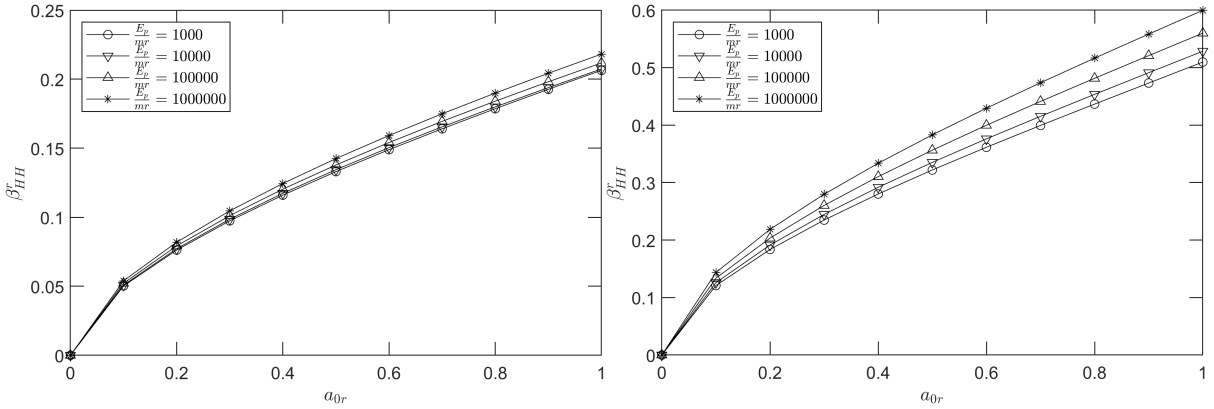

Figure 6.20: Variation of β^r_{ij} with normalized frequency for fixed-head piles (left: $n = 1$, right: $n = 0.5$, results averaged over Poisson's ratio)

6.3 Expressions for pile head impedance functions

From the forgoing discussions in subsections 6.1 and 6.2, the following points are summarized:

- For low frequency excitation, the dynamic pile head stiffness can reasonably be approximated by the static pile head stiffness for free-head piles, Figures 6.1 and 6.3. For fixed-head piles there is a reduction in stiffness from the static case.
- The Poisson's ratio is the least significant parameter affecting the pile head damping with maximum variations in the range of 10%.
- The hysteretic soil damping weight factor w_{ij}^{s} is practically independent of all parameters investigated.

Therefore, no new expressions are developed for the dynamic piled head stiffness for free-head piles and it is proposed that it be approximated by the static pile head stiffness given by (5.15) - (5.18). This is in line with that reported in similar works of Gazetas (1991), Syngros (2004), and Karatzia and Mylonakis (2017). On the other hand for fixed-head piles new curve fit expressions are proposed as follows:

$$K_{HH} = 0.80 \left(\frac{E_p}{mr} \right)^{0.36} \tag{6.7}$$

for piles embedded in soil with linearly increasing elastic modulus and

$$K_{HH} = 0.80 \left(\frac{E_p}{mr} \right)^{0.29} \tag{6.8}$$

for piles embedded in soil with parabolically increasing elastic modulus. Equation (6.7) and (6.8) are similar to their static counterparts in (5.25) and (5.26) with the exception that this expressions involve coefficients about 60% smaller than the static ones. Note that the Poisson's ratio term is not included in (6.7) and (6.8) but the expression was developed using K_{HH} values averages over the range of Poisson's ratios investigated. This is justified since the effect of the Poisson's ratio is limited as observed in the static case.

Table 6.1: Proposed mean values for material damping weight factor

Pile head condition	n	w^s_{HH}	w^s_{HM}	w^s_{MM}
Free-head	1	0.53	0.36	0.19
	0.5	0.65	0.45	0.23
Fixed-head	1	0.51	–	–
	0.5	0.63	–	–

In regards to the material damping, constant values of the weight factor are proposed by averaging results across all parameters investigated. These values are given in Table 6.1.

For the radiation damping ratio, the effect of the Poisson's ratio is neglected and results are averaged across it. Then, curve fitting is used to provide expressions for the radiation damping ratio as functions of the relative stiffness and normalized excitation frequency.

The proposed expression for β^r_{ij} are given by:

$$\beta^r_{HH} = 0.16 a_{0r}^{0.61} \left(\frac{E_p}{mr}\right)^{0.04} \tag{6.9}$$

$$\beta^r_{HM} = 0.09 a_{0r}^{0.62} \left(\frac{E_p}{mr}\right)^{0.05} \tag{6.10}$$

$$\beta^r_{MM} = 0.05 a_{0r}^{0.63} \left(\frac{E_p}{mr}\right)^{0.05} \tag{6.11}$$

for free-head piles embedded in soil with linearly increasing elastic modulus and

$$\beta^r_{HH} = 0.26 a_{0r}^{0.63} \left(\frac{E_p}{mr}\right)^{0.06} \tag{6.12}$$

$$\beta^r_{HM} = 0.16 a_{0r}^{0.65} \left(\frac{E_p}{mr}\right)^{0.07} \tag{6.13}$$

$$\beta^r_{MM} = 0.07 a_{0r}^{0.67} \left(\frac{E_p}{mr}\right)^{0.07} \tag{6.14}$$

for free-head piles embedded in soil with parabolically increasing elastic modulus. Similarly, the expressions for fixed head piles embedded in soil with linearly increasing elastic modulus is given by:

$$\beta_{HH}^{r} = 0.28 a_{0r}^{0.62} \left(\frac{E_p}{mr} \right)^{0.002} \tag{6.15}$$

and

$$\beta_{HH}^{r} = 0.43 a_{0r}^{0.63} \left(\frac{E_p}{mr} \right)^{0.02} \tag{6.16}$$

for fixed head piles embedded in soil with parabolically increasing elastic modulus.

The proposed pile head damping coefficients are compared against published works as shown in Figures 6.21 - 6.23. In the comparison, a soil damping ratio of $\beta_s = 5\%$ was taken while the pile material damping was not considered ($\beta_p = 0$) for compatibility with the published works. For free-head piles embedded in soil with linearly increasing elastic modulus, the proposed damping ratios are larger than those provided by Gazetas (1991) while being lower than those provided by Syngros (2004) in the lower frequency range with the exception of the swaying mode. For fixed head piles embedded in soil with linearly increasing elastic modulus, the proposed damping ratios are larger than those proposed by Syngros (2004) (Figure 6.23). On the other hand, for free-head piles embedded in soil with parabolicaly increasing elastic modulus, the proposed damping ratios are larger than those proposed by Gazetas (1991). Over all the proposed damping ratios are consistently larger than the damping ratios proposed by Gazetas (1991) while being lower than Syngros (2004).

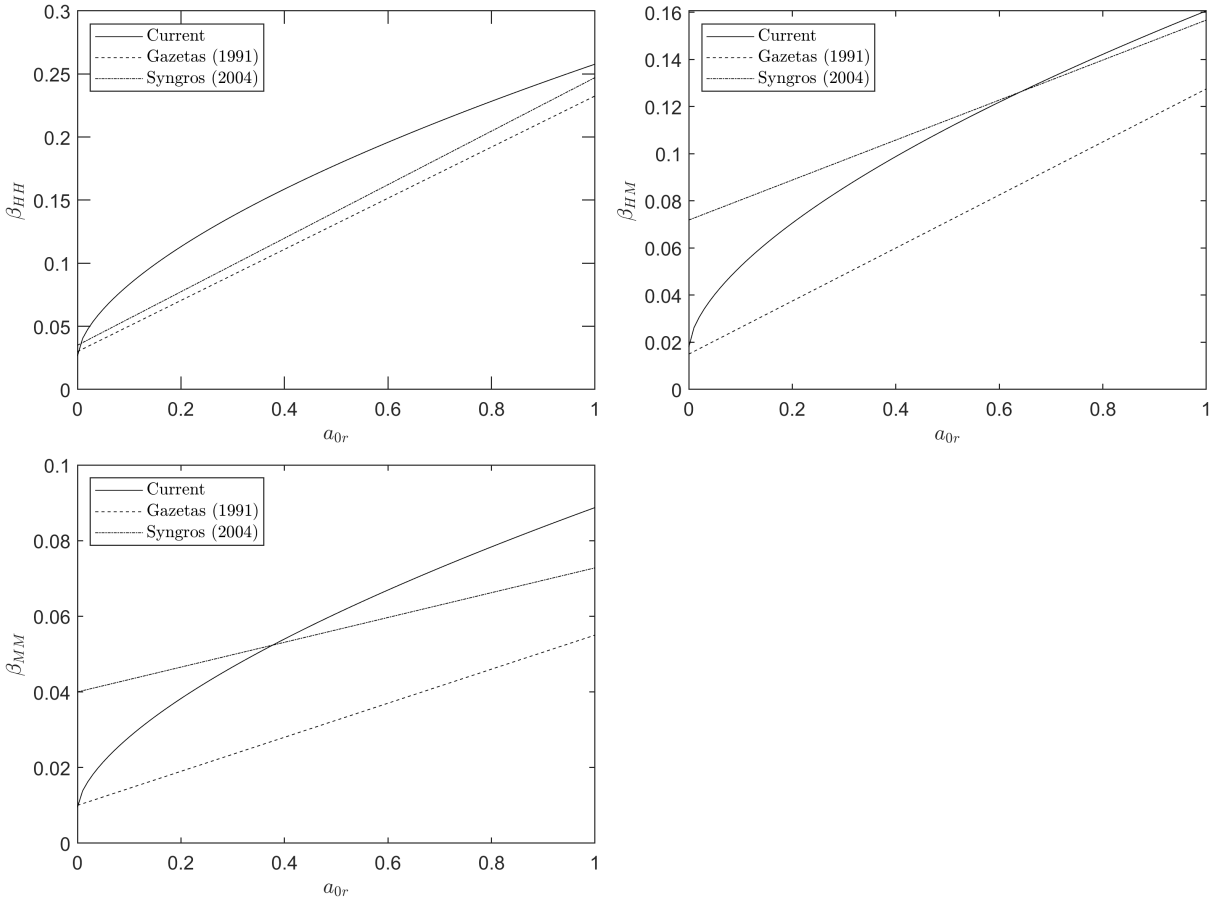

Figure 6.21: Comparison of proposed β_{ij} against published literature for free-head piles in soil with linearly increasing elastic modulus and $\beta_s = 5\%$

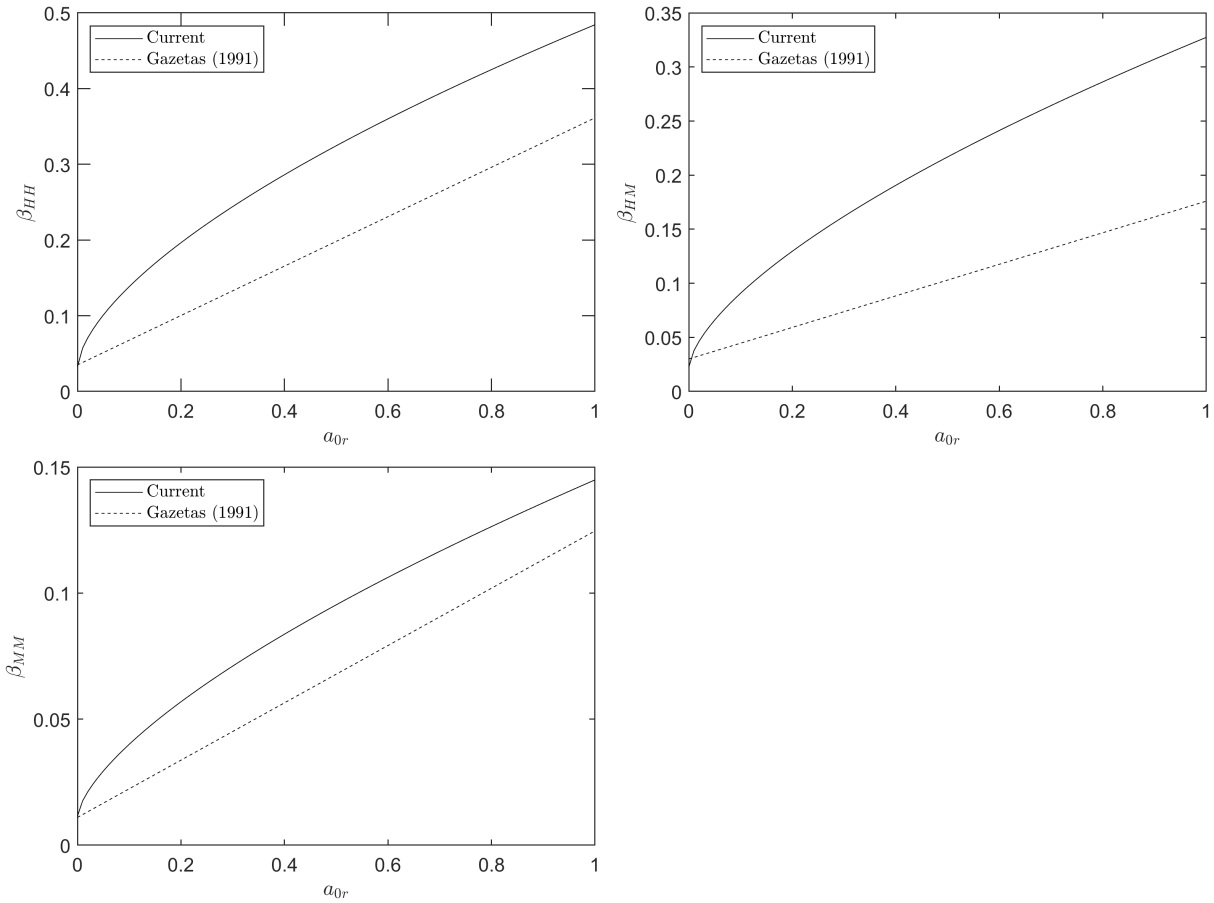

Figure 6.22: Comparison of proposed β_{ij} against published literature for free-head piles in soil with parabolically increasing elastic modulus and $\beta_s = 5\%$

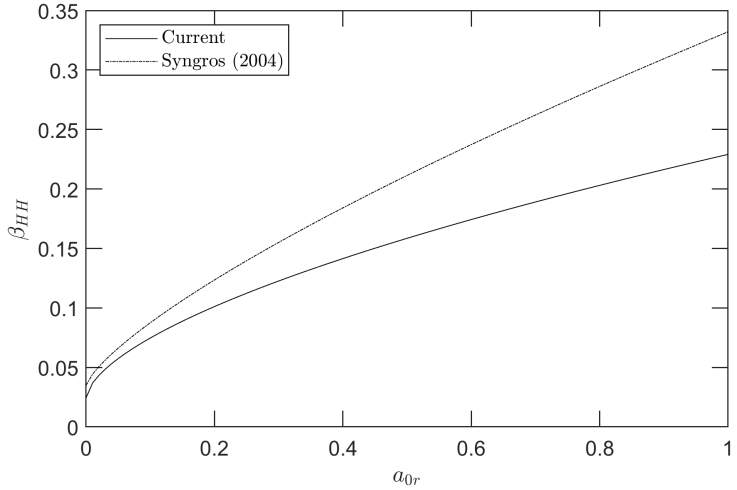

Figure 6.23: Comparison of proposed β_{ij} against published literature for fixed-head piles in soil with linearly increasing elastic modulus and $\beta_s = 5\%$

6.4 Effect of shear interaction in dynamic inertial response

Following from section 5.3, the effect of shear interaction, which is explicitly accounted for in Worku's 2014 Kerr-equivalent Pasternak subgrade is investigated for dynamic inertial interaction. The approach is the same with that of the static response, in that pile head response computed with and without the shear term are compared to investigate the effect of the shear term. For the dynamic inertial case, the approximate energy method with assumed shape functions is used.

As noted in the previous section, the dynamic pile head stiffness is approximated by the static one with the exception of fixed-head piles. Thus, the effect of shear interaction on this parameters will be similar to that for the static case discussed in section 5.3. Therefore in this section, emphasis is given to the effect of shear interaction on the pile head damping. It should be remembered that the approximate energy formulation used for dynamic inertial interaction is limited to long flexible piles.

Figure 6.24 presents the variation of the pile head damping ratio with excitation frequency for free-head piles in soil with linearly increasing elastic modulus. For the swaying and cross swaying-rocking modes the the damping ratio with and without the shear term are very similar with the damping ratio computed with the shear term included being slightly larger. For the rocking excitation mode, the difference between the damping ratio obtained with and without the shear term widens as the excitation frequency increases.

Figure 6.25, shows the the variation of the pile head damping ratio with excitation frequency for fixed-head piles in soil with linearly increasing elastic modulus. Alike, the free-head case, the effect of the shear term on β_{HH} is practicably negligible.

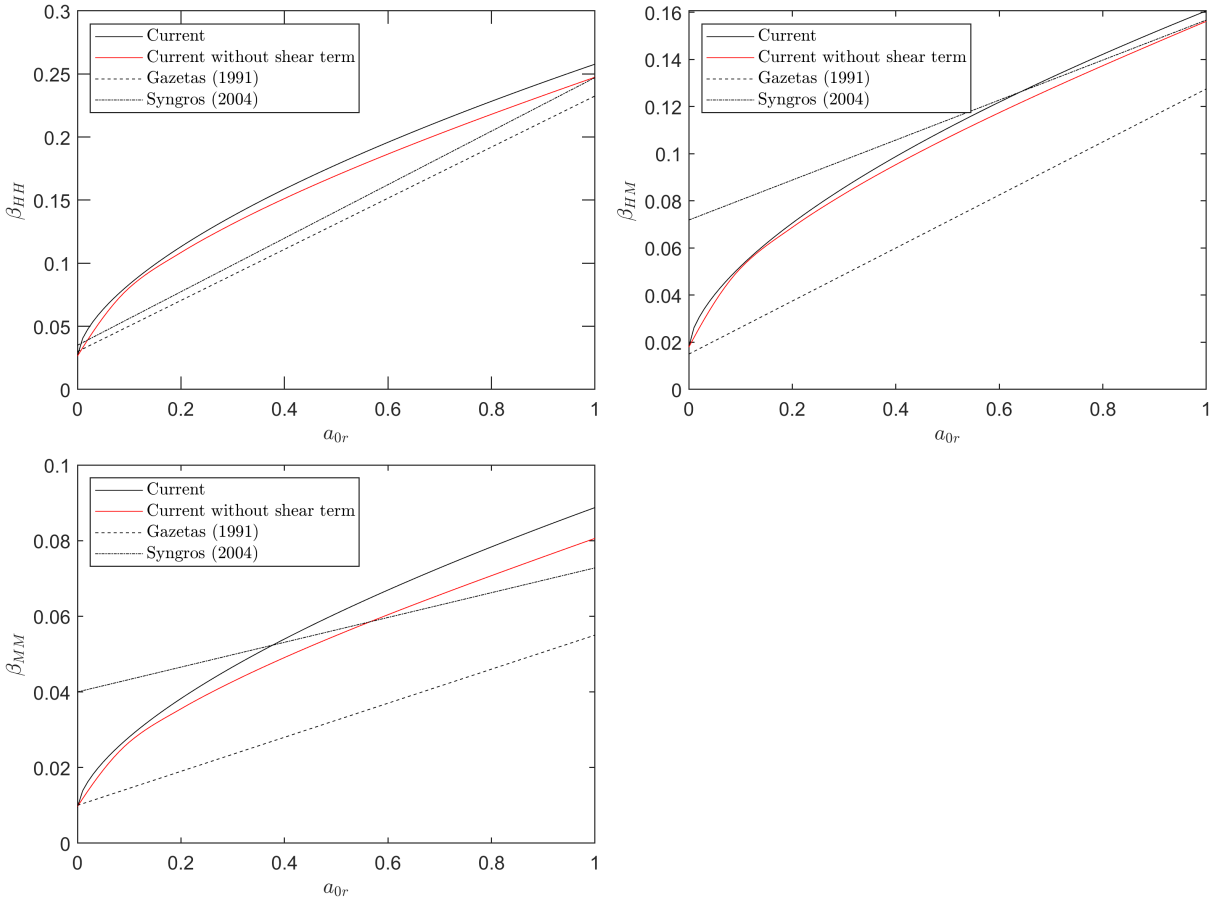

Figure 6.24: Variation of β_{ij} with a_{0r} for free-head piles in soil with linearly increasing elastic modulus, $^{E_p}/_{mr} = 10^4$ and $\beta^s = 5\%$ (results averaged over the Poisson's ratio)

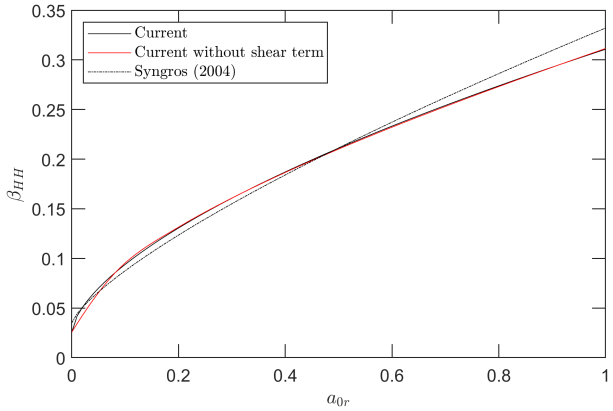

Figure 6.25: Variation of β_{ij} with a_{0r} for fixed-head piles in soil with linearly increasing elastic modulus, $^{E_p}/_{mr} = 10^4$ and $\beta^s = 5\%$ (results averaged over the Poisson's ratio)

For piles embedded in soil with parabolically increasing elastic modulus, the effect of the shear interaction is similar to that for linearly increasing elastic modulus with exception that the damping ratio formulated without the shear term is larger than the one with shear term for the rocking mode of oscillation. But in general, like the linearly increasing

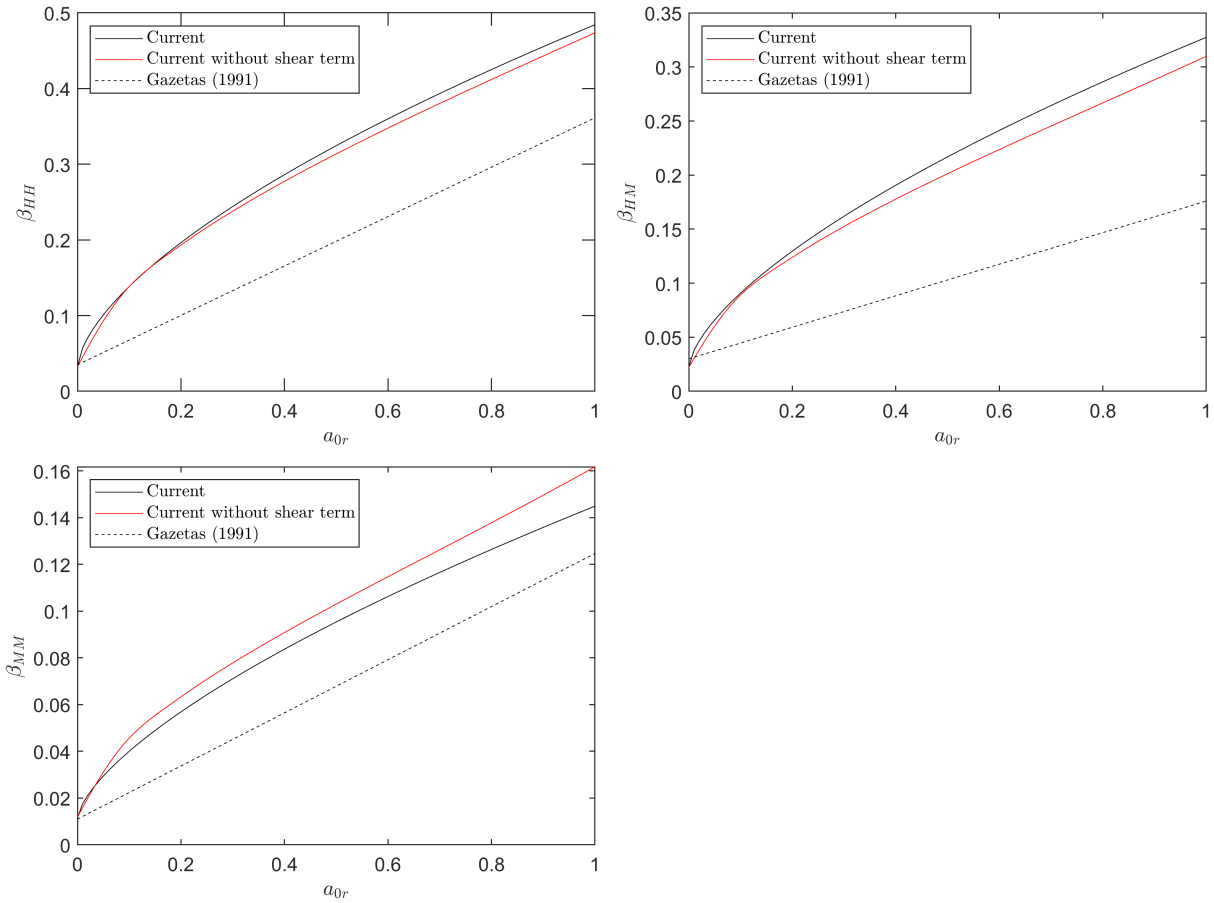

Figure 6.26: Variation of β_{ij} with a_{0r} for free-head piles in soil with parabolically increasing elastic modulus, $E_p/mr = 10^4$ and $\beta^s = 5\%$ (results averaged over the Poisson's ratio)

case, the difference between the damping ratio with and without the shear term are small (see Figures 6.26 and 6.27).

From the forgoing discussion the following points are summarized

- The effect of shear term is very minimal except for the rocking mode of excitation. Based what was observed from the effect of the shear term on the static response (Section 5.3), such minimal influence may be due to the fact that the above formulations are limited to long flexible piles.

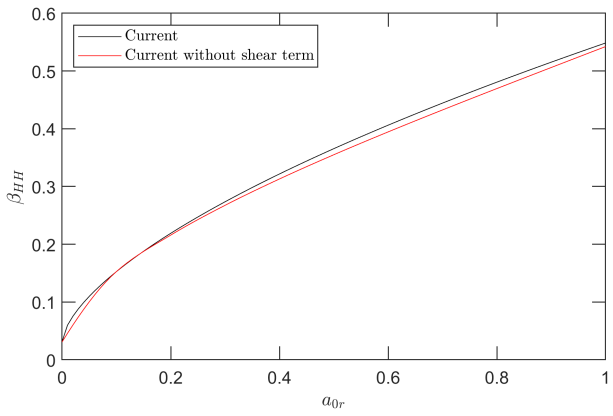

Figure 6.27: variation of β_{ij} with a_{0r} for fixed-head piles in soil with parabolically increasing elastic modulus, $E_p/mr = 10^4$ and $\beta^s = 5\%$ (results averaged over the Poisson's ratio)

Chapter 7

Conclusions and Recommendations

7.1 Conclusions

It is to be remembered that the primary objective of this thesis is to study the applicability of the Kerr-equivalent Pasternak-type continuum model developed by Worku (2014) for laterally loaded piles in non-homogeneous soils for both static and dynamic inertial cases. The specific objectives are to evaluate the calibration factor left open in the model for non-homogeneous profiles of the type $E_s(z) = mr\left(\frac{z}{r}\right)^n$, to formulate an expression for the critical (active) slenderness ratio, to study the response of a pile embedded in the non-homogeneous soil due static loads and dynamic inertial interaction and investigate the effect of shear interaction that is explicitly accounted for in the subgrade model.

To this end, an extensive finite element analysis was conducted and pile head displacements from the analysis were compared with those from the beam-on-Pasternak subgrade analysis to determine the calibration factor. The calibration factors were determined for linearly ($n = 1$) and parabolically ($n = 1/2$) increasing soil profiles. Expressions for the calibration factor were developed through curve fitting along with ranges for their applicability. The developed expressions were verified against finite element analysis and resulted in displacements within a mean value of 4% of the finite element results at the pile head.

It was also noted that the calibration factor mimics the pile head displacement, exhibit-

ing independence to the relative stiffness for short rigid piles and independence to the slenderness ratio for long flexible piles. Furthermore, the threshold values used in developing expressions for the calibration factor were found to be similar to the critical (active) slenderness ratio and the critical relative stiffness. Thus, mirroring the trends of the latter parameters and providing an indirect estimate for them.

Using the calibrated model, the static response of the pile is investigated using the beam-on-Pasternak subgrade analysis. The resulting boundary value problem was solved numerically. Expressions for the static pile head flexibility influence factors and stiffness coefficients were provided. These expressions, for the most part, were shown to be comparable with those reported in the literature. Furthermore, the fact that the subgrade model involved an explicit shear term was utilized as a good advantage to investigate the effect of shear interaction in static pile response. It was observed that neglecting the shear term resulted in overestimation of the pile head displacement with the most significant effects being observed for short rigid free-head piles. In addition, the use of a calibrated single parameter subgrade model that implicitly accounts for shear interaction, resulted in overestimation of the overall displacement profile.

The response of long flexible piles under dynamic loading in inertial interaction was also investigated. An approximate energy approach utilizing shape functions based on the response of a pile in homogenous medium was used. It was found that for low frequency excitations, the dynamic pile head stiffness can be estimated from the static pile head stiffness for free-head piles. For fixed-head piles, the dynamic pile head stiffness was about 60% less than the static pile head stiffness. It was noted that the radiation damping ratio is most affected by the pile-soil relative stiffness and the excitation frequency, while the material damping weight factors were practically independent of all parameters. Based on these observations, expressions were provided for the dynamic pile head stiffness, radiation damping ratio and material damping weight factors. The effect of the shear term in dynamic inertial interaction was also investigated. Negligible differences were observed with or without the shear term with the exception of the rocking mode of oscillation where differences between the two cases (with or without the shear term) increase with the excitation frequency. The limited effect of the shear term for the dynamic case is attributed to the fact that the analysis was limited to long flexible piles.

Overall, the Kerr-equivalent Pasternak-type continuum model subgrade model, even though developed for shallow foundations, is capable of providing reasonably accurate representation of the response of a single pile in static and dynamic inertial interaction in a non-homogenous medium provided the model is properly calibrated, as this work does.

7.2 Recommendations for future research

Based on the findings of this work and knowledge gained throughout the research process, the following recommendations are put forward for future research

- The current work is limited to a power function type of soil non-homogeneity, as noted in Section 2.2 there are many other types that incorporate attributes such as a bounded exponential form which is more realistic. Such types of non-homogeneity can be investigated using the same approach used here. Admittedly, such forms involve additional terms that increase the computational cost through increasing the number of parameters to be investigated. Research into piles embedded in soil with such forms of non-homogeneity conducted by Vrettos (1998) and Karatzia and Mylonakis (2017) and the limited summary provided by Selvadurai (2007) can serve as a starting point to this effect. Additionally, one of the most common forms of non-homogeneity, multi-layering, can also be investigated along similar lines. Research into single pile response in multilayered soil using alternative approaches conducted by Gazetas and Dobry (1984a) and Basu, Salgado, and Prezzi (2008) can be used as starting points.

- Another avenue for further research can be the inclusion of non-linear soil response. Such non-linearity may be handled by introducing iterative approaches to the current work.

- Further research may also be directed towards the investigation of pile group behavior using the work presented currently and in Lulseged (2021), Worku and Lulseged (2023a), and Worku and Lulseged (2023b). This may be done by using approaches such as the $p-$factor method (Rollins, Lane, and Gerber 2005; Reese and Van Impe

2010) where a factor is applied to the subgrade model for each pile to account for group effects.

- Finally, dynamic kinematic interaction, which is not investigated in this thesis, can be studied with the approaches used in this work. It should be noted that for homogenous soils such an investigation has already been undertaken by Lulseged (2021) and Worku and Lulseged (2023a).

References

AASHTO (2007). *AASHTO LRFD Bridge Design Specifications*. American Association of State Highway and Transportation Officials (AASHTO).

ABAQUS (2022). *ABAQUS/Standard User's Manual, Abaqus 2022*. Dassault Systèmes Simulia Corp.

ACI (2019). *Building Code Requirements for Structural Concrete and Commentary*. ACI 318M-19. American Concrete Institute.

Banergee, P. K. and R. M. Driscoll (1976). "Three-Dimensional Analysis of Raked Pile Groups". In: *Proceedings of the Institution of Civil Engineers* 61.4, pp. 653–671. DOI: 10.1680/iicep.1976.3336.

Banerjee, P. K. (1976). "Integral Equation Methods for Analysis of Piece-Wise Non-Homogeneous Three-Dimensional Elastic Solids of Arbitrary Shape". In: *International Journal of Mechanical Sciences* 18.6, pp. 293–303. ISSN: 0020-7403. DOI: 10.1016/0020-7403(76)90031-X.

Banerjee, P. K. and T. G. Davies (1978). "The Behaviour of Axially and Laterally Loaded Single Piles Embedded in Nonhomogeneous Soils". In: *Géotechnique* 28.3, pp. 309–326. ISSN: 0016-8505. DOI: 10.1680/geot.1978.28.3.309.

Basu, Dipanjan and William Higgins (2011). *Fourier Finite Element Analysis of Laterally Loaded Piles in Elastic Media*. DOI: 10.13140/RG.2.1.5061.6162.

Basu, Dipanjan, R. Salgado, and M. Prezzi (2008). "Analysis of Laterally Loaded Piles in Multilayered Soil Deposits". In: *Joint Transportation Research Program*.

Bowles E., Joseph (1997). *Foundation Analysis and Design*. 5th ed. McGraw-Hill.

BSI (2016). *Structural Timber-Strength Classes BS EN 338:2016*. BS EN 338:2016. British Standards Institute.

Butterfield, R. and P. K. Banerjee (1971). "The Elastic Analysis of Compressible Piles and Pile Groups". In: *Géotechnique* 21.1, pp. 43–60. ISSN: 0016-8505. DOI: 10.1680/geot.1971.21.1.43.

Collin, J. G. (2002). *Timber Pile Design and Construction Manual*. Timber Piling Council, American Wood Preservers Institute.

Davies, T. G. and P. K. Banerjee (1978). "The Displacement Field Due to a Point Load at the Interface of a Two Layer Elastic Half-Space". In: *Géotechnique* 28.1, pp. 43–56. ISSN: 0016-8505. DOI: 10.1680/geot.1978.28.1.43.

Davisson, M. T. and S. Prakash (1963). "A Review of Soil-Pole Behavior". In: *Highway Research Record* 39.

Day, R. A. and D. M. Potts (1994). "Zero Thickness Interface Elements—Numerical Stability and Application". In: *International Journal for Numerical and Analytical Methods in Geomechanics* 18.10, pp. 689–708. ISSN: 1096-9853. DOI: 10.1002/nag.1610181003.

Desai, C. S. et al. (1984). "Thin-Layer Element for Interfaces and Joints". In: *International Journal for Numerical and Analytical Methods in Geomechanics* 8.1, pp. 19–43. ISSN: 1096-9853. DOI: 10.1002/nag.1610080103.

Dobry, Ricardo et al. (1982). "Stiffness and Damping of Single Piles". In: *Journal of the Geotechnical Engineering Division* 108, pp. 439–459. DOI: 10.1061/AJGEB6.0001259.

ES EN 1992-1-1:2015 (2015). *Design of Concrete Structures, Part 1-1, General Rules and Rules for Buildings*. ES EN 1992-1-1:2015. Ministry of Construction.

ES EN 1993-1-1:2015 (2015). *Design of Steel Structures – Part 1-1: General Rules and Rules for Buildings*. ES EN 1993-1-1:2015. Ministry of Construction.

Filonenko-Borodich, M. M. (1940). "Some approximate theories of elastic foundation". In: *Uchenyie Zapiski Moskovkogo Gosudarstuennogo Universiteta Mekhanika* 46, pp. 3–18.

Forest Products Laboratory (1999). *Wood Handbook : Wood as an Engineering Material*. General technical report FPL ; GTR-113. Madison, WI: U.S. Department of Agriculture, Forest Service.

Fulan, Pan (1981). "Analysis of Variation of Poisson's Ratio with Depth of Soil". In: *International Conferences on Recent Advances in Geotechnical Earthquake Engineering and Soil Dynamics*.

Gazetas, George (1984). "Seismic Response of End-Bearing Single Piles". In: *International Journal of Soil Dynamics and Earthquake Engineering* 3.2, pp. 82–93. ISSN: 0261-7277. DOI: 10.1016/0261-7277(84)90003-2.

— (1991). "Foundation Vibrations". In: *Foundation Engineering Handbook*. Ed. by Hsai-Yang Fang. Boston, MA: Springer US, pp. 553–593. ISBN: 978-1-4757-5271-7. DOI: 10.1007/978-1-4757-5271-7_15.

Gazetas, George and Ricardo Dobry (1984a). "Horizontal Response of Piles in Layered Soils". In: *Journal of Geotechnical Engineering* 110.1, pp. 20–40. ISSN: 0733-9410. DOI: 10.1061/(ASCE)0733-9410(1984)110:1(20).

— (1984b). "Simple Radiation Damping Model for Piles and Footings". In: *Journal of Engineering Mechanics* 110.6, pp. 937–956. ISSN: 0733-9399. DOI: 10.1061/(ASCE)0733-9399(1984)110:6(937).

Gibson, R. E. (1967). "Some Results Concerning Displacements and Stresses in a Non-Homogeneous Elastic Half-space". In: *Géotechnique* 17.1, pp. 58–67. ISSN: 0016-8505. DOI: 10.1680/geot.1967.17.1.58.

Guo, W. D. (2012). *Theory and Practice of Pile Foundations*. 1st edition. Boca Raton, FL: CRC Press. 576 pp. ISBN: 978-0-415-80933-7.

Guo, W. D. and F. H. Lee (2001). "Load Transfer Approach for Laterally Loaded Piles". In: *International Journal for Numerical and Analytical Methods in Geomechanics* 25.11, pp. 1101–1129. ISSN: 1096-9853. DOI: 10.1002/nag.169.

Gupta, Dipanjan and Dipanjan Basu (2018). "Applicability of Timoshenko, Euler–Bernoulli and Rigid Beam Theories in Analysis of Laterally Loaded Monopiles and Piles". In: *Géotechnique* 68.9, pp. 772–785. ISSN: 0016-8505, 1751-7656. DOI: 10.1680/jgeot.16.P.244.

Hetényi, M. (1946). *Beams on Elastic Foundation: Theory with Applications in the Fields of Civil and Mechanical Engineering*. Ann Arbor, MI: University of Michigan press.

— (1950). "A General Solution for the Bending of Beams on an Elastic Foundation of Arbitrary Continuity". In: *Journal of Applied Physics* 21.1, p. 55. ISSN: 0021-8979. DOI: 10.1063/1.1699420.

Higgins, William et al. (2013). "Elastic Solutions for Laterally Loaded Piles". In: *Journal of Geotechnical and Geoenvironmental Engineering* 139.7, pp. 1096–1103. ISSN: 1943-5606. DOI: 10.1061/(ASCE)GT.1943-5606.0000828.

Horvath, J. S. (1983a). "Modulus of Subgrade Reaction: New Perspective". In: *Journal of Geotechnical Engineering* 109.12, pp. 1591–1596. ISSN: 0733-9410. DOI: 10.1061/(ASCE)0733-9410(1983)109:12(1591).

— (1983b). "New Subgrade Model Applied to Mat Foundations". In: *Journal of Geotechnical Engineering* 109.12, pp. 1567–1587. ISSN: 0733-9410. DOI: 10.1061/(ASCE)0733-9410(1983)109:12(1567).

— (2002). *Basic SSI Concepts and Applications Overview*. Bronx, New York: Manhattan College.

Karatzia, Xenia and George Mylonakis (2012). "Horizontal Response of Piles in Inhomogeneous Soil: Simple Analysis". In: SECOND INTERNATIONAL CONFERENCE ON PERFORMANCE-BASED DESIGN IN EARTHQUAKE GEOTECHNICAL ENGINEERING. Taormina, Italy.

— (2017). "Horizontal Stiffness and Damping of Piles in Inhomogeneous Soil". In: *Journal of Geotechnical and Geoenvironmental Engineering* 143.4, p. 04016113. ISSN: 1943-5606. DOI: 10.1061/(ASCE)GT.1943-5606.0001621.

Kerr, A. D. (1964). "Elastic and Viscoelastic Foundation Models". In: *Journal of Applied Mechanics* 31.3, pp. 491–498. ISSN: 0021-8936. DOI: 10.1115/1.3629667.

— (1965). "A Study of a New Foundation Model". In: *Acta Mechanica* 1.2, pp. 135–147. ISSN: 1619-6937. DOI: 10.1007/BF01174308.

Kerr, A. D. and W. J. Rhines (1967). *A Further Study of Elastic Foundation Models*. S-67-1. University Heights, New York: New York University, School of Engineering and Science, p. 25.

Kierzenka, J and Lawrence Shampine (2008). "A BVP Solver That Controls Residual and Error". In: *European Society of Computational Methods in Sciences and Engineering (ESCMSE) Journal of Numerical Analysis, Industrial and Applied Mathematics* 3, pp. 27–41.

Kuhlemeyer, Roger L. (1979). "Static and Dynamic Laterally Loaded Floating Piles". In: *Journal of the Geotechnical Engineering Division* 105.2, pp. 289–304. DOI: 10.1061/AJGEB6.0000771.

Kulhawy, Fred H and Paul W Mayne (1990). *Manual on Estimating Soil Properties for Foundation Design*. Electric Power Research Inst., Palo Alto, CA (USA); Cornell Univ., Ithaca ...

Lulseged, Abey (2021). "Static and Dynamic Lateral Response of Single Piles Using Kerr-Equivalent Pasternak Subgrade Model". Thesis. Addis Ababa University.

Mathematica (2022). *Mathematica, Version 13.2*. Champaign, IL: Wolfram Research Inc.

MATLAB (2022). *MATLAB, Version 9.12.0 (R2022a)*. Natick, Massachusetts: The MathWorks Inc.

Matlock, Hudson (1970). "Correlation for Design of Laterally Loaded Piles in Soft Clay". In: Offshore Technology Conference. OnePetro. DOI: 10.4043/1204-MS.

Mindlin, Raymond D. (1936). "Force at a Point in the Interior of a Semi-Infinite Solid". In: *Physics* 7.5, pp. 195–202. ISSN: 0148-6349. DOI: 10.1063/1.1745385.

Mylonakis, George (1995). "Contributions to Static and Seismic Analysis of Piles and Pile-Supported Bridge Piers".

— (2001). "Elastodynamic Model for Large-Diameter End-Bearing Shafts". In: *Soils and Foundations* 41.3, pp. 31–44. ISSN: 0038-0806. DOI: 10.3208/sandf.41.3_31.

Novak, Milos (1974). "Dynamic Stiffness and Damping of Piles". In: *Canadian Geotechnical Journal* 11.4, pp. 574–598. ISSN: 0008-3674. DOI: 10.1139/t74-059.

O'Neill, M. W., L. C. Reese, and W. R. Cox (1990). "Soil Behavior for Piles Under Lateral Loading". In: Offshore Technology Conference. OnePetro. DOI: 10.4043/6377-MS.

Pasternak, P. L. (1954). *On a new method of analysis of an elastic foundation by means of two foundation constants*. Moscow, Russia: Gosudarstvennoye Izdatel'stvo Literatury po Stroitel'stvu i Arkhitekture.

Pender, M. J. (1993). "Aseismic Pile Foundation Design Analysis". In: *Bulletin of the New Zealand Society for Earthquake Engineering* 26.1 (1), pp. 49–160. ISSN: 2324-1543. DOI: 10.5459/bnzsee.26.1.49-160.

PLAXIS 3D (2020). *PLAXIS 3D, CONNECT Edition V20 Update 3*. Exton, Pennsylvania: Bentley Systems, Incorporated.

Poulos, Harry (1971). "Behavior of Laterally Loaded Piles: I-Single Piles". In: *Journal of the Soil Mechanics and Foundations Division* 97.5, pp. 711–731. DOI: 10.1061/JSFEAQ.0001592.

Poulos, Harry and E. Davis (1980). *Pile Foundation Analysis and Design*. Wiley. 397 pp. ISBN: 978-0-471-09956-7.

Randolph, M. F. (1981). "The Response of Flexible Piles to Lateral Loading". In: *Géotechnique* 31.2, pp. 247–259. ISSN: 0016-8505. DOI: 10.1680/geot.1981.31.2.247.

Reddy, J. N. (2002). *Energy Principles and Variational Methods in Applied Mechanics*. 2nd edition. New York: Wiley. 608 pp. ISBN: 978-0-471-17985-6.

Reese, L. C. and W. F. Van Impe (2010). *Single Piles and Pile Groups Under Lateral Loading*. CRC Press. 529 pp. ISBN: 978-1-4398-9430-9. Google Books: buTqBgAAQBAJ.

Reissner, E. (1958). "A Note on Deflections of Plates on a Viscoelastic Foundation". In: *Journal of Applied Mechanics* 25.1, pp. 144–145. ISSN: 0021-8936. DOI: 10.1115/1.4011704.

Rollins, Kyle M., J. Dusty Lane, and Travis M. Gerber (2005). "Measured and Computed Lateral Response of a Pile Group in Sand". In: *Journal of Geotechnical and Geoenvironmental Engineering* 131.1, pp. 103–114. ISSN: 1090-0241. DOI: 10.1061/(ASCE)1090-0241(2005)131:1(103).

Scott, R. F. (1981). *Foundation Analysis*. 1st. Englewood Cliffs, NJ: Prentice Hall. 545 pp. ISBN: 978-0-13-329169-8.

Selvadurai, A. P. S. (2007). "The Analytical Method in Geomechanics". In: *Applied Mechanics Reviews* 60.3, pp. 87–106. ISSN: 0003-6900. DOI: 10.1115/1.2730845.

Selvadurai, A. P. S., B. M. Singh, and J. Vrbik (1986). "A Reissner-Sagoci Problem for a Non-Homogeneous Elastic Solid". In: *Journal of Elasticity* 16.4, pp. 383–391.

Shampine, L. F., I. Gladwell, and S. Thompson (2003). *Solving ODEs with MATLAB*. Cambridge: Cambridge University Press. ISBN: 978-0-521-82404-0. DOI: 10.1017/CBO9780511615542.

Sun, Keming (1994). "A Numerical Method for Laterally Loaded Piles". In: *Computers and Geotechnics* 16.4, pp. 263–289. ISSN: 0266-352X. DOI: 10.1016/0266-352X(94)90011-6.

Syngros, Konstantinos (2004). "Seismic Response of Piles and Pile-Supported Bridge Piers Evaluated Through Case Histories".

Terzaghi, K. (1955). "Evaluation of Coefficients of Subgrade Reaction". In: *Geotechnique* 5.4, pp. 297–326. ISSN: 17517656. DOI: 10.1680/geot.1955.5.4.297.

Vesic, A. (1961). "Beams on Elastic Subgrade and the Winkler's Hypothesis". In: *Proc. 5th Int. Conf. on SMFE*. Vol. 1, pp. 845–851.

Vesic, A. and S. K. Saxena (1970). *Analysis of Structural Behavior of AASHO Road Test Rigid Pavements*. National Cooperative Highway Research Program Report 97. Highway Research Board, p. 47.

Vlasov, V. Z. and N. N Leont'ev (1966). *Beams, Plates, and Shells on Elastic Foundations.* translated from Russian by Israel program for scientific translations.

Vrettos, Christos (1998). "The Boussinesq Problem for Soils with Bounded Non-Homogeneity". In: *International journal for numerical and analytical methods in geomechanics* 22.8, pp. 655–669.

Wilson, E. L. (1965). "Structural Analysis of Axisymmetric Solids." In: *AIAA Journal*. DOI: 10.2514/3.3356.

Winkler, E. (1867). *Die Lehre von der Elasticitaet und Festigkeit: mit besonderer Rücksicht auf ihre Anwendung in der Technik, für polytechnische Schulen, Bauakademien, Ingenieure, Maschinenbauer, Architecten, etc.* H. Dominicus.

Worku, Asrat (2010). "Part I: A Generalized Formulation of Continuum Models for Elastic Foundations". In: *GeoFlorida 2010*. American Society of Civil Engineers, pp. 1641–1650. DOI: 10.1061/41095(365)166.

— (2013). "Calibrated Analytical Formulas for Foundation Model Parameters". In: *International Journal of Geomechanics* 13.4, pp. 340–347. ISSN: 1943-5622. DOI: 10.1061/(ASCE)GM.1943-5622.0000214. URL: https://ascelibrary.org/doi/abs/10.1061/%28ASCE%29GM.1943-5622.0000214 (visited on 11/10/2021).

— (2014). "Development of a Calibrated Pasternak Foundation Model for Practical Use". In: *International Journal of Geotechnical Engineering* 8.1, pp. 26–33. ISSN: 1938-6362. DOI: 10.1179/1938636213Z.00000000055. URL: https://doi.org/10.1179/1938636213Z.00000000055 (visited on 11/10/2021).

Worku, Asrat and Yimer Degu (2010). "Part II: Application of Newly Derived and Calibrated Continuum Subgrade Models in the Analysis of Beams on Elastic Foundations". In: *GeoFlorida 2010*. Reston, VA: American Society of Civil Engineers, pp. 1651–1660. DOI: 10.1061/41095(365)167--.

Worku, Asrat and Abey Lulseged (2023a). "Kinematic Pile-Soil Interaction Using a Rigorous Two-Parameter Foundation Model". In: *Soil Dynamics and Earthquake Engineering* 165, p. 107701. ISSN: 0267-7261. DOI: 10.1016/j.soildyn.2022.107701.

— (2023b). "Lateral Static Response of Piles Based on a Full-Fledged Two-Parameter Foundation Model". In: *International Journal of Geomechanics* 23.2, p. 04022282. ISSN: 1943-5622. DOI: 10.1061/(ASCE)GM.1943-5622.0002628.

Appendix A

Derivation of equivalent base shear, Q_L

In the case of the free-base boundary, effects of the soil below the pile is taken into consideration, since the Pasternak subgrade model accounts for shear interaction. This effect can be represented by an equivalent shear force, Q_L, at the base of the pile (Sun 1994; Guo 2012). Considering the soil segment below the pile, from the Pasternak subgrade model:

$$k_p(z)u(z) - G_p(z)\frac{d^2u(z)}{dz^2} \quad = 0, \quad z > L \tag{A.1}$$

Applying (3.6) and (3.7)-(3.20) to (A.1) with the conditions that $z = L$, $u(z) = u_L$and $z \to \infty$, $u(z) \to 0$

$$\frac{(0.4\nu_s + 0.67)}{\chi} mr \left(\frac{z}{r}\right)^n u(z) - \frac{(2.72\nu_s + 4.56)}{1 + \nu_s} \chi mr^3 \left(\frac{z}{r}\right)^n \frac{d^2u(z)}{dz^2} = \quad 0, \quad z > L \tag{A.2}$$

$$z = L, \quad u(z) = u_L$$

$$z \to \infty, \quad u(z) \to 0$$

for $z > L$, $\left(\frac{z}{r}\right)^n \neq 0$, hence this terms can be canceled out. This simplifies the expression to a second order ODE with constant coefficients.

$$k_{pr}u(z) - G_{pr}\frac{d^2u(z)}{dz^2} = \quad 0, \quad z > L \tag{A.3}$$

$$z = L, \quad u(z) = u_L$$
$$z \to \infty, \quad u(z) \to 0$$

where:

$$k_{pr} = \frac{(0.4\nu_s + 0.67)}{\chi} mr \tag{A.4}$$
$$G_{pr} = \frac{(2.72\nu_s + 4.56)}{1 + \nu_s} \chi m r^3 \tag{A.5}$$

using the characteristic equation method the solution becomes:

$$u(z) = u_L \exp\left[-\sqrt{\frac{k_{pr}}{G_{pr}}}\,(z - L)\right] \tag{A.6}$$

Note that the ratio $\dfrac{k_p(z)}{G_p(z)}$ is constant and equal to $\dfrac{k_{pr}}{G_{pr}} = \dfrac{k_{pL}}{G_{pL}}$. Hence (A.6) may be expressed as:

$$u(z) = u_L \exp\left[-\sqrt{\frac{k_{pL}}{G_{pL}}}\,(z - L)\right] \tag{A.7}$$

Considering the shear force at the pile base,

$$
\begin{aligned}
Q_L &= \tau \times 1 \\
&= G_{pL} \left. \frac{du}{dz} \right|_{z=L} \\
&= G_{pL} \frac{d}{dz} \left\{ u_L \exp \left[-\sqrt{\frac{k_{pL}}{G_{pL}}} \, (z - L) \right] \right\}_{z=L} \\
Q_L &= -u_L \sqrt{k_{pL} G_{pL}}
\end{aligned} \tag{A.8}
$$

Appendix B

Derivation of energy equations for approximate analysis in inertial interaction

This section formulates the energy equations in 3.45 and 3.46. The is done on a component-by-component bases. The pile head impedance given by $\mathcal{K}_{\mathrm{x}} = K_x + iC_x$, involves two components the real part, the equivalent pile head stiffness, and the imaginary part the equivalent pile head damping. Following Mylonakis (1995), two displacement shape function are defined φ_i and φ_j. This formulation is similar to the unit dummy displacement method described by Reddy (2002). In the formulation to follow, φ_j will be treated as virtual displacement while φ_i is treated as an actual displacement; this choose does not affect the final solution.

First considering the pile head stiffness, the virtual work done by the spring reaction force, F_i^k, associated with the pile head stiffness element (spring) in moving through the virtual displacement φ_j can be computed as follows:

$$\begin{aligned} W^{H,K} &= F_i^k \varphi_j \\ &= K_{ij} \varphi_i \varphi_j \end{aligned} \tag{B.1}$$

where K_{ij} is the stiffness coefficient of the element and φ_i is the actual displacement associated with the reaction force.

Similarly the virtual work done by the viscous dashpot, whose reaction force, by definition, is proportional to the velocity of motion, can be computed as follows:

$$W^{H,C} = F_i^C \varphi_j \tag{B.2}$$

The dashpot reaction force, F_i^Ccan be computed as follows:

$$F_i^C = C_{ij} \frac{d\varphi_i}{dt} \tag{B.3}$$

Considering harmonic excitation of the form $\varphi(z,t) = 1 \times e^{i\omega t}$, the dashpot reaction force can be expressed as:

$$F_i^C = iC_{ij}\varphi_i \tag{B.4}$$

Note the coefficient i in Equation (B.4) is the imaginary unit, i.e. $i = \sqrt{-1}$.

Inserting (B.4) into (B.2) one obtains:

$$W^{H,C} = iC_{ij}\varphi_i\varphi_j \tag{B.5}$$

The imaginary unit can be dropped as formulation is done on a component-by-component basis and the imaginary part represents the damping component in the impedance equation. The above two expressions for work are equal to the combined contribution of the distributed elements along the pile length. The virtual work done by each component in moving through the virtual displacement φ_j is computed as follows:

B.1 Contribution of the pile flexural stiffness

Considering the Euler-Bernoulli beam theory, the internal virtual work done by (or on) a bending beam can be computed by considering the strain energy stored in the beam as follows (Reddy 2002):

$$W^I = \int_0^L \int_A \sigma_{z,i}\epsilon_{z,j} dA dz \tag{B.6}$$

Where L is the length of the pile, A is the cross-sectional area. Assuming no axial load is applied and neglecting higher order terms, the strains associated with the displacements φ_i and φ_j can be expressed as follows:

$$\epsilon_{z,i} = z\frac{d^2\varphi_i}{dz^2} \tag{B.7}$$

$$\epsilon_{z,j} = z\frac{d^2\varphi_j}{dz^2} \tag{B.8}$$

Expanding (B.6) and inserting (B.7) and (B.8), one obtains:

$$W^I = \int_0^L \int_A \sigma_{z,i}\epsilon_{z,j} dA dz \tag{B.9}$$

$$= \int_0^L \int_A E_p\epsilon_{z,i}\epsilon_{z,j} dA dz \tag{B.10}$$

$$= \int_0^L \int_A E_p z\frac{d^2\varphi_i}{dz^2} z\frac{d^2\varphi_j}{dz^2} dA dz \tag{B.11}$$

$$W^I = \int_0^L E_p I_p \frac{d^2\varphi_i}{dz^2}\frac{d^2\varphi_j}{dz^2} dz \tag{B.12}$$

Assuming the pile to be homogenous and prismatic, the total virtual work becomes:

$$W^I = E_p I_p \int_0^L \frac{d^2\varphi_i}{dz^2}\frac{d^2\varphi_j}{dz^2} dz \tag{B.13}$$

B.2 Contribution of the subgrade

The contribution from the subgrade involves two components, contribution from the stiffness (spring) element and contribution from the shear element. First considering the spring element, the total virtual work done by the distributed spring element is given by:

$$W^{k_p} = \int_0^L f_i^k(z)\varphi_j dz \tag{B.14}$$

where $f_i^k(z)$ is the reaction force in the distributed springs given by $f_i^k(z) = k_p(z)\varphi_i$, where $k_p(z)$ is the stiffness of the distributed spring elements. Hence, the total virtual work becomes:

$$W^{k_p} = \int_0^L k_p(z)\varphi_i\varphi_j dz \tag{B.15}$$

Moving on to the total virtual work done by the shear element, first considering the total strain energy stored in the element

$$W^{G_P} = \int_0^L \int_A \tau_{x,i}\gamma_{x,j} dA dz \tag{B.16}$$

The shear strains associated with the displacements φ_i and φ_j can be expressed as:

$$\gamma_{x,i} = \frac{d\varphi_i}{dz} \tag{B.17}$$

$$\gamma_{x,j} = \frac{d\varphi_j}{dz} \tag{B.18}$$

From the consideration that $\tau_{x,i} = -G_p\gamma_{x,i}$, assuming unity for the dimensions of the element, i.e. $A = 1$, and inserting (B.17) and (B.18) into (B.16) one obtains:

$$W^{G_P} = \int_0^L -G_p \gamma_{x,i} \gamma_{x,j} dz \tag{B.19}$$

$$W^{G_P} = -\int_0^L G_p(z) \frac{d\varphi_i}{dz} \frac{d\varphi_j}{dz} dz \tag{B.20}$$

B.3 Contribution of the pile inertia

From the Hamilton's principle for continuum solids, the virtual work done by the inertial force ma_i in moving through the virtual displacement φ_j is given by (Reddy 2002):

$$W^D = \int_V \rho \frac{\partial^2 \varphi_i}{\partial t^2} \varphi_j dV \tag{B.21}$$

Where ρ is the volumetric mass density of the pile. Since the expression is being developed for a linear structural element (a pile), only the axial direction is considered, hence:

$$W^D = \int_0^L \bar{m} \frac{\partial^2 \varphi_i}{\partial t^2} \varphi_j dz \tag{B.22}$$

where $\bar{m}$ is the mass per unit length of the pile and L is the length of the pile. Assuming harmonic excitation of the form $\varphi(z,t) = 1 \times e^{i\omega t}$,

$$W^D = -\int_0^L \bar{m} \omega^2 \varphi_i \varphi_j dz \tag{B.23}$$

Assuming the density of the pile to be constant with depth, the total virtual work done becomes:

$$W^D = -\bar{m} \omega^2 \int_0^L \varphi_i \varphi_j dz \tag{B.24}$$

B.4 Contribution of the dashpot

The distributed dashpot elements represent both viscous radiation dashpots and hysteretic material damping components, i.e. $C^s + C^p + C^r$.

First, the work done by the distributed dashpot elements for radiation damping can be computed as follows:

$$W^{cr} = \int_0^L f_i^{cr}(z)\varphi_j dz \tag{B.25}$$

where $f_i^{cr}(z)$ is the reaction force of the distributed dashpots. This force is proportional to the velocity of motion is given by:

$$f_i^{cr}(z) = c(z)\frac{d\varphi_i}{dt} \tag{B.26}$$

where $c(z)$ is the damping coefficient for the distributed dashpots. Assuming harmonic excitation of the form $\varphi(z,t) = 1 \times e^{i\omega t}$,

$$f_i^{cr}(z) = ic(z)\varphi_i \tag{B.27}$$

Inserting (B.27) into (B.25), one obtains the total virtual work done by the distributed dashpot elements as follows:

$$W^{cr} = i\int_0^L c(z)\varphi_i\varphi_j dz \tag{B.28}$$

Note that the imaginary unit can be dropped, for similar reasons stated for the equivalent pile head damping term above (Equation (B.5)).

The hysteretic material damping components are associated with the pile damping represented by the the damping ratio β_p and soil damping ratio, β_s. Both terms are considered to be constant. From an equivalent 1-DOF system the damping coefficient is given by $C = \frac{2k\beta}{\omega}$. Since both material damping components are constant the work done by the

associated dashpot components can simply be found by summing each contribution along the pile length. Hence,

$$W^{cm} = \frac{2\beta_p}{\omega} W^I + \frac{2\beta_s}{\omega} \left(W^{k_p} + W^{G_p} \right) \tag{B.29}$$

Combining (B.28) and (B.29) the total dashpot contribution is given by:

$$W^c = \frac{2\beta_p}{\omega} W^I + \frac{2\beta_s}{\omega} \left(W^{k_p} + W^{G_p} \right) + \int_0^L c(z)\varphi_i\varphi_j dz \tag{B.30}$$

expanding the above equation,

$$W^c = \frac{2\beta_p}{\omega} E_p I_p \int_0^L \frac{d^2\varphi_i}{dz^2}\frac{d^2\varphi_j}{dz^2} dz + \frac{2\beta_s}{\omega} \left(\int_0^L k_p(z)\varphi_i\varphi_j dz - \int_0^L G_p(z)\frac{d\varphi_i}{dz}\frac{d\varphi_j}{dz} dz \right) + \int_0^L c(z)\varphi_i\varphi_j dz \tag{B.31}$$

Finally each of the contributions can be summed up and equated to the virtual work done at the pile head. First for the virtual work associated with the stiffness elements, this includes the spring element at the pile head (B.1) and the beam flexural stiffness (B.13), beam inertia (B.24), distributed springs (B.15) and distributed shear elements (B.20). Hence, equating the work done at the pile head with contribution of distributed elements, one obtains:

$$\begin{aligned} W^{H,K} &= W^I + W^{k_p} + W^{G_P} + W^D \\ K_{ij}\varphi_i\varphi_j &= E_p I_p \int_0^L \frac{d^2\varphi_i}{dz^2}\frac{d^2\varphi_j}{dz^2} dz + \int_0^L k_p(z)\varphi_i\varphi_j dz - \int_0^L G_p(z)\frac{d\varphi_i}{dz}\frac{d\varphi_j}{dz} dz - \bar{m}\omega^2 \int_0^L \varphi_i\varphi_j dz \end{aligned} \tag{B.32}$$

Since either φ_i and φ_j can be treated as virtual displacements in the formulation without affecting the generality of the solution, they can be chosen arbitrarily provided they are consistent with the displacement boundary conditions. Hence, following Mylonakis (1995) this displacements are defined as shape function associated with either a unit

displacement or rotation at the pile head. Thus, the pile head stiffness is given by:

$$K_{ij} = E_p I_p \int_0^L \frac{d^2\varphi_i}{dz^2}\frac{d^2\varphi_j}{dz^2}dz + \int_0^L k_p(z)\varphi_i\varphi_j dz - \int_0^L G_p(z)\frac{d\varphi_i}{dz}\frac{d\varphi_j}{dz}dz - \bar{m}\omega^2 \int_0^L \varphi_i\varphi_j dz \tag{B.33}$$

The equivalent pile head dashpot represents the combination of material (soil and pile) and radiation damping, i.e. $C^s + C^p + C^r$. The virtual work done by the pile head radiation dashpot coefficient, C^r, is equal to the total virtual work done by the radiation component of the distributed dashpot elements given by (B.28).

Therefore, the equivalent pile head damping coefficient can be determined by equating the expressions in (B.5) and (B.31) and setting φ_i and φ_j to be unity at the pile head, resulting in the expression:

$$C_{ij} = \frac{2\beta_p}{\omega}E_p I_p \int_0^L \varphi_i''\varphi_j'' dz + \frac{2\beta_s}{\omega}\left[-\int_0^L G_p(z)\varphi_i'\varphi_j' dz + \int_0^L k_p(z)\varphi_i\varphi_j dz\right] + \int_0^L c_r(z)\varphi_i\varphi_j dz \tag{B.34}$$